FORSCHUNGSZENTRUM JÜLICH GmbH

KFA

Institut für Kernphysik

In-Beam γ-Ray Spectroscopy of N=84 Nuclei above Gd and the Impact of the $(\pi h_{11/2} \nu h_{9/2})1^+$ Attraction on their Yrast Lines

Chengteng Zhang

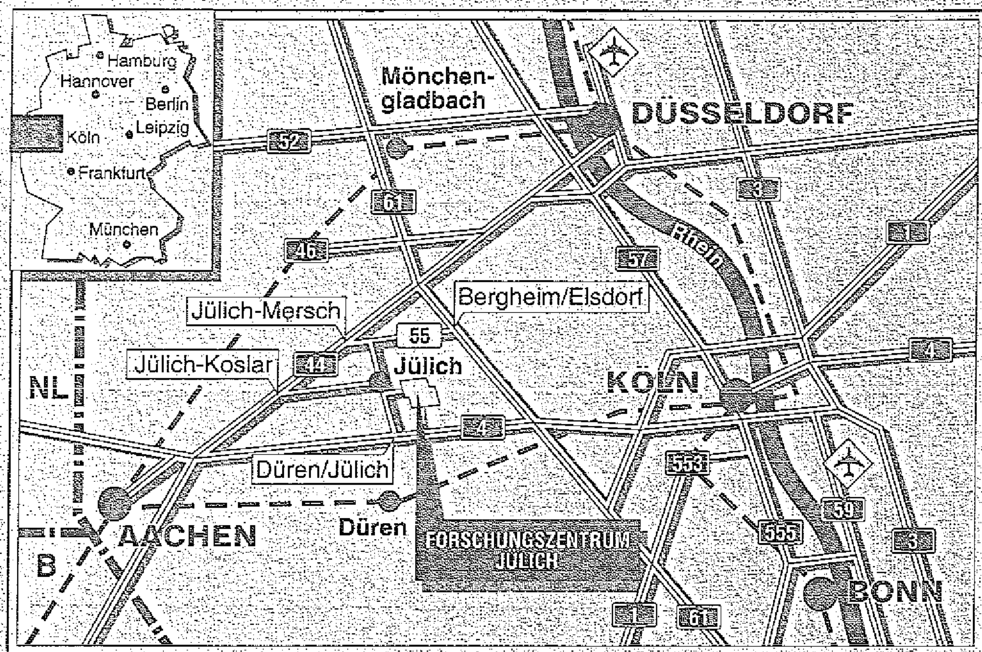

Berichte des Forschungszentrums Jülich ; 2857
ISSN 0944-2952
Institut für Kernphysik Jül-2857
D 38 (Diss. Universität Köln)

Zu beziehen durch : Forschungszentrum Jülich GmbH · Zentralbibliothek
D-52425 Jülich · Bundesrepublik Deutschland
Telefon : 02461/61-6102 · Telefax : 02461/61-6103 · Telex : 833556-70 kfa d

In-Beam γ-Ray Spectroscopy of N=84 Nuclei above Gd and the Impact of the $(\pi h_{11/2} \nu h_{9/2})1^+$ Attraction on their Yrast Lines

Chengteng Zhang

Table of Contents

page

Chapter 1 Introduction 1

Chapter 2 Experiments and Data Analysis 6

2.1 The Osiris γ-spectrometer 7

2.2 The Nordball γ-spectrometer 9

2.3 Standard $\gamma\gamma$-coincidence matrices 10

2.4 $\gamma\gamma$-n coincidences 11

2.5 Angular distributions from coincidence data 14

Chapter 3 Level Scheme 20

3.1 The nucleus $^{151}_{67}Ho_{84}$ 20

3.2 The nucleus $^{152}_{68}Er_{84}$ 31

3.2 The nucleus $^{153}_{69}Tm_{84}$ 36

3.3 The nucleus $^{154}_{70}Yb_{84}$ 43

Chapter 4 Shell Model Analysis 52

4.1 Multiparticle shell model calculations 52

4.2 Configuration assignments 56

4.3 Characteristic properties of the $\pi h^n_{11/2}\nu f^2_{7/2}$ and $\pi h^n_{11/2}\nu f_{7/2}h_{9/2}$ yrast lines 63

4.3.1 The $\pi h^n_{11/2}\nu f^2_{7/2}$ yrast line 65

4.3.2 The significant impact of the strong $(\pi h_{11/2}\nu h_{9/2})1^+$ attraction on the $\pi h^n_{11/2}\nu f_{7/2}h_{9/2}$ yrast line 66

Chapter 5 Low-Lying High-Spin States of Opposite Parity 76

Chapter 6 Synopsis 81

References

Zusammenfassung

In In-beam γ-Experimenten wurden Hochspinanregungen der vier N=84 Isotone ^{151}Ho, ^{152}Er, ^{153}Tm und ^{154}Yb untersucht. Die Kerne wurden mit Schwerionenprojektilen der Massen 28 bis 56 in Fusions-Verdampfungsreaktionen erzeugt und ihre γ-Strahlung mit den Vieldetektorspektrometern Nordball des Niels Bohr Instituts und Osiris am Hahn-Meitner Institut gemessen. In den Yrast-Zerfallsschemata wurden alle γ-Übergänge mit Intensitäten oberhalb 1% (in ^{154}Yb 5%) des Gesamtquerschnitts für die Erzeugung des Ausgangskerns eingeordenet. Die Spins der Niveaus konnten bestimmt werden bis 10 MeV (Yb 8 MeV) Anregungsenergie; die Niveauparitäten wurden für Zustände unterhalb 5-7 MeV festgelegt.

Die Resultate zeigen, daß im Yrast-Zerfall dieser vier N=84 Kerne die Vielvalenzteilchenkonfigurationen $\pi h^n_{11/2}\nu f^2_{7/2}$ und $\pi h^n_{11/2}\nu f_{7/2}h_{9/2}$ (n=Z–64) stark bevölkert werden. Ihre maximal ausgerichteten Zustände von $43/2^-$ in ^{151}Ho (bei 4.8 MeV Anregung), 24^+ in ^{152}Er (7.5 MeV) und $51/2^-$ in ^{153}Tm (6.9 MeV) wurden identifiziert, während im ^{154}Yb der höchste beobachtete $(\pi h^6_{11/2}\nu f_{7/2}h_{9/2})24^+$ Zustand 0.5 MeV unterhalb des bei 9.6 MeV erwarteten voll ausgerichteten 26^+ Niveaus gefunden wurde. Die Experimente ergeben einen relativen glatten Verlauf der $\pi h^n_{11/2}\nu f^2_{7/2}$ Yrastlinie, im Gegensatz zur Yrastlinie der $\pi h^n_{11/2}\nu f_{7/2}h_{9/2}$ Konfiguration, wo die starke $(\nu f_{7/2}h_{9/2})8^+$ Nukleon-Nukleon-Attraktion einzelne Yrastniveaus selektiv absenkt.

Theoretische Ergebnisse aus Schalenmodellrechnungen dieser beiden Vielteilchenkonfigurationen sind in hervorragender Übereinstimmung mit dem Experiment. Diese Rechnungen sind parameterfrei, da sämtliche in der Theorie erforderlichen dynamischen Größen (Nukleon-Nukleon-Wechselwirkungen und Einteilchenenergien) in früheren Arbeiten experimentell bestimmt wurden.

Ein interessantes hier identifiziertes Kernstrukturphänomen wurde bei Yrastzuständen der $\pi h^n_{11/2}\nu f_{7/2}h_{9/2}$ Konfiguration beobachtet, wo für spezifische Spinwerte

die stark attraktive $(\pi h_{11/2} \nu h_{9/2})1^{+}$ Kopplung dominant wird. Dadurch wird die Anregungsenergie unter das höchste Yrastniveau der nächst niedrigeren Senioritätsstufe abgesenkt, während sonst die Seniorität monoton mit dem Spin ansteigt. Diese senioritätsinvertierten Yrastzustände werden für die Kerne oberhalb Dysprosium erwartet und wurden erstmalig in den vier untersuchten N=84 Isotonen systematisch identifiziert.

1 Introduction

The classical heavy nuclei with stable spherical shape are located along the major shell closures for either protons or neutrons, or in their close neighbourhood. These include the Sn isotopes with 50 protons, the N=82 isotones, the neutron deficient Pb nuclei with Z=82, and the N=126 isotones above ^{208}Pb. The structure of these nuclei can be described by the nuclear shell model based on the principles of independent nucleon motion in a spherical potential.

A special feature characterizes the group of spherical nuclei near N=82, where a significant energy gap in the proton single particle spectrum separates the low-lying $g_{7/2}$ and $d_{5/2}$ proton orbitals from the above $h_{11/2}$, $s_{1/2}$ and $d_{3/2}$ orbitals (Fig. 1.1), and it is found that the Z=64 nucleus ^{146}Gd has many properties of a doubly closed core. This feature greatly simplifies shell model analysis in the region above ^{146}Gd, where in general only the $h_{11/2}$ proton will play a significant role in the yrast-line configurations.

Experimental data on the N=82 isotones above Gd exist up to the Z=72 8-valence-proton nucleus ^{154}Hf. In the even-Z species ^{148}Dy, ^{150}Er, ^{152}Yb and ^{154}Hf, 10^+ isomers of $\pi h^2_{11/2}$ character are found near 3 MeV, and corresponding $\pi h^3_{11/2}$ $27/2^-$ isomers were observed at similar energies in the odd-Z isotones ^{149}Ho, ^{151}Tm and ^{153}Lu. The experimental πh^n yrast-level energies in these nuclei agree excellently with theoretical values calculated with the shell model using the π-π two-body residual interactions from the observed level energies in the ^{148}Dy two-proton nucleus. The maximum spin that can be formed by $h_{11/2}$ protons is 18^+, and is expected in the six-proton nucleus ^{152}Yb but has not yet been observed. But for 5, 4, 3, and 2 valence protons the $\pi h^n_{11/2}$-states with maximum spins of $35/2^-$, 16^+, $27/2^-$, and 10^+ were identified through in-beam measurements in the respective isotones, all in similarly good agreement with theory.

Naturally, the yrast lines become much more complicated when neutrons are added.

At N=83, the lowest $f_{7/2}$ valence neutron will combine with the $h^{n}_{11/2}$ proton spectra and form corresponding $\nu f_{7/2}$ and $(\pi h_{11/2}\nu f_{7/2})9^{+}$ ground states, and 3 MeV-isomers with spins $27/2^{-}$ and 17^{+} in the stretched coupling, but little is known about the configuration of the higher-lying yrast states in these nuclei.

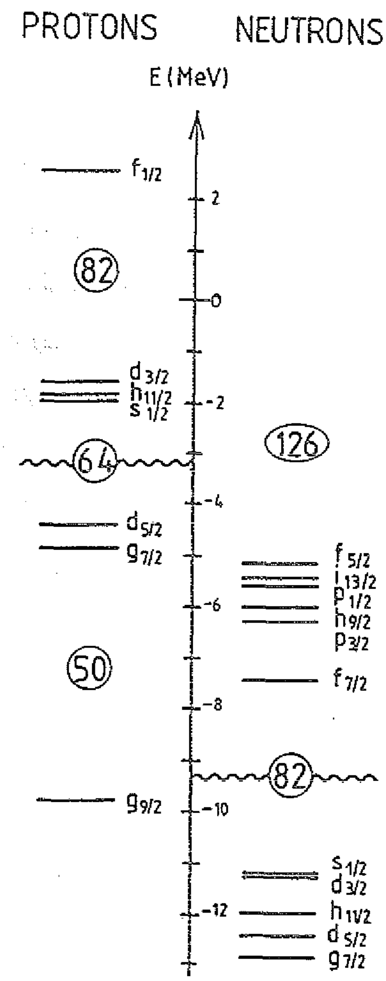

Fig. 1.1 Single-particle diagrams for ^{146}Gd.

Two $f_{7/2}$ valence neutrons, at N=84, can provide up to 6 units of angular momentum, and the 6—>4—>2—>0 triple E2 transition sequence forms the lowest portion of the yrast cascade, in odd-Z nuclei connecting the $(\pi h_{11/2}\nu f^{2}_{6})23/2^{-}$ state to the $11/2^{-}$ ground state. The next high-j neutron orbital above $f_{7/2}$ is $h_{9/2}$, which in ^{147}Gd lies at 1.4 MeV (Fig.1.1). Together with one $f_{7/2}$ neutron it forms a low-lying 8^{+} state, which is also strongly populated in the yrast cascade. Above it, only the $i_{13/2}$ orbital could provide more neutron spin, but this state lies at high excitation and strongly admixes with 3 quasi-particle levels such that it is in general not prominent in the low-lying yrast states.

Instead, above 8^{+}, the next yrast state is $\pi h^{2}_{11/2}$ coupled to 10, followed again by the 2^{+} to 8^{+} couplings of the two valence neutrons. This principle structure of the valence particle yrast lines in nuclei above Gd with 82 to 84 neutrons is schematically displayed in Fig. 1.2, which gives the maximum spin of the valence particle yrast cascade as a function of proton and neutron number.

In the N=84 nuclei these multi-particle yrast levels were known so far up to $27/2^{-}$ in ^{149}Tb, to 18^{+} in ^{150}Dy and ^{152}Er, and $43/2^{-}$ in ^{151}Ho. The principle aim of the present

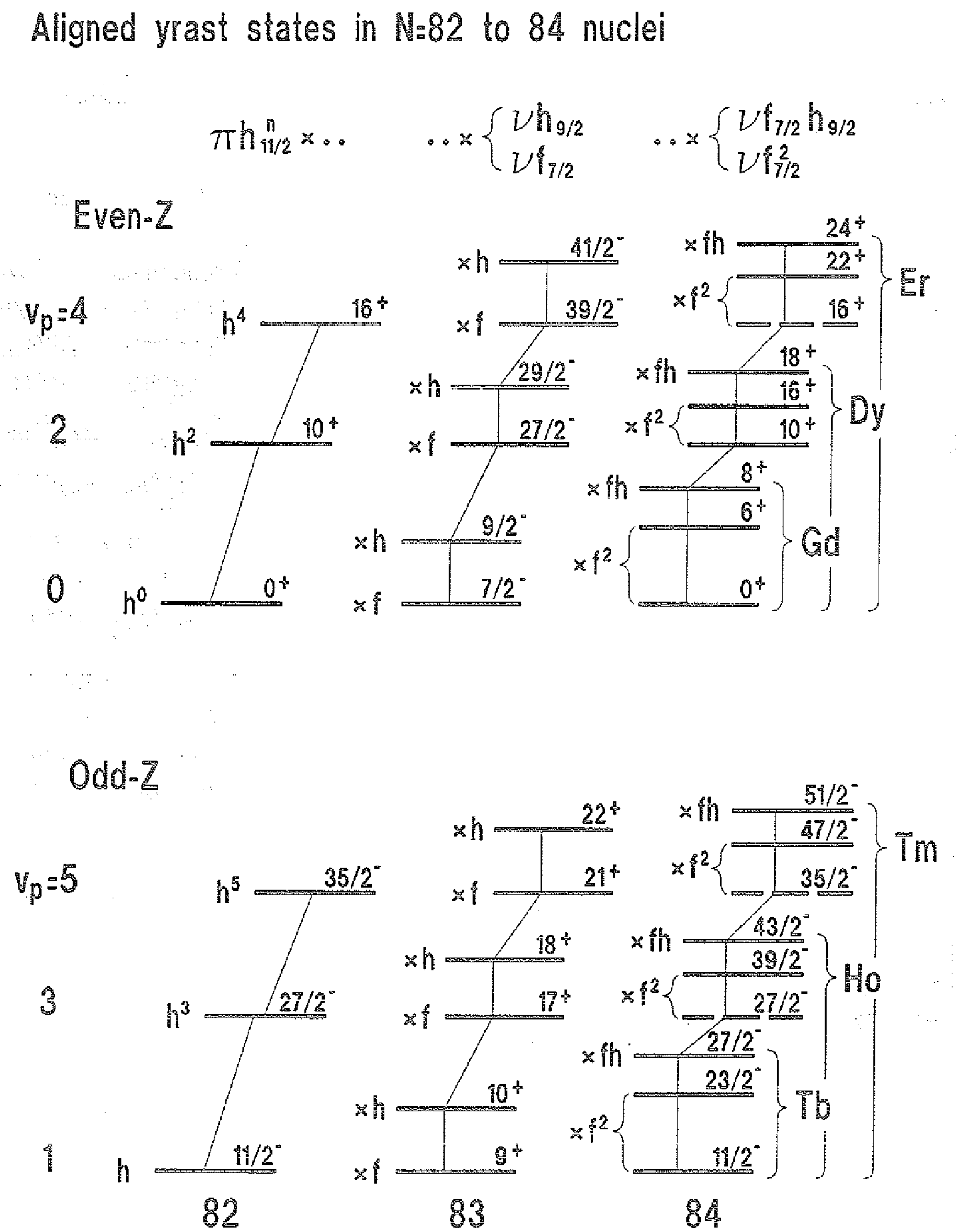

Fig. 1.2 Schematic yrast lines in N=82,83 and 84 nuclei above ^{146}Gd.

Table 1.1: Overview of the $\gamma\gamma$-coincidence experiments performed on Nordball and Osiris γ-spectrometers

Date	Place	Beam energy	Reaction used
June,1990	Osiris,HMI*	255 MeV	$^{106}Cd(^{54}Fe,\alpha 3p)^{153}Tm_{84}$ $^{106}Cd(^{54}Fe,\alpha 2p)^{154}Yb_{84}$ $^{106}Cd(^{54}Fe,3pn)^{156}Lu_{85}$ $^{106}Cd(^{54}Fe,2pn)^{157}Hf_{85}$ $^{106}Cd(^{54}Fe,\ 3p)^{157}Lu_{86}$
Jan., 1993	Nordball,NBI	145 MeV	$^{127}I(^{29}Si,\ 5n)^{151}Ho_{84}$
Jan., 1993	Nordball,NBI	174 MeV	$^{122}Te(^{35}Cl,\alpha 2n)^{151}Ho_{84}$ $^{122}Te(^{35}Cl,\ 4n)^{153}Tm_{84}$ $^{122}Te(^{35}Cl,p4n)^{152}Er_{84}$
April,1993	Osiris,HMI	270 MeV	$^{102}Pd(^{58}Ni,\alpha 3p)^{153}Tm_{84}$ $^{102}Pd(^{58}Ni,\alpha 2p)^{154}Yb_{84}$ $^{102}Pd(^{58}Ni,3pn)^{156}Lu_{85}$ $^{102}Pd(^{58}Ni,2pn)^{157}Hf_{85}$ $^{102}Pd(^{58}Ni,\ 3p)^{157}Lu_{86}$
May, 1993	Nordball,NBI	140 MeV	$^{130}Ba(^{28}Si,p4n)^{153}Tm_{84}$ $^{130}Ba(^{28}Si,\ 4n)^{154}Yb_{84}$

*: Combined with neutron detector
HMI: Hahn-Meitner-Institut, Berlin
NBI: Niels Bohr Institutet, København

thesis is to investigate further these specific multi-particle yrast lines at N=84, if possible extend them to their maximum spin and identify them in the so far largely unknown nuclei ^{153}Tm and ^{154}Yb.

For this purpose we have carried out in-beam γ-spectroscopic measurements using the Compton-suppressed multi-dectector arrays Osiris and Nordball, which allowed us to identify and characterize γ-transitions down to 1% of the formation cross-section of the respective nucleus. For the very neutron deficient ^{154}Yb and ^{153}Tm nuclei the exit channel cross-section was below 10% of the fusion cross-section for forming the compound nucleus. A list of the different experiments including the compound-evaporation reactions investigated is given in Table 1.1. The data from these measurements allowed us to establish the high-spin states in the N=84 isotones ^{151}Ho, ^{152}Er, ^{153}Tm, and ^{154}Yb up to 10 MeV excitation and about 25$\hbar$ angular momentum.

During the past years the empirical two-body residual interactions have been determined in a number of studies for the πh, νh, and νf nucleons through identification of the respective two-nucleon multiplets in the two-valenceparticle nuclei of ^{146}Gd. We have used this knowledge and carried out multi-particle shell model calculations for the $\pi h^n \nu f^2$ and $\pi h^n \nu f h$ configurations. These results are in excellent agreement with experiment and could trace the yrast states of these two configurations up to their highest spins.

These quantitative calculations reveal important deviations from the principle yrast line structure as shown in Fig. 1.2, which are caused by the proton-neutron residual interaction and are related to the unusually strong attraction of the $\pi h_{11/2} \nu h_{9/2}$ GT-partners in the 1^+ coupling. This interaction is selectively activated in specific proton angular momentum couplings that lie above the yrast line. With the addition of an $h_{9/2}$ neutron these complex states are significantly lowered in energy and become yrast states. This effect has been observed systematically at the predicted spins and energies in the four N=84 nuclei, and violates the regular increase of proton seniority along the yrast line as apparent from Fig. 1.2.

2 Experiments and Data Analysis

In in-beam nuclear structure research using γ-ray spectroscopy the high-spin states in the nucleus are often populated after particle evaporation from statistically equilibrated compound nuclei formed at high angular momentum in HI-induced fusion reactions. Naturally, the γ-radiation associated with such reactions is of tremendous complexity. After evaporation of the last particle the residual nucleus decays through thousands of competitive de-excitation pathways down to the yrast line. The associated numerous and weak statistical γ-rays are not resolved and form a continuum background in the γ-ray spectrum. Moreover, in a typical reaction about five to fifteen different nuclei are formed with sizable cross-section through evaporation of different number and kinds of particles. In addition, an appreciable portion of the total reaction cross-section leads to deep-inelastic, fusion-fission, or other binary reactions which all are associated with γ-emission. Thus, the γ-rays emitted from the target typically originate from 10–100 different nuclides, many of them formed with cross-sections within one tenth of the strongest final products.

Typical in-beam γ-ray experiments require the detection and characterization of γ-rays of an intensity down to 1% of the formation cross-section of the nuclide under study. Under the adverse conditions described above, and having in mind that the formation cross-section is often well below 10% of the reaction cross-section, it is clear that γ-ray spectrometers suitable for in-beam measurements must meet extreme demands in resolving power and detection sensitivity.

The presently used multidetector spectrometers consisting of many Compton-superessed Ge-detectors, and often combined with charged particle- or neutron detectors, were developed during the past 10 years to meet these severe demands. The results presented in this thesis were obtained with two such multidetector arrays, the Osiris spectrometer at the VICKSI cyclotron of the Hahn-Meitner Institute in Berlin, and the Nordball spectrometer at the Tandem accelerator of the Niels Bohr

Institute. In this chapter the two instruments, and special conditions during our experiments, will be briefly described and the methods of the data analysis will be presented.

2.1 The Osiris γ-spectrometer

The Osiris multidetector array [Lie 84] consists of 12 germanium detectors surrounded by 12 BGO-Anti–Compton–Shields. They are placed in two cones with 150° opening angle. In standard experiments the Osiris ring is oriented in the beam direction, such that the detectors cover the angular range between + 25° and + 155° to the beam direction.

In our first experiment, with ^{54}Fe on ^{106}Cd, a large four-sector neutron detector at 0° was used for identification of previously unknown fusion-evaporation exit channels, which required to orient the Osiris ring perpendicular to the beam direction, as shown in Fig. 2.1. In this geometry it is however not possible to measure the γ-ray angular distributions since all detectors have now the same angle of ± 25° relative to the alignment plane of the compound nuclei perpendicular to the beam direction.

A second experiment was therefore carried out, with the detectors mounted in a different support frame where they are placed in three cones at 61°, 101°, and 149° to the beam direction, with 4 detectors at each angle. In this experiment the same ^{160}W compound nucleus was formed with ^{58}Ni beam on ^{102}Pd, but at slightly lower excitation energy in order to enhance production of the $^{157}Hf_{85}$ nucleus which is the topic of a seperate thesis made in the group [Saa 93] and was only weakly populated in the first Osiris experiment.

We mention that in the first experiment one of the shields contained a high-resolution planar Ge-detector for resolving the K_α X–rays to provide Z-identification of exit channels. In the second experiment 12 coaxial detectors were used.

The Memphis 2000 system was employed for data acquisition. A coincidence event was defined by the occurrence of fast pulses from at least two Compton-suppressed

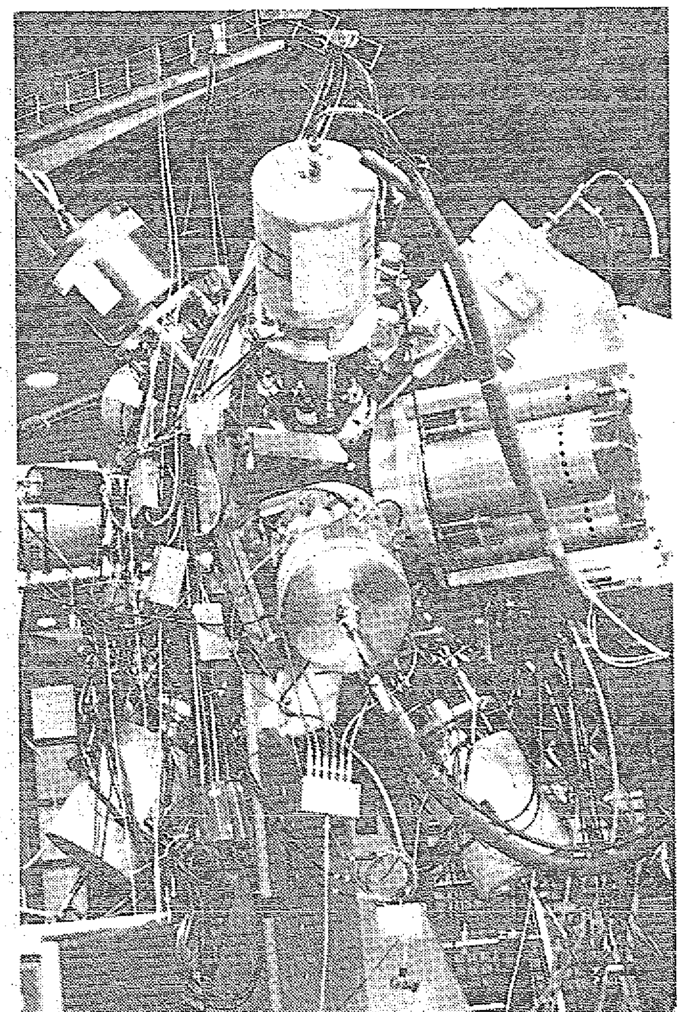

Fig. 2.1 The Osiris γ-spectrometer.

Ge-signals within a 300ns time interval after the beam pulse. For each event, the γ-ray energy and the arrival time relative to the beam pulse for the coincident detectors were written on tape.

2.2 The Nordball γ-spectrometer

The Nordball spectrometer [Her 86, Sle 89] combines 20 Compton-suppressed Ge-detectors with a 4π inner-ball 60 unit-BaF_2 multiplicity filter, as shown in Fig. 2.2. The spherical Nordball support frame was constructed to have 20 hexagons and 12 pentagons. Every hexagon accepts a BGO-shielded Ge-detector unit, while each of ten pentagons supports 6 elements of BaF_2 multiplicity filter, and the remaining two are used for beam line and Faraday cup. In this geometry the 20 Ge-detectors are positioned on four cones viewing the target under 37° and 79° in the forward and backward direction relative to the beam axis.

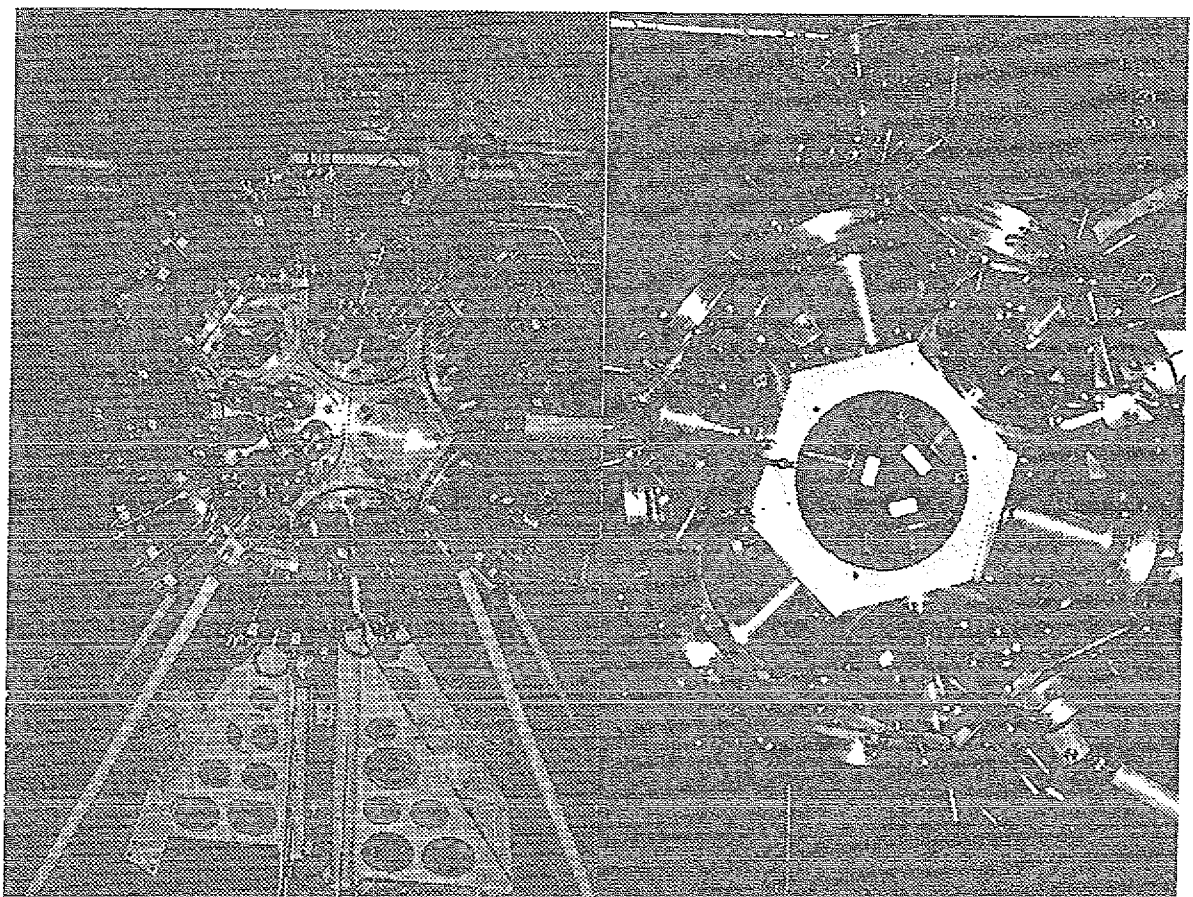

Fig. 2.2 The Nordball γ-spectrometer and its supporting frame.

The heavy ion beams from the Tandem accelerator are essentially DC beams, and therefore the reaction time is defined by the first signal from the BaF_2 multiplicity ball. A coincidence between at least two Ge-detectors within 100ns after the BaF_2 signal establishes an accepted event. For each coincident Ge-detector the γ-ray energy and the time difference from the first BaF_2 signal are written on tape.

Three reactions were performed at Nordball (Table 1.1). In all measurements one coaxial detector was replaced by a planar detector. During two of the measurements, with ^{29}Si and ^{35}Cl beams, one coaxial detector deteriorated badly and was therefore rejected in the data analysis.

2.3 Standard $\gamma\gamma$-coincidence matrices

The $\gamma\gamma$-coincidence matrices were utilized to construct the nuclear level scheme. The on-line coincidence data were stored event-by-event in multi-parameter format on exabyte tape. After the experiments these list-mode data were conventionally sorted into two-dimensional Energy(γ)–Energy(γ) matrices with specifically chosen time windows on the $t_{\gamma RF}$ parameter specifying the time between the nuclear reaction and the individual γ-ray. As mentioned, in the Osiris experiments the reaction time was defined by the radio frequency of the cyclotron, while the first γ-signal from the BaF_2 multiplicity ball was used in Nordball. In the standard prompt coincidence matrix the time window was defined as 0 to 80ns (Osiris) or 0 to 100ns (Nordball) after the reaction. Naturally, for further coincidence analysis these matrices were symmetrized, such that gates on one axis included the complete coincidence statistics.

An exception were the planar-coaxial coincidences, and matrices with non-identical timing conditions for the two coincident detectors prepared for locating isomeric states in the yrast decay. In the data discussed here such delayed-prompt matrices were prepared with the condition that the second γ-ray arrives delayed, in general chosen in an interval from 30 to 300ns after the first γ-ray which is emitted in the reaction. Finally, for determination of ns-half-lifes $E_{\gamma_1}-t_{\gamma_1 RF}$ and $E_{\gamma_1}-t_{\gamma_1\gamma_2}$ matrices were prepared, where gate setting on the E_{γ_2} parameter selected the yrast decay of the specific exit channel.

As generally in HI-induced in beam experiments, with their prohibitively rich singles spectra, the γ-ray energies and intensities were extracted from coincidence data using the standard symmetrized prompt matrix. The energy- and efficiency calibrations were measured with standard radioactive sources of ^{152}Eu, ^{133}Ba and ^{56}Co. The quoted γ-ray energy errors are related to the deviation found in the energy-shifted spectra from the standard source energies (at most 0.13 keV up to E_{γ}=1.6 MeV), or for weak lines to spectral complexity or to counting statistics.

2.4 $\gamma\gamma$-n coincidence

The large volume four-sector neutron detector at Osiris, combined with the planar X–ray detector was vital for identification of the largely unknown fusion-evaporation products from the $^{160}W_{86}$ compound nucleus, formed at 57 MeV excitation in the ^{54}Fe+ ^{106}Cd reaction. The neutrons were separated from the γ's by pulse shape analysis exploting the different rise-times of their respective signals. The neutron signals were converted into logical bits giving the number of neutrons detected. This information was written on tape for each coincidence event. In the measurement we obtained 0.6 million γ-γ-n out of totally 47 million coincidence events which is not sufficient to prepare a matrix with satisfactory statistics. Only the one dimensional $\gamma\gamma$-coincidence projection originating from those events was therefore sorted; an example is shown in Fig. 2.4.1.

For the very neutron-deficient ^{160}W compound nucleus at 57 MeV excitation charged particle evaporation of three protons, four protons, and three protons together with one neutron were predicted to be dominant exit channels in CASCADE calculations. Since also α-particles are emitted one expects strong population of four different elements, namely Hf, Lu; and Yb following proton evaporation, and Yb and Tm when also an α particle is evaporated (see Fig. 2.4.2). The coincidence data readily identified families of γ-rays belonging to an individual exit channel. The

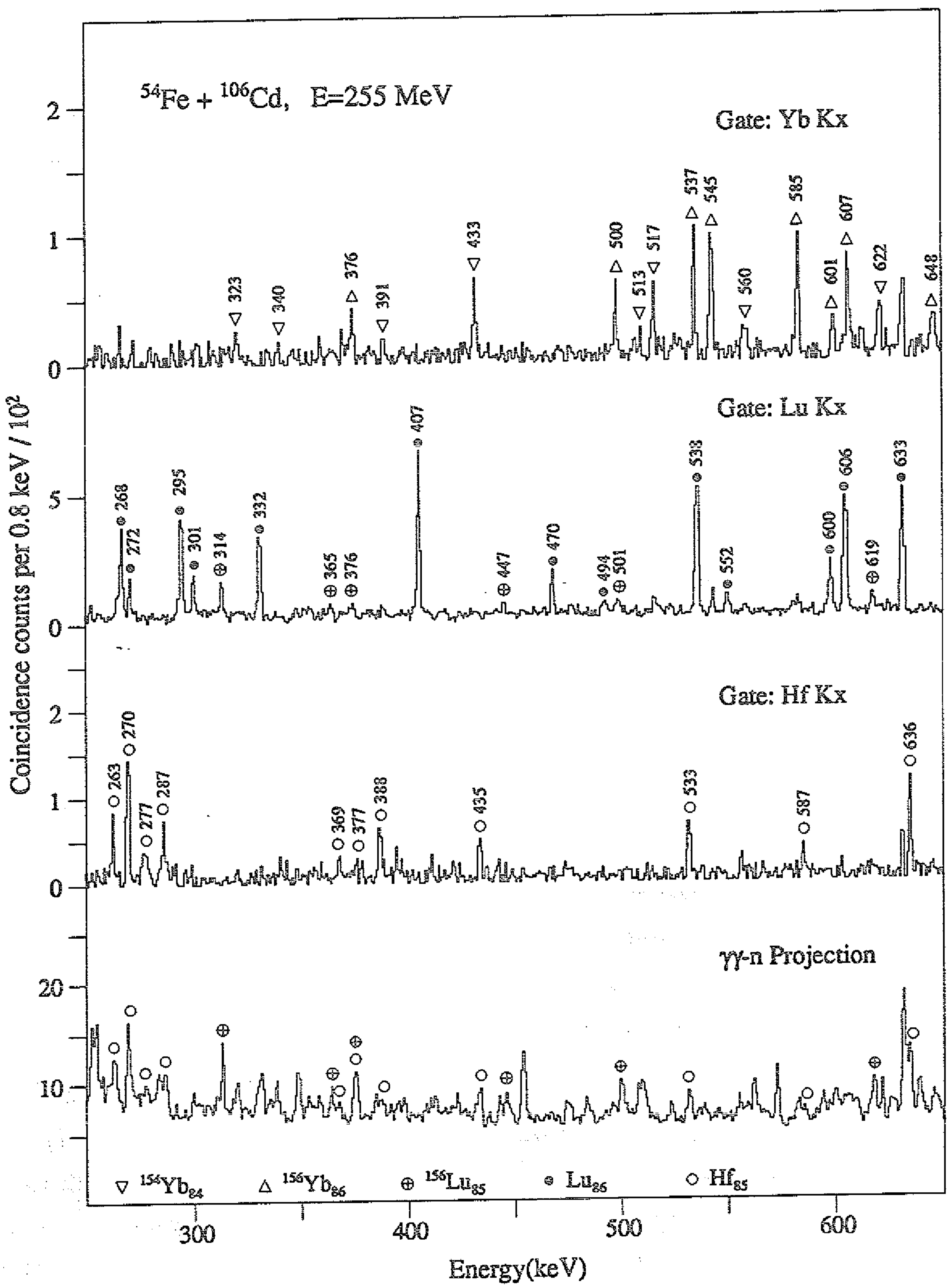

Fig. 2.4.1 Gamma-ray spectra observed in coincidence with the Kα X-rays of Yb, Lu and Hf, and with neutrons.

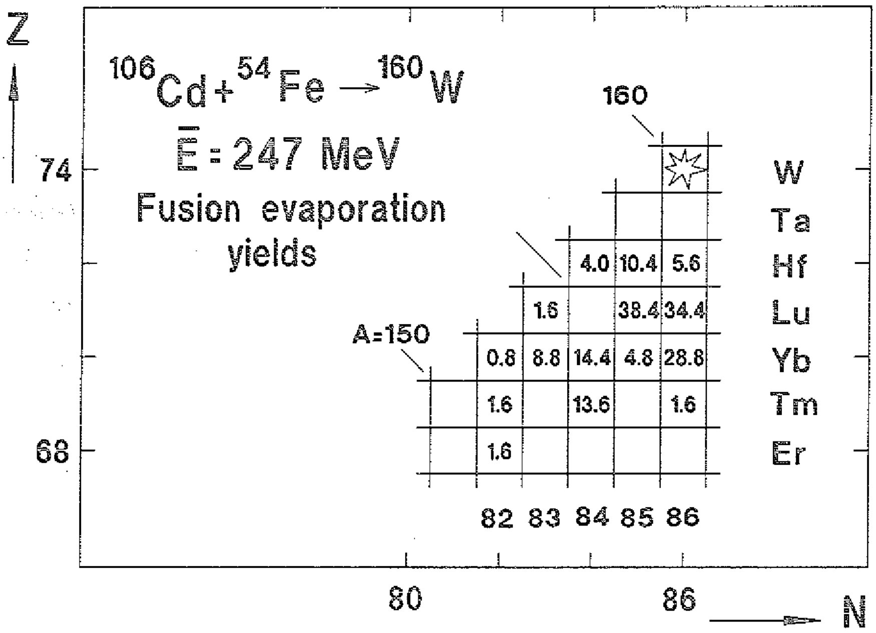

Fig. 2.4.2 Cross-sections for identified fusion-evaporation exit-channels observed with 255 MeV ^{54}Fe ions on ^{106}Cd. The yields are given in mb.

planar detector resolved the characteristic K_α X–rays of neighbouring elements and thus the γ-ray coincidences with the planar detector could be used for elemental assignment for the separate families (Fig. 2.4.1). Finally, the neutron coincidences gave the isotopic assignment. From Fig. 2.4.1 it is apparent that neutrons are observed for the N=85 exit channels. The N=84 exit channels are dominantly reached through α-particle evaporation; N=83 exit channels were too weak to be investigated (Fig. 2.4.2). The spectra in the figure demonstrate the separation of $^{156}Lu_{85}$ and $^{157}Lu_{86}$ by means of the neutron-$\gamma\gamma$ coincidences. The high-spin level schemes of these nuclei, and of $^{157}Hf_{85}$ have been established and will be reported [Zhal 93, Saa 93] elsewhere.

2.5 Angular distributions from coincidence data

The initial spin direction of a statistically equilibrated compound nucleus formed at high angular momuntum in a fusion reaction is aligned in the plane perpendicular to the beam direction. The nucleus decays subsequently by particle evaporation to a stage, where the nuclear excitation above the yrast line is below the particle binding energy. From here, further cooling down to the yrast line occurs by emission of the 'statistical γ-rays', which are followed by the yrast γ-ray cascade down to the nuclear ground state.The evaporation of a few particles carries away only a small amount of angular momentum and gives rise to little change of the direction of the nuclear spin. The alignment may decrease slightly during the emission of non-stretched statistical γ-rays, but it is still possible to measure the anisotropies of γ-transitions coming from the lower excitation levels along the yrast line, where stretched transitions dominate.

The method of singles angular distribution measurements has been successfully applied in in-beam γ-ray experiments for many years [Fer 65]. The angular distribution function is given as

$$W(E_\gamma(\vartheta)) = 1 + A_2 P_2(\cos\vartheta) + A_4 P_4(\cos\vartheta), \qquad 2.5.1$$

where A_2, A_4 are the angular distribution coefficients specifying the multipole order.

As we mentioned above, the γ-ray spectra following H.I. induced fusion-evaporation reaction are prohibitively complex, such that useful angular distribution data in general cannot be obtained from in-beam singles spectra. In comparison, the use of coincidence data introduces significant advantages;

(◦) The γ-lines are better separated and the background is smeared out in the two dimensions.

(◦) Even if a peak is contaminated in the singles spectrum, there are usually several coincidence gates in which it is not.

(∘) Weak transitions, which disappear in the background of the γ-singles spectrum, can be analysed in a coincidence spectrum.

Rather than A_2 and A_4 values, the coincidence data give the Directional Correlations of γ-rays deexciting Oriented states (DCO ratio), which allow to determine the multipole order. But in contrast to singles angular distribution data, the results extracted from coincidence measurements will also contain contributions originating from the angular correlation between γ-rays, which do not affect singles angular distribution data. The corresponding theory is well developed and was discussed by Steffen and Alder, and by Krane et al. [Ste 75, Kra 73].

The coincidence intensity W of the transition $E_{\gamma 1}$, measured in detectors at the angle ϑ_1, gated with the coincident transition $E_{\gamma 2}$ in detectors at the angle ϑ_2, is denoted by $W(E_{\gamma 1}(\vartheta_1), E_{\gamma 2}(\vartheta_2))$. Similarly, the intensity of the transition $E_{\gamma 1}$, measured in detectors at the angle ϑ_2, gated with the coincident transition $E_{\gamma 2}$ in detectors at the angle ϑ_1, is denoted by $W(E_{\gamma 1}(\vartheta_2), E_{\gamma 2}(\vartheta_1))$. The DCO-ratio for the transition $E_{\gamma 1}$ is defined as the intensity $W(E_{\gamma 1}(\vartheta_1), E_{\gamma 2}(\vartheta_2))$, divided by the intensity $W(E_{\gamma 1}(\vartheta_2), E_{\gamma 2}(\vartheta_1))$;

$$DCO(E_{\gamma 1}) = \frac{W(E_{\gamma 1}(\vartheta_1), E_{\gamma 2}(\vartheta_2))}{W(E_{\gamma 1}(\vartheta_2), E_{\gamma 2}(\vartheta_1))} , \qquad 2.5.2$$

where the index 2 denotes the gating transition. There are, however, limitations in the DCO method. Since the DCO ratio contains also the angular correlation between the two coincident γ-transitions, only transitions with known multipolarity, e.g. of stretched quadrupole type can be used for gating. This gives rise to problems in the spherical nuclei, where extensive sequences of stretched E2 transitions do not exist.

It therefore was desirable to find [Dri 90] a new definition of the DCO ratio such that the contribution to the intensities of the coincident γ-rays originating from the angular correlation (between gating and displayed γ-transition) would cancel, but the contribution from the angular distribution originating exclusively from the alignment due to the reaction geometry would prevail. This is trivially fulfilled if the gating detector would cover 4π solid angle. But the above condition can also be met even with a limited number of observation angles if the nuclear initial spin is sharply defined in the reaction plane.

The intensity of a coincidence peak between two transitions of $E_{\gamma 1}$ and $E_{\gamma 2}$ at different polar angles ϑ_1 and ϑ_2, as defined in Eq. 2.5.2, can be calculated from the singles γ-angular distribution function as

$$W(E_{\gamma 1}(\vartheta_1), E_{\gamma 2}(\vartheta_2)) = W(E_{\gamma 1}(\vartheta_1)) \cdot W(E_{\gamma 2}(\vartheta_2)), \qquad 2.5.3$$

and

$$W(E_{\gamma 1}(\vartheta_2), E_{\gamma 2}(\vartheta_1)) = W(E_{\gamma 1}(\vartheta_2)) \cdot W(E_{\gamma 2}(\vartheta_1)). \qquad 2.5.4$$

Similarly, the intensity of a coincidence peak between two γ-rays of $E_{\gamma 1}$ and $E_{\gamma 2}$, detected at the same angles ϑ_1 or ϑ_2 can be expressed as

$$W(E_{\gamma 1}(\vartheta_1), E_{\gamma 2}(\vartheta_1)) = W(E_{\gamma 1}(\vartheta_1)) \cdot W(E_{\gamma 2}(\vartheta_1)), \qquad 2.5.5$$

and

$$W(E_{\gamma 1}(\vartheta_2), E_{\gamma 2}(\vartheta_2)) = W(E_{\gamma 1}(\vartheta_2)) \cdot W(E_{\gamma 2}(\vartheta_2)). \qquad 2.5.6$$

The ADO ratio (Angular Distributions of γ-rays deexciting Oriented states) is defined as

$$ADO = \frac{W(E_{\gamma 1}(\vartheta_1), E_{\gamma 2}(\vartheta_1)) + W(E_{\gamma 1}(\vartheta_1), E_{\gamma 2}(\vartheta_2))}{W(E_{\gamma 1}(\vartheta_2), E_{\gamma 2}(\vartheta_1)) + W(E_{\gamma 1}(\vartheta_2), E_{\gamma 2}(\vartheta_2))}. \qquad 2.5.7$$

With the equations 2.5.3, 2.5.4, 2.5.5 and 2.5.6, one obtains

$$ADO = \frac{W(E_{\gamma 1}(\vartheta_1))}{W(E_{\gamma 1}(\vartheta_2))} = \frac{1 + A_2 P_2(\cos\vartheta_1) + A_4 P_4(\cos\vartheta_1)}{1 + A_2 P_2(\cos\vartheta_2) + A_4 P_4(\cos\vartheta_2)} . \qquad 2.5.8$$

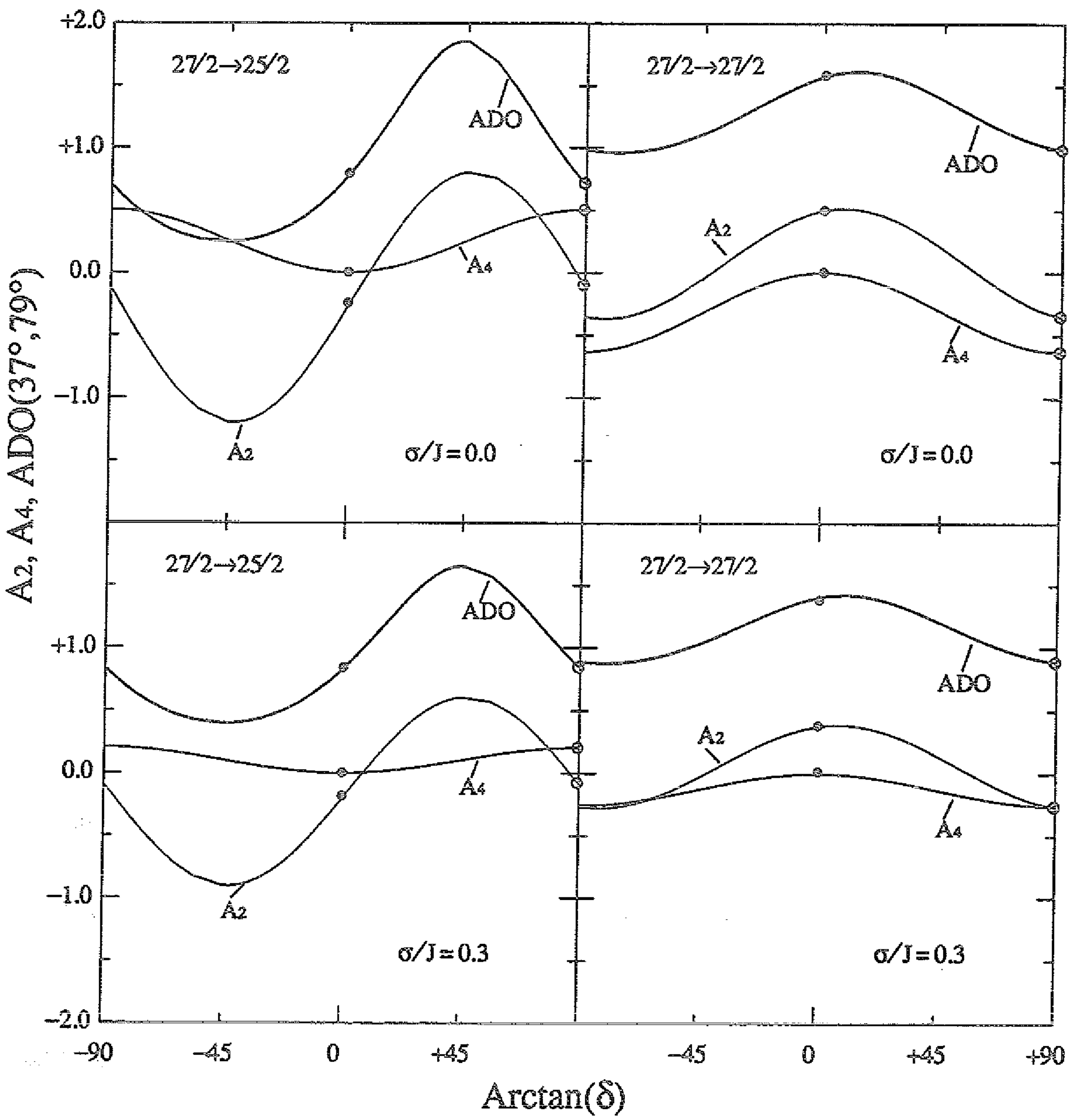

Fig. 2.5.1 The A_2 and A_4 coefficients, and the ADO ratios for the Nordball geometry, calculated for complete ($\sigma/J=0$) and partial ($\sigma/J=0.3$) alignment of dipole/quadrupole mixed radiation with mixing ratio δ. Results are shown for $\Delta I=0$ and $\Delta I=1$ transitions with $I_i=27/2$. The values for pure dipole radiation (dots) and for pure quadrupole (bubbles) are marked.

There is an obvious advantage with the ADO definition. Since it is related only to the angular distribution of the transition of interest, several clean coincidence gates can be summed up to improve the counting statistics, where the multipolarity of the gating transition needs not to be of only stretched type.

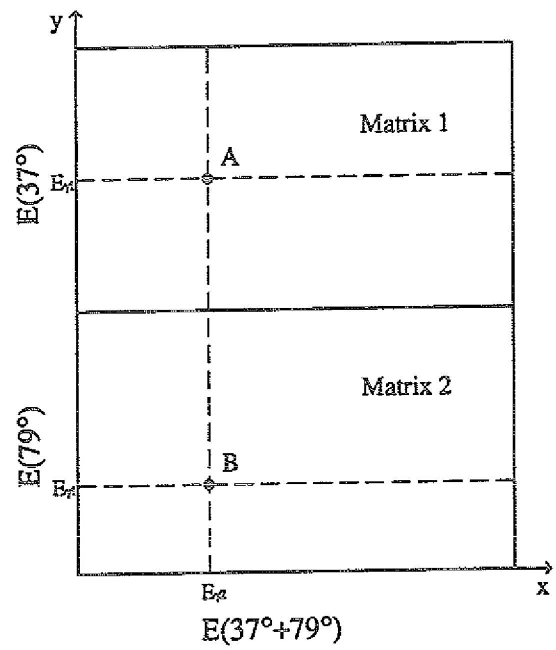

Fig. 2.5.2 Schematic display of coincidence matrices prepared for analysis of ADO ratios.

The dependence of the ADO value measured with the Nordball geometry on the mixing ratio δ for a $27/2 \longrightarrow 27/2$ or $27/2 \longrightarrow 25/2$ dipole/quadrupole mixed transition is plotted in Fig. 2.5.1, where also the A_2 and A_4 angular distribution coefficients are included. The figure shows the well-known fact that the ADO-ratios for dipole-quadrupole mixed transitions may often not be conclusive for spin assignments if independent information on the mixing ratio δ does not exist. The typical ADO values for stretched dipole and quadrupole transitions emitted from fully aligned nuclei (σ/J=0.0) are 0.7 and 1.4; rather insensitive to the initial spin.

Two $E\gamma$–$E\gamma$ matrices were produced for ADO determinations, as shown in Fig. 2.5.2 . The γ-rays measured by the detectors at 37 and 79 degree rings were projected along the display axis in matrix number 1 and number 2, while their coincidence partners were projected along the gate axis. When the $\gamma\gamma$-coincidence events were detected at the same detector ring, they were counted twice in both directions. The experimental ADO ratio is defined as the ratio of the integrated area of coincidence peak A, divided by the area of coincidence peak B, both corrected for detector efficiency;

$$ADO = \frac{\text{Area}(A)}{\text{Area}(B)} \times \frac{\text{Eff.}(79^\circ)}{\text{Eff.}(37^\circ)}. \qquad 2.5.9$$

Also in this case, the efficiency curves for the respective detector rings were obtain-

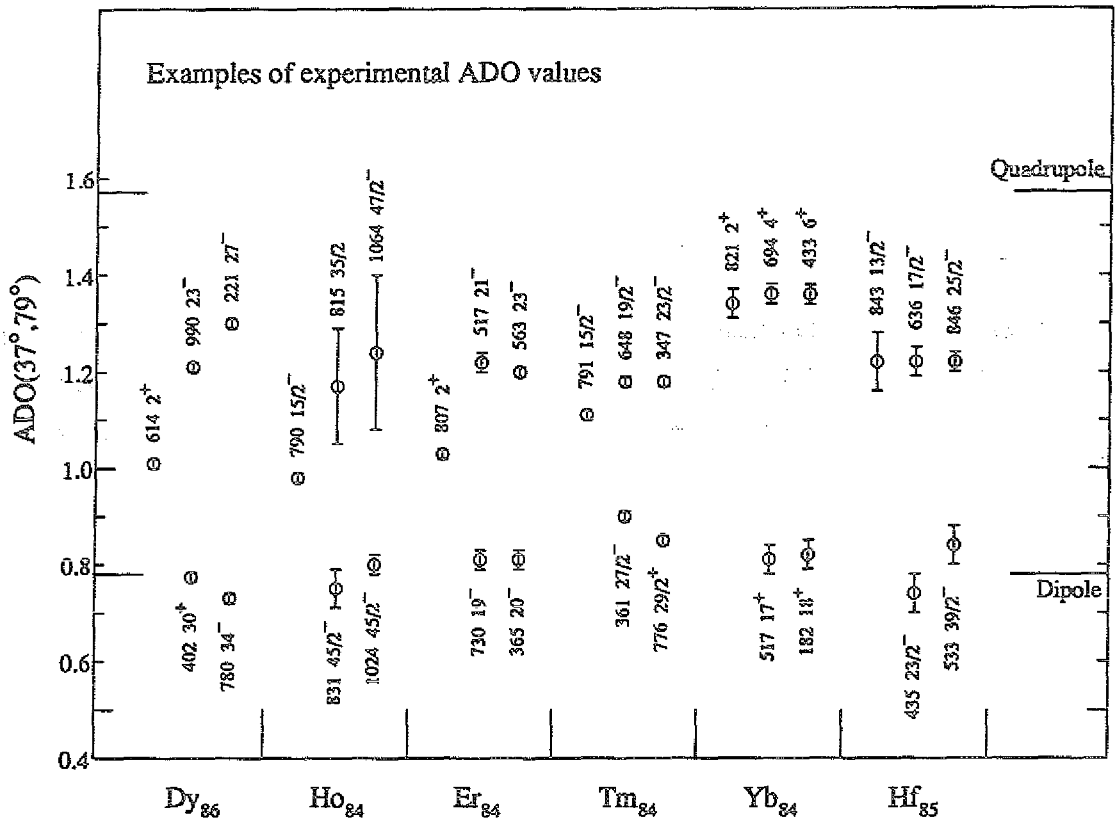

Fig. 2.5.3 ADO-ratios of stretched transitions measured in the present experiments in rare earth nuclei above Tb, which all have ns-isomers in their yrast cascades. Transition energy in keV and initial spin are specified for each point. Unattenuated theoretical ADO values for stretched quadrupole and stretched dipole transitions (for I_i=27/2) are shown to the right. The largest difference of ADO ratio between quadrupole and dipole transitions are found for Yb, where the 4f atomic shell is completed. In all cases the ADO-value for the lowest E2 yrast transition is included. In Dy, Ho, and Er it is found to be fully attenuated; the other transitions shown for these nuclei lie above the isomer or are essentially fed promptly.

ed from calibrations using ^{152}Eu, ^{130}Ba and ^{57}Co standard sources placed precisely in the target position.

Examples of measured ADO ratios for streched γ-transitions of different nuclei are plotted in Fig. 2.5.3. The data clearly distinct dipole and quadrupole radiations. All points lie clearly inside the maximun values for pure dipole and quadrupole transitions, which is related to the partial alignment in the respective initial states. Values measured close to 1.0 as the low-lying intense transitions in Dy, Ho and Er indicate completely destroyed alignment caused by hyperfine interaction during isomeric decays.

3 Level Schemes

In this chapter the results obtained from the experiments at the Nordball and Osiris spectrometers listed in Table 1.1 will be discussed in separate sections for each of the four N=84 nuclei investigated. The level schemes will be presented, and we will discuss the assignments of level spins and parities, and the properties of the nano-second-isomers identified in ^{151}Ho and ^{154}Yb.

3.1 The nucleus $^{151}_{67}Ho_{84}$

The $^{151}Ho_{84}$ nuclide has two low-lying isomers which both decay by α-emission and β-decay. From their $\Delta l=0$ α-decays to the ^{147}Tb single proton nucleus [Lia 87] the isomers are known to be $\pi h_{11/2}$ and $\pi s_{1/2}$, with the $T_{1/2}$=35s $11/2^-$ activity at 0 keV and the 47s metastable $1/2^+$ state at 41keV excitation energy. The $\pi h_{11/2}$ nature of the ground state is independently established [Tot 79] from its fast Gamow-Teller decay (log ft≈4.4) to the 527keV $\nu h_{9/2}$ excitation in $^{151}Dy_{85}$. Similar as in the case of ^{149}Dy [Mec 89], the ^{151}Er ground state β-decay also proceeds to both ^{151}Ho isomers. These decay data [Bar 88] have established in ^{151}Ho above the $s_{1/2}$ metastable state the $d_{3/2}$, $d_{5/2}$, and $g_{7/2}$ single proton states, and a few yet uninterpreted excitations decaying to the $\pi h_{11/2}$ ground state.

Only one in beam-study of ^{151}Ho has so far been reported, carried out by Gizon et al. in 1981 [Giz 81]. They produced ^{151}Ho with ^{16}O and ^{12}C beams on self-supporting metallic targets of ^{141}Pr and ^{144}Sm and recorded $\gamma\gamma$-coincidences with two 15% efficiency coaxial Ge(Li)-detectors. In addition they measured γ-ray angular distributions and linear polarizations for the ^{151}Ho transitions. These results established ^{151}Ho levels up to 6.6 MeV and suggested firm I^π values up to $49/2^-$ at 6.18 MeV, where the levels up to $43/2^-$ at 4.81 MeV are established by the prominent yrast decay cascade of nine intense stretched γ-transitions. For the other levels below that energy only tentative I^{π} assignments could be specified. These authors also noticed several ns-isomers in the yrast cascade which are of crucial significance for the measurement of γ-angular distributions as we will discuss below.

In our present experiments carried out with the Nordball γ-ray detector we populated the ^{151}Ho levels with the ^{127}J(^{29}Si,5n) reaction at 145 MeV beam energy. Due to the low melting point of iodine, the target was prepared as a 3mg/cm^2 layer of ^{nat}PbJ_2 iodide evaporated on an 8mg/cm^2 ^{208}Pb backing to stop the recoiling compound nuclei. In the Nordball coincidence experiment the beam current was ~3.6 · 10^{10} particles /sec, chosen to give ~3 to 4·10^3/sec Compton-suppressed γ-singles rate in each of the 18 coaxial detectors, and ~1.6·10^3/sec in the planar detector. The total γγ-coincidence counting rate was about 1600/sec. A total of 65 million good coincidence events were collected in 16 hours effective beam time, which gave 0.68 million total coincidence counts in the full absorption peak of the 789.6 keV $15/2^- \longrightarrow 11/2^-$ ground state transition in ^{151}Ho.

In another Nordball experiment (Table 1.1) aimed to investigate ^{153}Tm with a ^{35}Cl beam on a ^{122}Te, the ^{151}Ho nucleus was also populated after α2n evaporation, but this exit channel was comparatively weak, such that the data were more strongly polluted. They gave no additional information on ^{151}Ho, but we used them to check the angular distributions measured for the intense yrast transitions.

The data from the ^{127}J+ ^{29}Si measurement are summarised in Table 3.1, and in the level scheme of Fig 3.1.1. It was built exploiting the extensive γγ-coincidence relationship from the coincidence matrix analysis. Examples are shown in Fig 3.1.2 and Fig 3.1.3. The Fig 3.1.2, giving the coincidences with the four lowest and most intense yrast γ- rays in the nucleus, identifies all observed ^{151}Ho transitions and gave the essential information for the transition energies and intensities of Table 3.1. For a few favourable low-energy transitions the α_{tot} values could be extracted from the γ-intensity balance. These results are listed in column 4 of Table 3.1 and compared with theoretical values in Fig 3.1.4.

From our coincidence data we could confirm the nine main-cascade yrast levels up

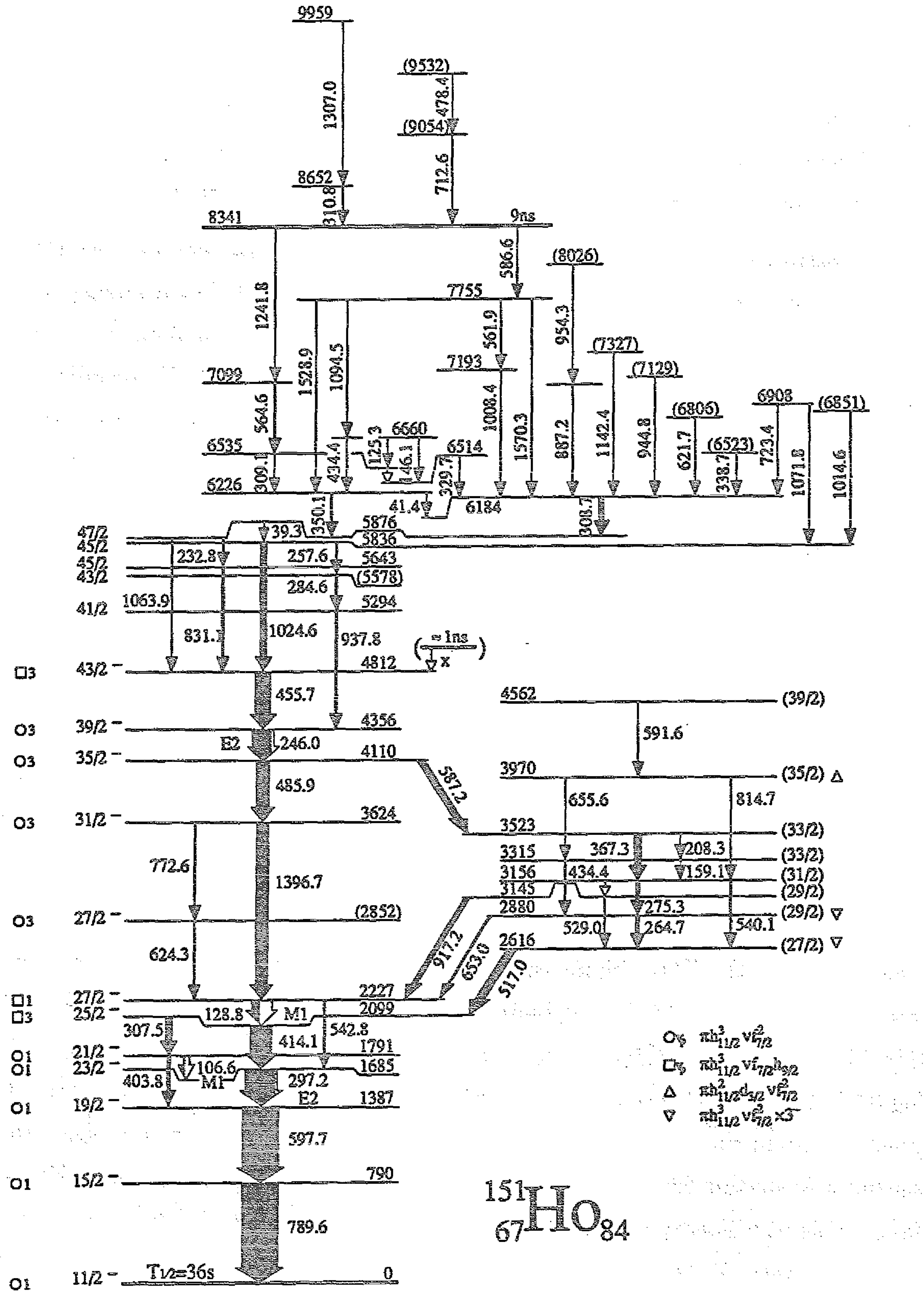

Fig. 3.1.1 The ^{151}Ho high-spin states observed in the ^{127}I(^{29}Si,5n) reaction. The widths of the arrows are proportional to the total- or γ-intensities. Multipolarities are labeled when obtained from conversion information. White arrows are drawn for unobserved low energy γ-rays inferred from coincidence data. The configuration assignments are discussed in Section 4.2 and Section 5. For the tentative 1 ns half-live, cf. discussion in the text.

Table 3.1: Gamma-transitions in ^{151}Ho observed in the ^{127}I(^{29}Si,5n) reaction at 145 MeV performed on Nordball

E_γ^a (keV)	Rel. γ-ray[b] Intensity	ADO[c] ratio	α_{tot}^d	Multi-polarity[e]	Placement E_i(keV)	$I_i^\pi \rightarrow I_f^\pi$
11.0(2)[f]					3155.6	(31/2)→(29/2)
20.8(2)[f]					6534.8	
39.3(2)[g]	w				5875.6	$47/2^- \rightarrow 45/2^-$
41.4(2)[g]	w				6225.7	
106.6(1)	42(4)	1.08(9)	3.3(3)	M1	1791.1	$21/2^- \rightarrow 23/2^-$
125.3(1)	12(2)	1.5(4)			6660.1	
128.8(1)	235(5)	1.09(2)	1.39(4)	M1	2227.4	$27/2^- \rightarrow 25/2^-$
146.1(2)	2(1)				6660.1	
159.1(1)	17(2)	1.16(15)			3314.7	(33/2)→(31/2)
208.3(1)	19(2)	1.00(12)			3522.9	(33/2)→(33/2)
211.7(1)	11(2)					
232.8(1)	35(2)	0.84(5)			5875.6	$47/2^- \rightarrow 45/2^-$
246.0(1)	524(12)	1.03(2)	0.13(2)	E2	4356.0	$39/2^- \rightarrow 35/2^-$
257.6(1)	49(3)	0.86(4)			5836.0	$45/2^- \rightarrow 43/2$
264.7(1)	108(4)	0.89(3)	0.17(3)	M1	2880.3	(29/2)→(27/2)
275.3(1)	106(4)	0.95(3)	0.03(3)	E1	3155.6	(31/2)→(29/2)
284.6(1)	51(3)	0.80(4)			(5578.4)	43/2 →41/2
294.6(1)	22(2)					
297.2(1)	823(17)	1.01(1)	0.056(8)	E2	1684.5	$23/2^- \rightarrow 19/2^-$
307.5(2)	192(11)	1.14(3)			2098.6	$25/2^- \rightarrow 21/2^-$
308.7(3)	151(11)				6184.3	
309.1(3)	25(6)				6534.8	
310.8(2)	31(4)	0.81(10)			8652.0	
329.7(1)	16(2)	0.84(9)			6514.0	
338.7(1)	14(2)				(6523.0)	
350.1(1)	42(2)	0.99(5)			6225.7	
367.3(1)	194(6)	0.91(2)	0.08(2)	M1	3522.9	(33/2)→(31/2)
403.8(1)	94(4)	0.91(4)			1791.1	$21/2^- \rightarrow 19/2^-$
414.1(1)	594(12)	0.89(1)			2098.6	$25/2^- \rightarrow 23/2^-$
434.4(2)	36(4)	0.90(6)			3314.7	(31/2)→(29/2)
434.4(2)	21(3)				6660.1	
451.4(1)	18(2)					
455.7(1)	438(8)	1.06(1)			4811.7	$43/2^- \rightarrow 39/2^-$
478.4(1)	23(2)	0.94(10)			(9532.2)	
485.9(1)	381(8)	0.99(2)			4110.0	$35/2^- \rightarrow 31/2^-$
517.0(1)	229(7)	0.90(2)			2615.6	$(27/2) \rightarrow 25/2^-$
529.0(1)	26(2)	1.26(13)			3144.6	(29/2)→(27/2)

to be continued

Table 3.1: continued

Eγ (keV)	Rel. γ-ray Intensity	ADO ratio	α_{tot}	Multi-polarity	Placement E(keV)	Placement $I_i^\pi \rightarrow I_f^\pi$
540.1(1)	55(5)	1.05(8)			3155.7	(31/2)→(27/2)
541.4(2)	11(2)					
542.8(2)	50(3)	0.95(5)			2227.4	$27/2^- \rightarrow 23/2^-$
561.9(2)	20(2)	1.4(3)			7754.6	
564.6(1)	53(3)	1.03(6)			7099.4	
586.6(3)	21(2)				8341.2	
587.2(2)	192(16)	0.98(2)			4110.0	$35/2^- \rightarrow (33/2)$
591.6(1)	25(2)	1.65(28)			4561.9	(39/2)→(35/2)
597.7(1)	1000(21)	1.00(1)			1387.3	$19/2^- \rightarrow 15/2^-$
621.7(2)	15(3)				(6806.0)	
624.3(1)	42(3)	0.92(6)			(2851.7)	$27/2^- \rightarrow 27/2^-$
653.0(1)	43(3)	0.74(6)			2880.3	$(29/2) \rightarrow 27/2^-$
655.6(1)	15(2)	0.78(16)			3970.3	(35/2)→(33/2)
712.6(1)	26(2)	0.85(8)			(9053.8)	
723.4(1)	w				6908.1	
772.6(1)	41(3)	1.06(7)			3624.1	$31/2^- \rightarrow 27/2^-$
789.6(1)	1000(21)	0.98(1)			789.6	$15/2^- \rightarrow 11/2^-$
814.7(1)	31(2)	1.17(12)			3970.3	(35/2)→(31/2)
831.1(1)	62(3)	0.74(4)			5642.8	$45/2^- \rightarrow 43/2^-$
860.7(1)	12(2)					
887.2(1)	28(3)	0.81(7)			7071.5	
896.5(1)	13(2)					
917.2(1)	131(5)	0.85(3)			3144.6	$(29/2) \rightarrow 27/2^-$
937.8(1)	68(4)	0.77(4)			5293.8	$41/2 \rightarrow 39/2^-$
944.8(2)	13(2)	0.94(17)			(7129.1)	
954.3(2)	8(2)	0.98(27)			(8025.8)	
1008.4(1)	26(2)	1.48(17)			7192.7	
1014.6(1)	21(2)				(6850.9)	
1024.6(1)	177(6)	0.79(2)			5836.3	$45/2^- \rightarrow 43/2^-$
1063.9(2)	22(2)	1.24(16)			5875.6	$47/2^- \rightarrow 43/2^-$
1071.8(3)	16(3)	0.70(10)			6908.1	
1094.5(2)	23(2)	1.11(12)			7754.6	
1142.4(2)	11(2)				(7326.7)	
1241.8(1)	24(2)	1.01(12)			8341.2	
1307.0(2)	10(2)	0.87(22)			9959.0	
1396.7(2)	342(8)	1.08(2)			3624.1	$31/2^- \rightarrow 27/2^-$
1435.9(2)	30(2)					

to be continued

Table 3.1: continued

Eγ (keV)	Rel. γ-ray Intensity	ADO ratio	α_{tot}	Multi-polarity	Placement E(keV)	$I_i^{\pi} \rightarrow I_f^{\pi}$
1528.9(2)	27(2)	1.36(12)			7754.6	
1570.3(2)	20(2)	1.18(15)			7754.6	

[a] For errors cf. Sect. 2.3.1
[b] Extracted from coincidence data.
[c] Coincidence intensity ratio I(37°)/I(79°) determined in sum gates of γ-transitions in coincidence with analysed γ-ray, cf. Sect. 2.4
[d] Determined from intensity balance
[e] Multipolarity listed when obtained from α_{tot} data, possible E2 contributions to M1 transitions not listed
[f] Not observed, but firmly inferred from coincidence data
[g] Observed in Planar-Coaxial coincidence data

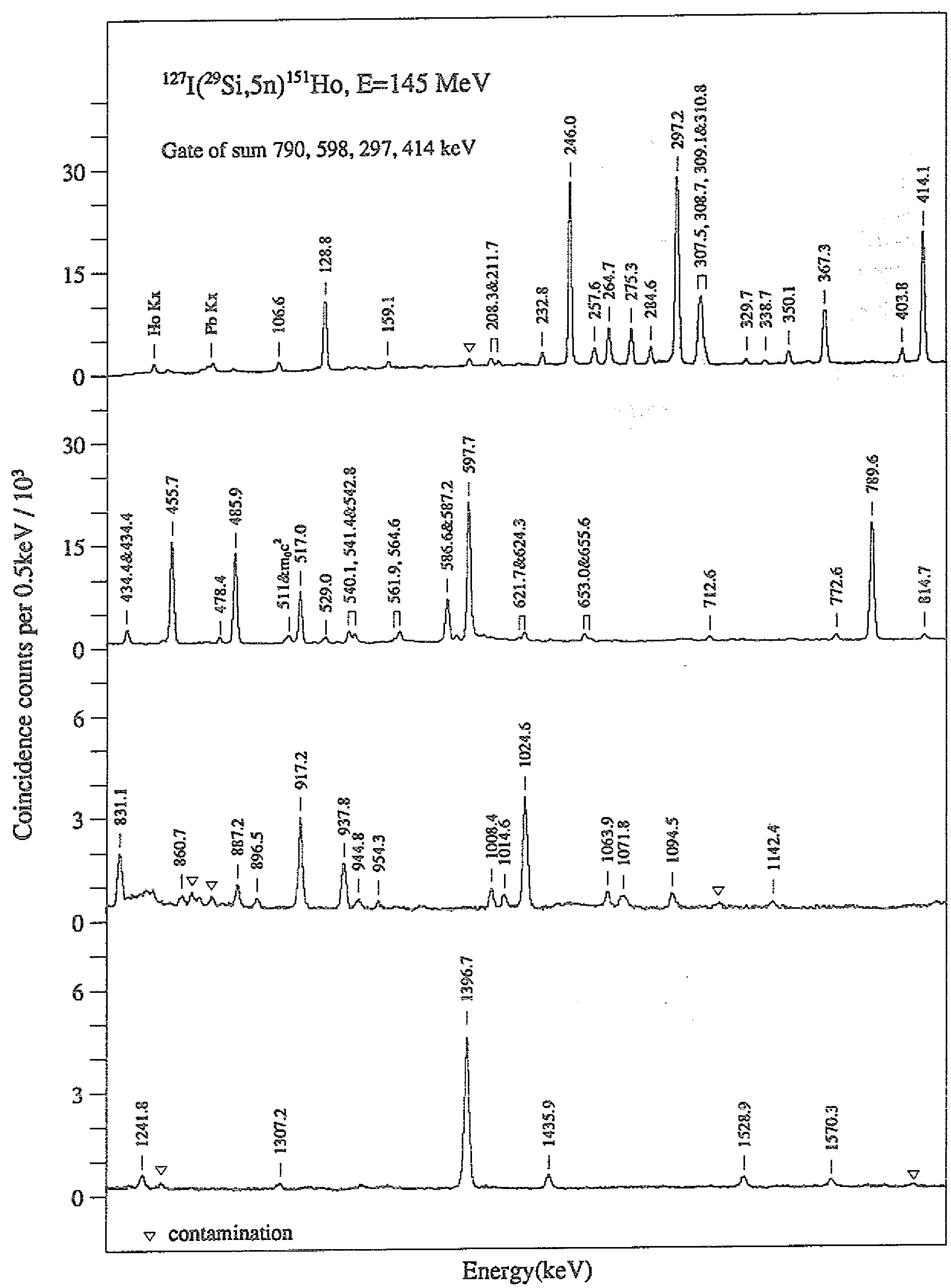

Fig. 3.1.2 *The ^{151}Ho γ-rays observed in the summed gates of the lowest four yrast γ-transitions.*

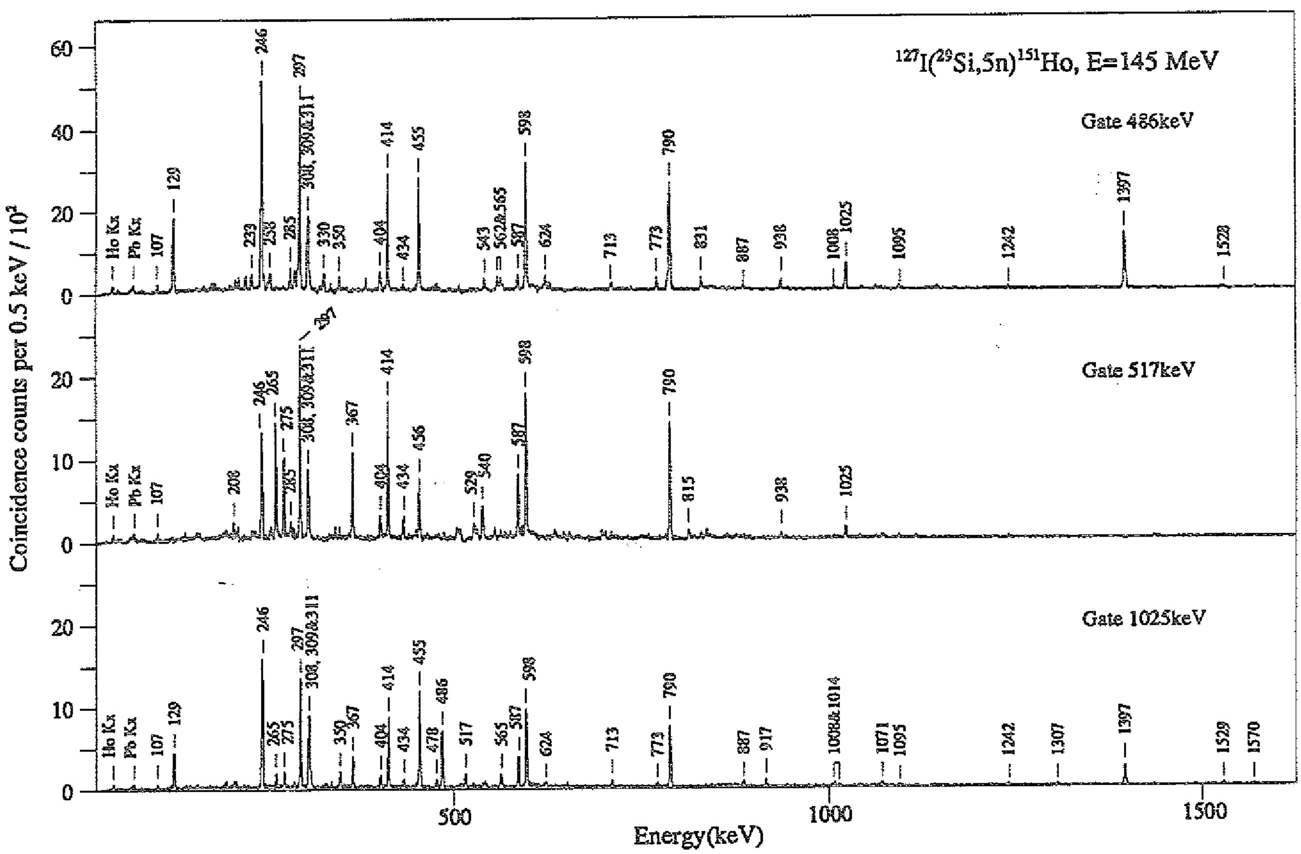

Fig. 3.1.3 Examples of coincidence gates on selected ^{151}Ho transitions.

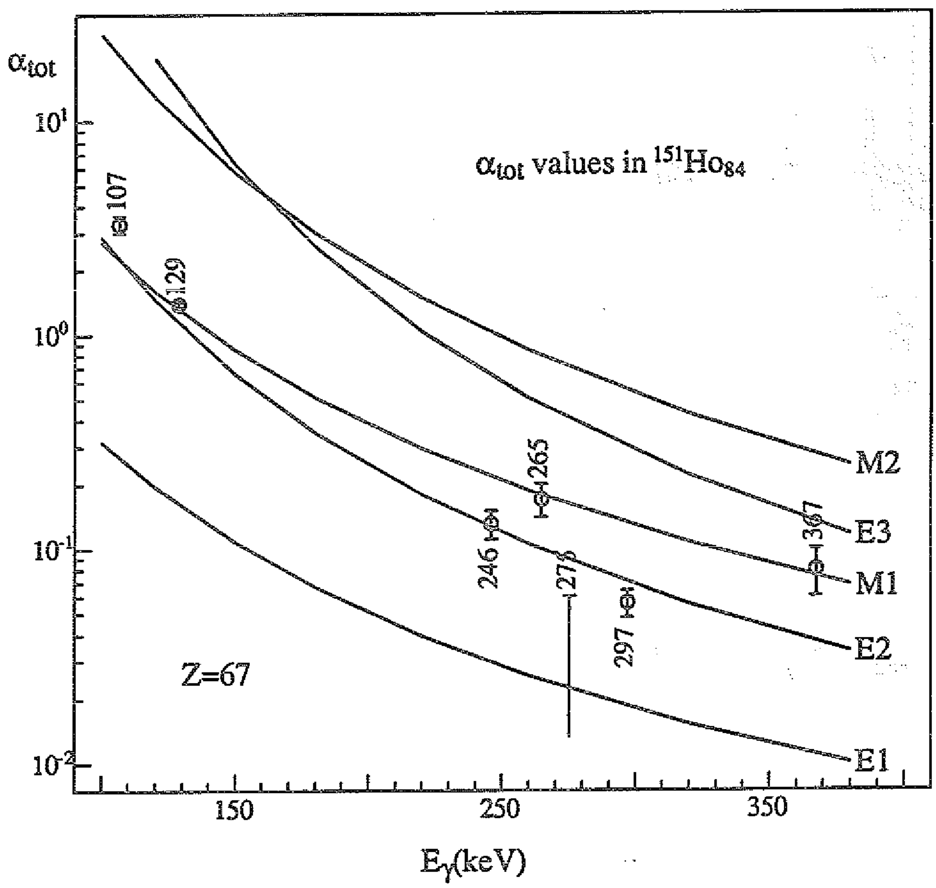

Fig. 3.1.4 Total conversion coefficients from intensity balance of transitions in $^{151}Ho_{84}$.

to the 4.812 MeV $43/2^-$ state reported in the previous study [Giz 81], but all other ^{151}Ho states reported there are not in accord with our results. An important additional finding in our data is the 106.6 keV M1 transition connecting the low-lying 1.791 and 1.685 MeV levels. This new transition removes the previous severe intensity imbalance at the 1.791 MeV state and gives a firm $21/2^-$ assignment for it, instead of the earlier $23/2^-$.

Above the $43/2^-$ state we identified seven levels up to 6.226 MeV which still receive an appreciable fraction of the yrast decay intensity. The number of parallel decay branches in the yrast cascade increases drastically above 6.2 MeV, involving numerous high-energy γ-rays. The states with parallel decay branchings to lower-lying known levels are still quite firm, but many weakly populated states, including several monopode levels are more tentative and given in parentheses. A technical difficulty here is that four γ-rays between 308 and 311 keV occur in the ^{151}Ho yrast decay, all in mutual coincidence, which precludes conclusive spin assignments for the states above 6.2 MeV, although for the stronger above-lying γ-rays the angular distribution data would still be conclusive.

At the 4.110 MeV $35/2^-$ level one third of the decay proceeds through a 587 keV transition to a group of six closely spaced levels that decay back to the $27/2^-$ and $25/2^-$ yrast states. The four γ-rays of the prominent decay cascade 367, 275, 265, and 517 keV all have ΔI=1 dipole angular distributions suggesting four of the level spins as shown in the scheme. The remaining 3.145 MeV state is fixed by its 917 keV dipole decay as 29/2, making the very intense unobserved 11 keV transition presumably M1. The 3.315 MeV state is specified as 33/2 as it is fed from the 3.970 MeV 35/2 state through the 656 keV dipole transition. Intensity balance suggests M1, (E1), and M1 for the three intense 367, 275, and 265 keV transitions, but still the level parities remain unspecified.

Gizon et al. [Giz 81] have already noted that there occur several ns-half-lives in the ^{151}Ho yrast cascade, and they are also evident from our data. However, the only clear-cut result is a $T_{1/2}$=9.2(20) ns half-life found in the $t_{\gamma RF}$ distribution of the 1242 keV line, where clearly no prompt contribution is present (Fig. 3.1.5). We therefore firmly assign this half-life to the 8.341 MeV level. The transitions above that state contained no such long component, but had also shorter delayed contributions, except for the 1307 keV line which was clearly prompt. The time distributions for the γ-rays emitted from levels between 8.1 and 5.2 MeV give no clear indication for other half-lifes above ~ 7ns.

There is clear but indirect evidence that an additional delay is present from the transitions below the 4.812 MeV $43/2^-$ state, but extraction of the half-life is difficult since it is of the order of only a few ns and thus too short for reliable determination from Ge timing data. The best estimate comes from comparison of the $t_{\gamma RF}$ distributions for the two high energy 1025 keV $45/2^- \longrightarrow 43/2^-$ and 1397 keV $31/2^- \longrightarrow 27/2^-$ transitions (Fig 3.1.5), where the 1397 keV $t_{\gamma RF}$ curve is clearly delayed with respect to the 1025 keV transition, evincing a half-life of the order of 1ns for one of the four intermediate levels.

An important clue for the location of this half-life comes from our measured coincidence angular distribution data. Whereas the 1064 keV E2 transition feeding the 4.812 MeV $43/2^-$ state has an ADO-value of 1.24(16), the value for the 456 keV E2

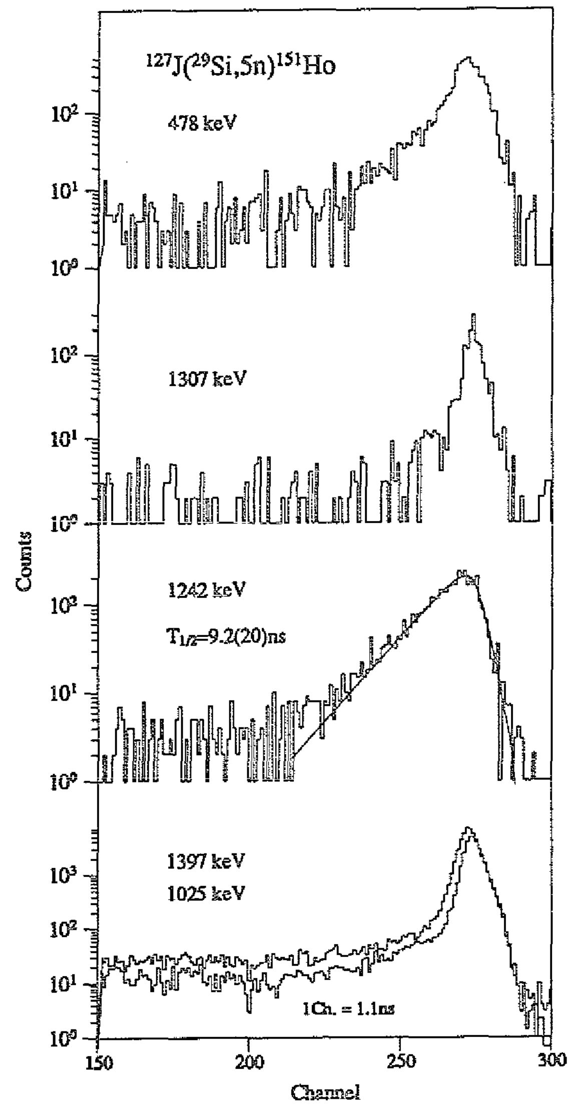

Fig. 3.1.5 Selected $t_{\gamma RF}$ time distributions for transitions in ^{151}Ho.

de-excitation transition is only 1.06(1). Similarly, the dipole transitions originating above the $43/2^-$ state have ADO values between 0.77 and 0.86, whereas the 587 keV transition connecting the 4.11 MeV $35/2^-$ to the 33/2 state has 0.98(2), also suggesting significant attenuation of the alignment. These findings would be consistent with attribution of the half-life to the $43/2^-$ state. But then its 456 keV E2 de-excitation transition would be rather slow, having a transition strength of only $0.4B_w$. This is a rather large retardation for an E2 transition in an N=84 nucleus. We note however that the intensities of the three transitions feeding the $43/2^-$ level carry only 58% of the 456 keV de-excitation transition intensity, while the unobserved side-feeding to the near lying states above and below is much smaller. This would alternatively leave the speculative possibility that the isomer could lie slightly above the $43/2^-$ state, and decay to it through an unobserved low-energy line. Although we could not identify γ-rays feeding this presumed isomer, we nevertheless show it tentatively in Fig 3.1.1 and give its half-life derived above as a lower limit. The data however cannot distinguish between the two alternatives.

We mention that our conclusions are in accord with the observations of Gizon et al. who also in their $t_{\gamma RF}$ data more tentatively noted a delay of less than 2ns for all transitions in the main yrast cascade. In their experiments, fortunately, and in contrast to ours, the alignment was not fully destroyed in this isomeric state. They could still obtain angular distribution and polarization data for the 9 lowest yrast transitions that have provided the firm I^π assignments up to $43/2^-$, while the data from our experiments with two different production reactions both gave unsatisfactory angular distribution results below the 1ns isomer.

3.2 The nucleus $^{152}_{68}Er_{84}$

The yrast states in this nucleus, which we will also discuss in Chapter 4, have very recently been studied [Kuh 92] in high-quality in-beam γ-ray experiments with Osiris at the HMI, and with HERA in Berkeley. The aim of these $^{116}Sn(^{40}Ar,4n)$ measurements was to observe superdeformed bands, which were not found, but the ^{152}Er

high-spin levels were established up to 15 MeV excitation. Spins and parities were assigned up to 28^+ at ~10 MeV, and the shell model configurations for the lower-lying states were discussed.

Similar as we noted in the previous section for holmium, also in erbium hyperfine interactions severely attenuate the nuclear alignment. Since ^{152}Er has high-spin ns-isomers [Kuh 92], at 13.5 MeV (11ns), and below at $I^{\pi}=28^+$(35ns), 16_2^+(6ns), 16_1^+ (1.5ns), and 8^+(2ns), the angular distribution data from these experiments were largely inconclusive. Therefore, only angular correlation results–which are less clear-cut–could be used to infer transition multipolarities.

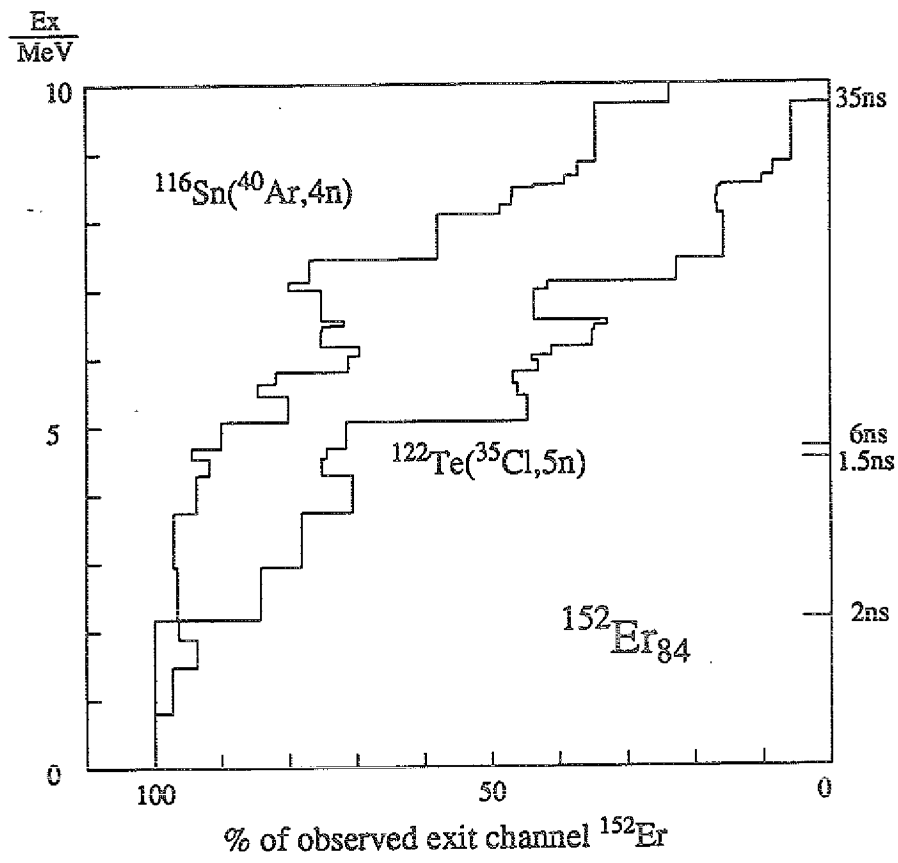

Fig. 3.2.1 Total population intensities for high-spin levels in ^{152}Er observed with two different production reactions.

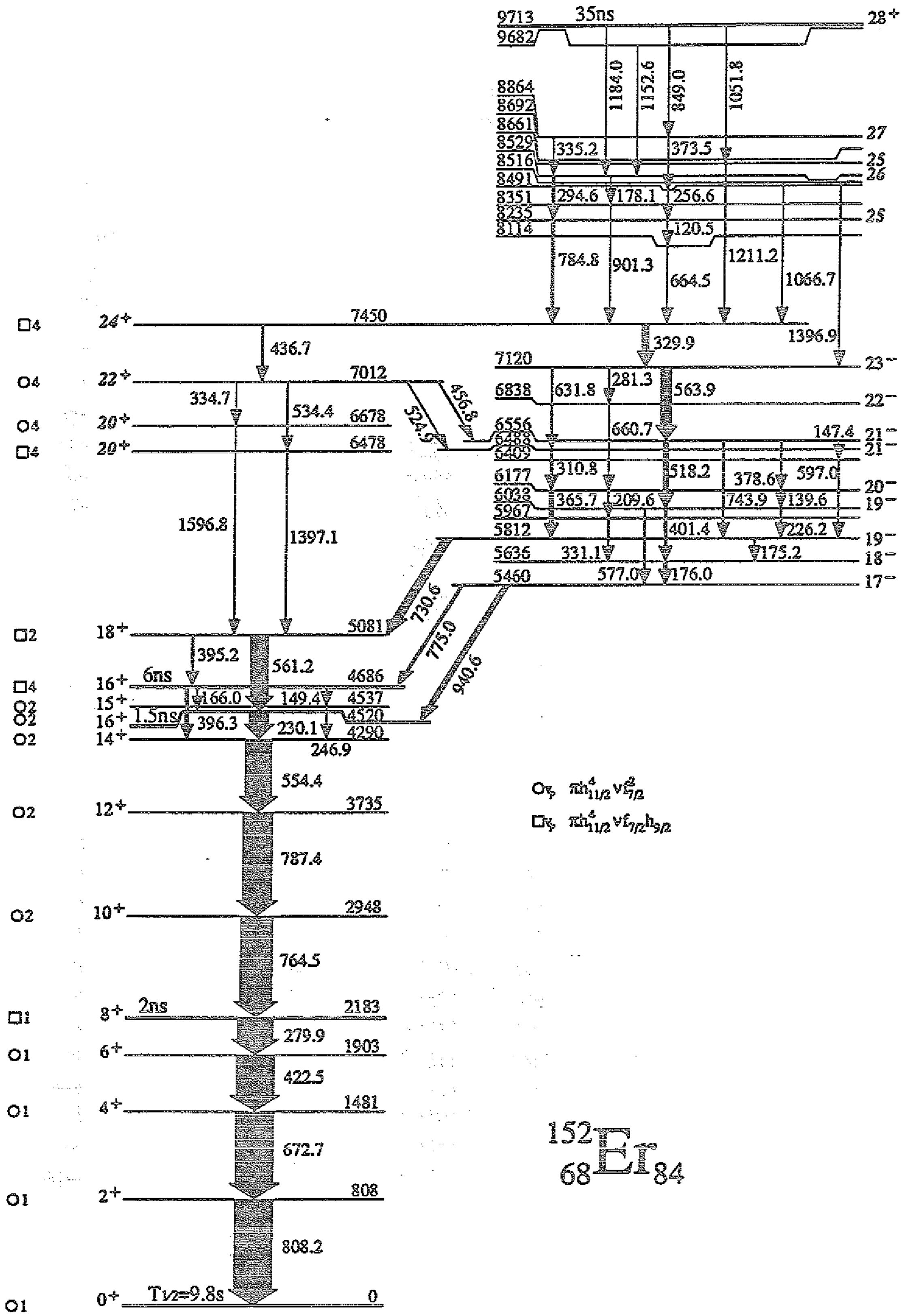

Fig. 3.2.2 The high-spin states of ^{152}Er as established by A. Kuhnert et. al [Kuh 92] but shown with the transition energies and intensities measured in the present study. Modified spin-parity assignments are given with skew numbers.

Table 3.2: Gamma-transitions in ^{152}Er observed in the ^{122}Te(^{35}Cl,p4n) reaction at 174 MeV performed on Nordball

E_γ^a (keV)	Rel. γ-ray[b] Intensity	ADO[c] ratio	E_i (keV)	E_γ^a (keV)	Rel. γ-ray[b] Intensity	ADO[c] ratio	E_i (keV)
120.5(2)	6(1)	0.83(3)	8235	518.2(1)	136(4)	1.25(1)	6556
139.6(2)	14(1)	1.14(3)	6177	524.9(1)	15(1)	0.79(1)	7012
147.4(2)	11(1)		6556	534.4(2)	19(1)	1.25(2)	7012
149.4(2)	38(2)	1.11(2)	4686	554.4(1)	707(14)	1.04(1)	4290
166.0(2)	23(1)	1.08(2)	4686	561.2(2)	469(11)	1.22(2)	5081
175.2(2)	30(5)		5812	563.9(2)	291(7)	1.10(2)	7120
176.0(2)	100(10)		5636	577.0(2)	47(2)	1.13(2)	6038
178.1(2)	10(2)		8529	597.0(2)	24(4)		6409
209.6(1)	28(1)	0.84(2)	6177	631.8(1)	51(2)	1.19(1)	7120
226.2(1)	42(5)	1.39(1)	6038	660.7(1)	17(2)	0.78(2)	6838
230.1(1)	529(9)	1.12(1)	4520	664.5(2)	3(1)		8114
246.9(1)	28(2)	1.16(2)	4537	672.7(1)	1000(20)	0.99(1)	1481
256.6(1)	24(1)	0.69(3)	8491	730.6(1)	223(5)	0.79(1)	5812
279.9(1)	939(19)	1.03(1)	2183	743.9(2)	45(2)	1.05(2)	6556
281.3(2)	30(1)		7120	764.5(1)	842(17)	0.98(1)	2948
294.6(1)	79(2)	0.78(1)	8529	775.0(1)	61(2)	0.83(2)	5460
310.8(1)	77(2)	0.81(1)	6488	784.8(1)	89(3)	0.96(2)	8235
329.9(2)	178(4)	0.80(1)	7450	787.4(1)	782(16)	1.03(1)	3735
331.1(2)	41(1)	1.05(1)	5967	808.2(1)	1000(20)	1.01(1)	808
334.7(2)			7012	849.0(2)	22(2)	0.77(2)	9713
335.2(2)	20(1)	0.85(2)	8864	901.3(1)	9(1)	0.67(4)	8351
365.7(1)	120(3)	0.79(1)	6177	940.6(1)	132(3)	0.80(1)	5460
373.5(2)	26(2)	0.69(3)	8864	1051.8(2)	19(2)	1.07(3)	9713
378.6(2)	21(2)	0.87(1)	6556	1066.7(2)	16(2)		8516
395.2(2)	54(5)		5081	1152.6(2)	4(1)		9682
396.3(2)	94(5)		4686	1184.0(2)	15(2)	0.86(3)	9713
401.4(1)	77(3)	0.86(1)	6038	1211.2(2)	35(2)	0.88(2)	8661
422.5(1)	1000(20)	1.02(1)	1903	1396.9(3)	5(2)		8516
436.7(1)	44(2)	1.17(1)	7450	1397.1(3)	27(5)		6478
456.8(2)	26(2)	1.05(1)	7012	1596.8(2)	4(4)		6678

[a] For errors cf. Sect. 2.3
[b] Extracted from coincidence data.
[c] Coincidence intensity ratio I(37°)/I(79°) determined in sum gates of γ-transitions in coincidence with analysed γ-ray, cf. Sect. 2.4

In our (^{35}Cl,4n) Nordball experiment for $^{153}Tm_{84}$ discussed in the next section, the neighbouring ^{152}Er isotone formed through p4n evaporation is twice as strongly populated as ^{153}Tm. Due to the available recent results[Kuh 92] we did not fully analyse our own data on this nucleus. But since in our reaction the ^{152}Er is formed at significantly lower angular momentum, such that a much larger fraction of the yrast decay intensity enters below the 35ns 28^{+} isomer at 10MeV (see Fig. 3.2.1), we find only weakly attenuated angular distributions for γ-rays from levels between 5 and 9 MeV, which provide useful check for the previous results.

The γ-intensties and ADO-values from our data are listed in Table 3.2. In Fig. 3.2.2 we show the level scheme as established in Ref. [Kuh 92] up to the 9.7 MeV isomer, but with the γ-ray intensities from our data. We have also included a few modified I^{π} assignments, and will briefly discuss them. Our results confirm the previous spin assignments up to I=24 at 7.450 MeV, but for the above lying 784.8 keV line our data prefer dipole rather than quadrupole character as previously proposed. It moreover appears to us that the intense 330 keV dipole transition from the 7.450 MeV state, instead of M1[Kuh 88] or E2 [Kuh 92], rather should have E1 character, which also seems to us in accord with the published conversion electron spectrum. This inverts four level parities, and removes the previous difficulty in decay of the 6.478 MeV state where the unusual M2 decay competing against possible M1 and E2 de-excitation branches is eliminated. Finally, we invert the 1597–335 keV cascade connecting the I=22 and 18^{+} states, which is equally compatible with the data, and is motivated in Chapter 4, or more explicitely, we do it because we have a theory.

3.3 The nucleus $^{153}_{69}Tm_{84}$

The Z=69 nucleus ^{153}Tm, similar as its ^{151}Ho N=84 isotone, has also two low-lying α- and β-decaying isomers, formed by the odd proton in the $s_{1/2}$ or $h_{11/2}$ shell model orbital. This was first shown by a high-resolution study of ^{153}Tm α-decay [Sch 87], where the previously single 5.11 MeV α-transition [Hag 77] was shown to be a closely spaced doublet, with $\Delta E=7\pm.4$ keV , and where the half-lives of 1.5s and 2.5s were established for the $11/2^-$ and $1/2^+$ activities, respectively. The known 49.0 keV $1/2^+$ excitation [Fir 88] in the α-daughter $^{149}Ho_{82}$ gives 43 keV for the $1/2^+$ state in ^{153}Tm. This was later confirmed in a ^{153}Yb β-decay study [Kor 89], where also ^{153}Tm excited states γ-decaying to both isomers were observed (cf. Chap. 3.1). Moreover, also in ^{153}Tm the $\pi h_{11/2}$ isomer decays via a fast Gamow-Teller transition to the $\nu h_{9/2}$ state at 299 keV in ^{153}Er [Kor 89]. From earlier in beam measurements [Rat 84] an yrast cascade of eight transitions had been established, where the six lowest yrast level energies are confirmed in our present study.

In our measurements, first in-beam results on ^{153}Tm were obtained from the ^{54}Fe+ ^{106}Cd experiment at 255 MeV, primarily aimed to study $^{154}Yb_{84}$, where ^{153}Tm was excited via the α3p evaporation channel(Table 1.1). But much superior data came from the later Nordball experiment using the reaction ^{122}Te(^{35}Cl,4n), where a 1.6mg/cm^2 ^{122}Te metallic target with 94.7% enrichement, evaporated on an 8mg/cm^2 ^{208}Pb backing, was bombarded with 174 MeV ^{35}Cl beam. The Nordball configuration was the same as described in chapter 2, identical as used in the ^{151}Ho study.

The results from this experiment are compiled in Table 3.3 and in the level scheme of Fig. 3.3.1. The coincidences with the three lowest intense yrast γ-rays in Fig. 3.3.2 identified the ^{153}Tm γ-lines and gave their relative intensities. In the table we also list the intensities from the ^{54}Fe-induced experiment obtained in a similar manner. The Fig. 3.3.3 shows examples of individual gates used to construct the level scheme. For seven intense low-energy transitions the data gave the α_{tot}-values in Fig 3.3.4 and Table 3.3, which were vital for assigment of the level parities. Of crucial

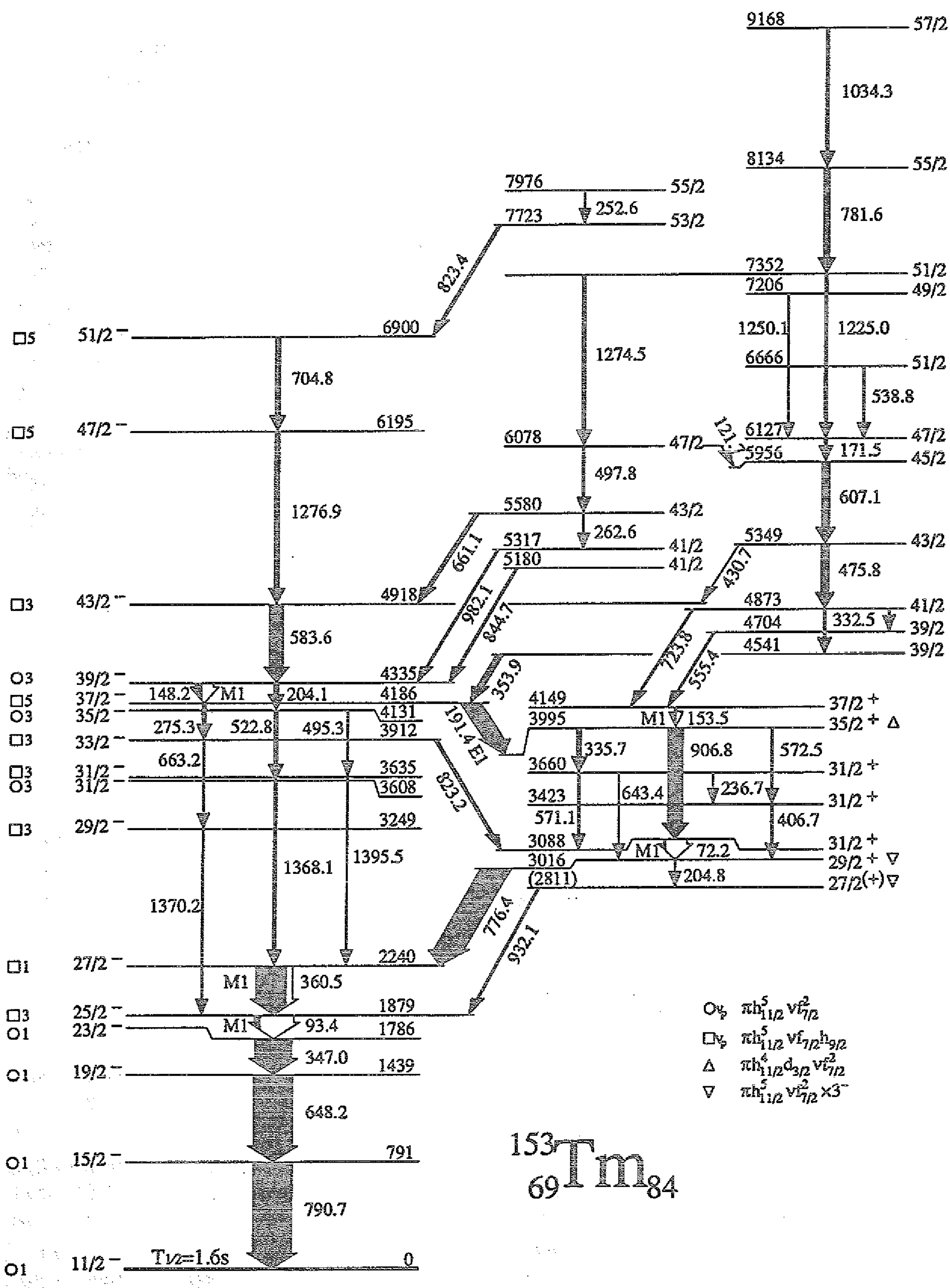

Fig. 3.3.1 *The ^{153}Tm high-spin states observed in the ^{122}Te(^{35}Cl,4n) reaction (cf. caption to Fig. 3.1.1).*

Table 3.3: Gamma-transitions in ^{153}Tm observed in the ^{122}Te(^{35}Cl,4n) reaction at 174 MeV performed on Nordball and in the ^{106}Cd(^{54}Fe,α3p) reaction at 255 MeV on Osiris

E_γ^a (keV)	Rel. γ-ray Intensity[b] (^{35}Cl,4n)	(^{54}Fe,α3p)	ADO[c] ratio	α_{tot}^d	Multi-polarity[e]	Placement E_i(keV)	$I_i^\pi \rightarrow I_f^\pi$
72.2(2)[f]	71(9)		1.03(7)	7.3(30)	M1	3088	$31/2^+ \rightarrow 29/2^+$
93.4(1)	185(10)	150(14)	1.06(3)	4.75(46)	M1	1879	$25/2^- \rightarrow 23/2^-$
121.9(1)	25(3)		0.96(13)			6078	$47/2 \rightarrow 45/2$
148.2(1)	172(9)	95(5)	1.04(3)	1.58(15)	M1	4335	$39/2^- \rightarrow 37/2^-$
153.5(1)	55(4)	37(4)	0.96(5)	0.6(2)	M1	4149	$37/2 \rightarrow 35/2$
168.8(2)[g]	61(12)	48(5)	0.96(3)[h]			4873	$41/2 \rightarrow 39/2$
169.3(2)[i]	41(6)		0.96(3)[h]				
171.5(1)	89(5)	29(4)	0.95(3)			6127	$47/2 \rightarrow 45/2$
191.5(1)	453(16)	246(8)	0.98(1)	≤0.06	E1	4187	$37/2^- \rightarrow 35/2^+$
204.1(2)[j]	144(12)[j]	59(5)	1.28(4)[j]			3523	$39/2^- \rightarrow 35/2^-$
204.8(2)[k]	48(32)[k]					3016	$29/2 \rightarrow 27/2$
236.7(1)						3660	$31/2^+ \rightarrow 31/2^+$
252.6(1)	34(2)	19(5)	0.81(8)			7976	$55/2 \rightarrow 53/2$
262.6(1)	49(2)					5580	$43/2 \rightarrow 41/2$
275.1(1)	120(4)	50(6)	1.16(4)			4187	$37/2^- \rightarrow 33/2^-$
332.5(1)	91(3)	47(6)	0.87(3)			4873	$41/2^- \rightarrow 39/2$
335.7(1)	130(4)	61(6)	1.28(4)			3995	$35/2^+ \rightarrow 31/2^+$
347.0(1)	951(23)	1000(38)	1.17(1)	0.06(6)	E2	1786	$23/2^- \rightarrow 19/2^-$
353.9(1)	166(5)	46(6)	0.84(3)			4541	$39/2 \rightarrow 37/2^-$
360.5(1)	777(18)	675(33)	0.89(1)	0.12(3)	M1	2240	$27/2^- \rightarrow 25/2^-$
406.7(1)	74(3)	52(8)	0.89(5)			3423	$31/2^- \rightarrow 29/2^+$
430.7(1)	18(2)		1.72(36)			5349	$43/2 \rightarrow 43/2^-$
475.8(1)	206(6)	125(9)	0.88(2)			5349	$43/2 \rightarrow 41/2$
495.3(1)	30(2)	42(6)	1.18(11)			4131	$35/2^- \rightarrow 31/2^-$
497.8(1)	78(3)		1.18(6)			6078	$47/2 \rightarrow 43/2$
522.8(1)	110(4)	65(7)	1.10(5)			4131	$31/2^- \rightarrow 27/2^-$
538.8(1)	66(3)		1.12(8)			6666	
555.4(1)	44(3)	44(8)	0.78(7)			4704	$39/2 \rightarrow 37/2^+$
571.1(2)	67(4)	49(8)	1.29(9)			3660	$31/2^+ \rightarrow 31/2^+$
572.5(1)	64(3)		1.18(11)			3995	$35/2^+ \rightarrow 31/2^+$
583.6(1)	369(10)	169(12)	1.24(2)			4918	$43/2^- \rightarrow 39/2^-$
607.1(1)	221(7)		0.83(3)			5956	$45/2 \rightarrow 43/2$
643.4(1)	42(3)		0.68(5)			3660	$31/2^+ \rightarrow 29/2^+$
648.2(1)	1000(25)	1000(45)	1.17(1)			1439	$19/2^- \rightarrow 15/2^-$
661.6(1)	95(5)		0.91(5)			5580	$43/2 \rightarrow 43/2^-$
663.2(1)	56(3)		1.57(15)			3912	$29/2^- \rightarrow 25/2^-$
704.8(1)	133(5)		1.45(7)			6900	$51/2^- \rightarrow 47/2^-$

to be continued

Table 3.3: continued

Eγ (keV)	Rel. γ-ray Intensity (^{35}Cl,4n)	(^{54}Fe,α3p)	ADO ratio	α_{tot}	Multi-polarity	Placement E_i(keV)	$I_i^\pi \rightarrow I_f^\pi$
723.8(1)	44(3)		1.14(12)			4873	41/2 → 37/2
776.4(1)	681(17)	583(15)	0.84(1)			3016	$29/2^+ \rightarrow 27/2^-$
781.6(1)	169(6)		1.15(5)			8134	55/2 → 51/2
790.8(1)	1000(25)	1000(45)	1.10(1)			791	$15/2^- \rightarrow 11/2^-$
808.0(1)	49(3)		0.89(8)				
823.2(2)	61(10)[l]	87(9)	0.86(12)			3912	$33/2^- \rightarrow 31/2^+$
823.4(2)[m]	77(11)[m]		0.88(3)			7724	$53/2 \rightarrow 51/2^-$
844.7(1)	57(3)		0.84(5)			(5180)	$41/2 \rightarrow 39/2^-$
906.8(1)	398(10)	239(11)	1.20(2)			3995	$35/2^+ \rightarrow 31/2^+$
932.1(1)	48(3)	32(9)	0.81(10)			(2811)	$27/2^+ \rightarrow 25/2^-$
982.1(1)	49(3)		0.72(7)			5317	$41/2 \rightarrow 39/2^-$
1034.3(1)	93(4)		1.05(6)			9168	57/2 → 55/2
1225.0(1)	84(4)		1.16(9)			7352	51/2 → 47/2
1250.1(1)	39(3)		1.19(16)			7206	49/2 → 45/2
1274.5(1)	105(4)		1.14(16)			7352	51/2 → 47/2
1276.9(1)	137(5)	50(11)	1.28(5)			6195	$47/2^- \rightarrow 43/2^-$
1368.1(1)	84(8)	56(11)	1.23(8)			3608	$35/2^- \rightarrow 31/2^-$
1370.2(2)	43(6)		1.19(26)			(3249)	$33/2^- \rightarrow 29/2^-$
1395.5(2)	36(2)					3635	$31/2^- \rightarrow 27/2^-$
1435.9(1)	30(2)		1.27(19)				
1468.0(2)	15(2)		1.14(24)				

[a] for errors cf. Sect. 2.3.1
[b] Extracted from coincidence data.
[c] Coincidence intensity ratio I(37°)/I(79°) in sum gates 791keV, 648keV and 347keV transitions
[d] Determined from intensity balance
[e] Multipolarity listed when obtained from α_{tot} data, possible E2 contributions to M1 transitions not listed
[f] Obtained from planar-coaxial coincidence data
[g] Determined in 153keV gate
[h] Could not be resolved from the value obtained for the transition with almost equal energy
[i] Determined in 845keV gate
[j] Determined in 361keV gate
[k] Determined in 932keV gate
[l] Corrected for contribution from analogous 823.4keV transition
[m] Obtained from sum gates 1368keV, 523keV and 204keV transitions

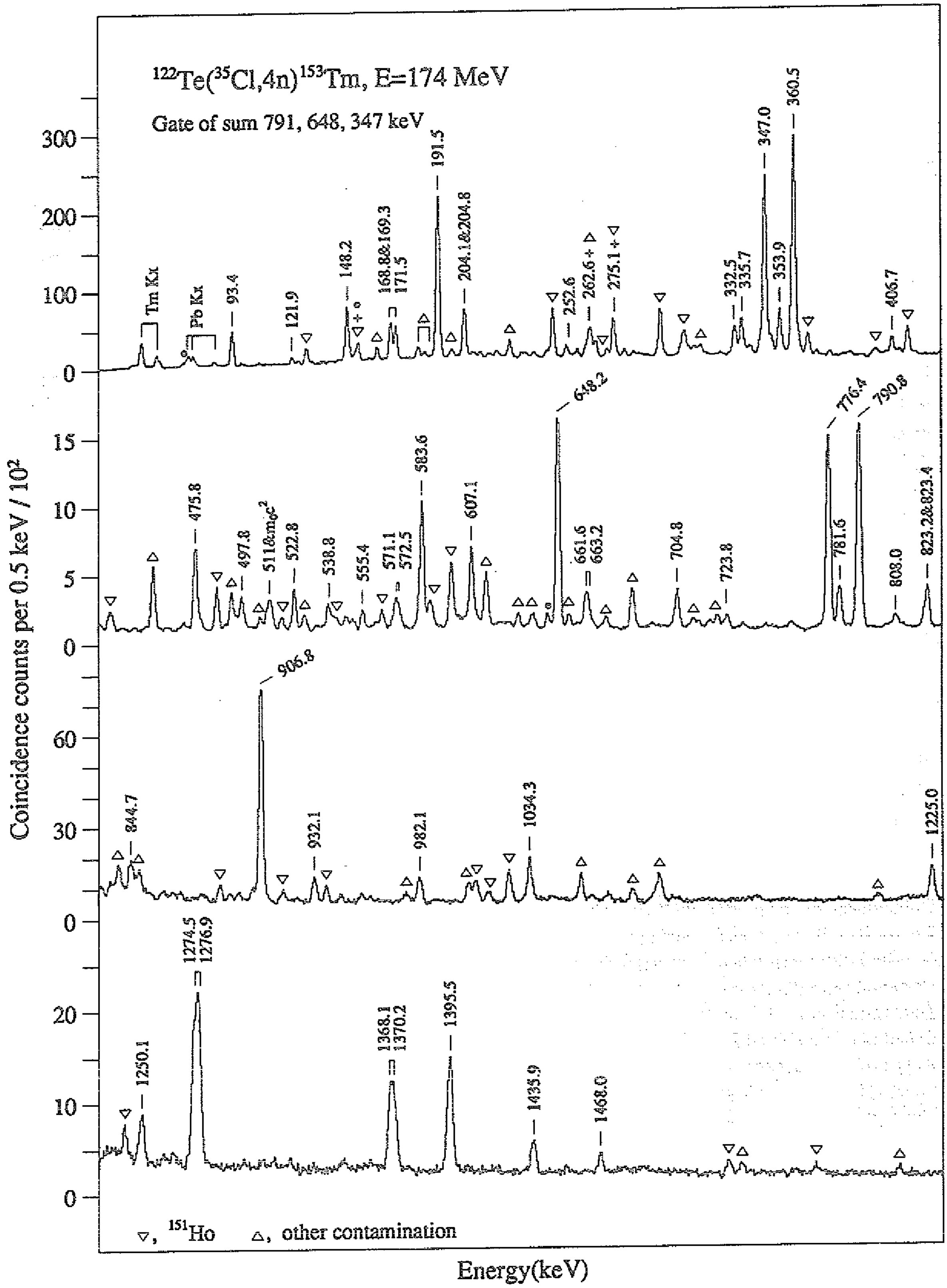

Fig. 3.3.2 The ^{153}Tm γ-rays observed in the summed gates of the lowest three yrast γ-transitions.

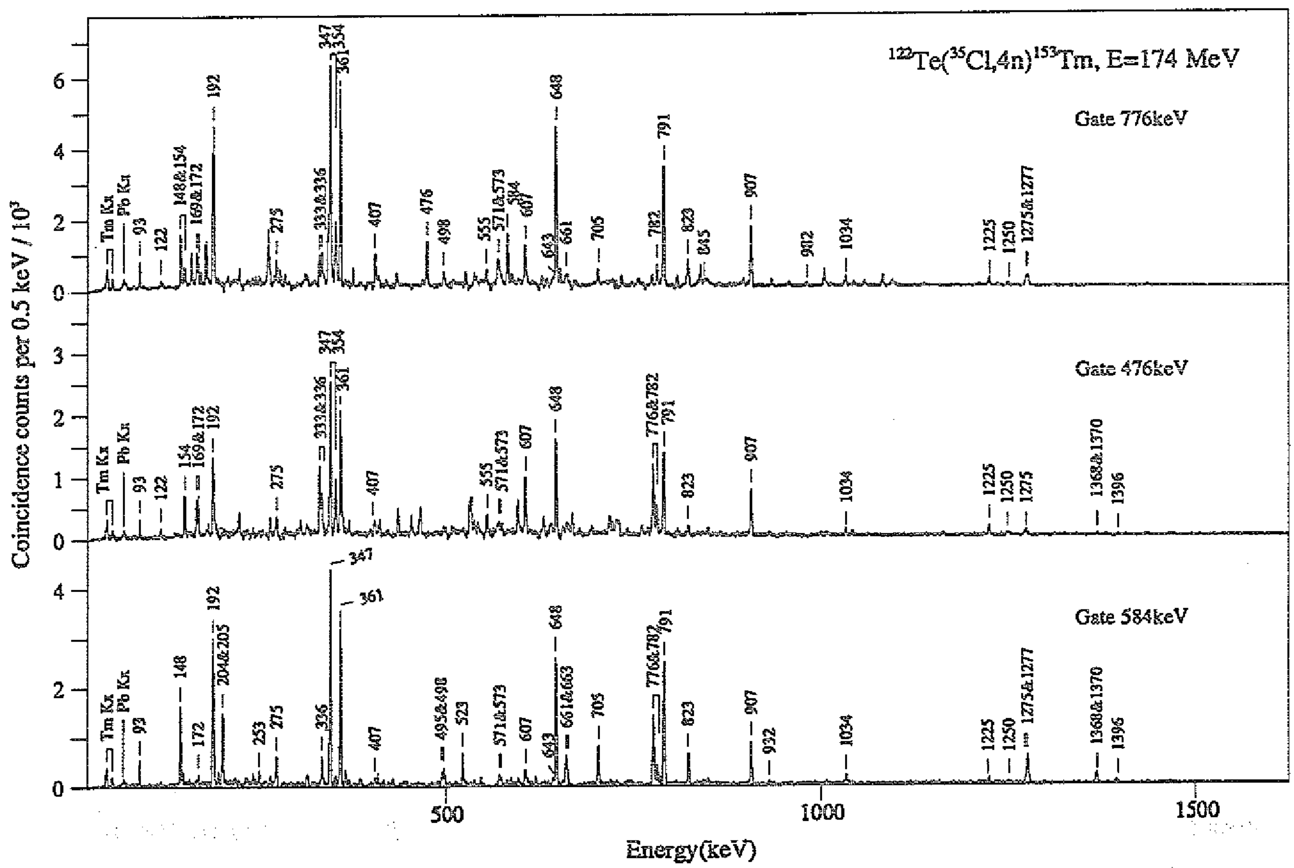

Fig. 3.3.3 Examples of coincidence gates on selected ^{152}Tm transitions.

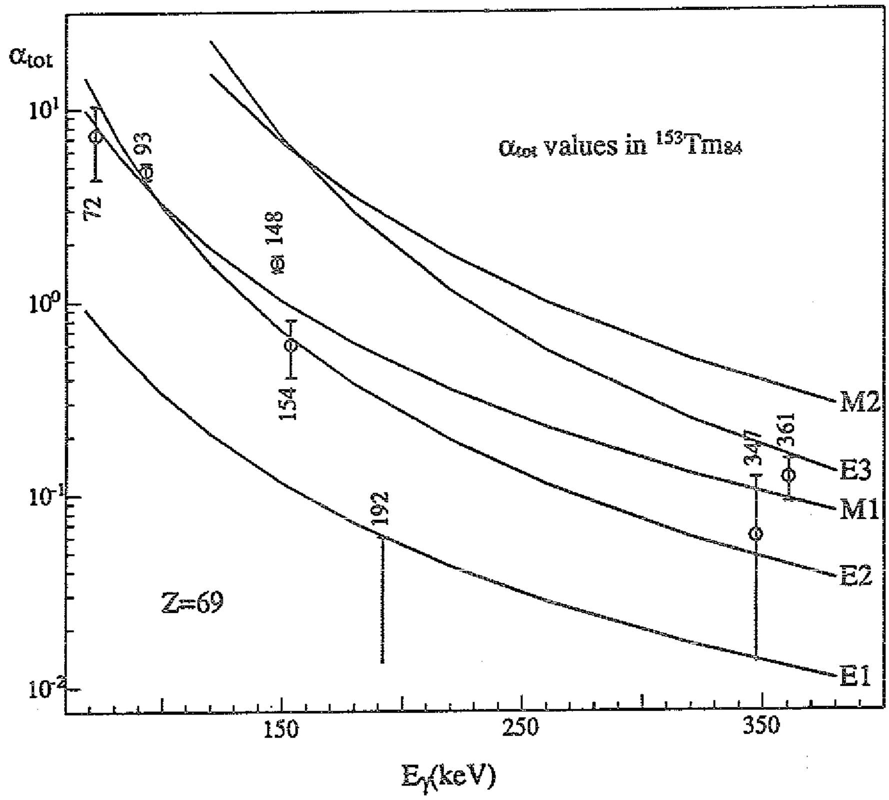

Fig. 3.3.4 Total conversion coefficients from intensity balance of transitions in $^{153}Tm_{84}$.

importance was the α_{tot} value of the 72.2 keV γ-ray connecting the 3.088 and 3.016 MeV states. It was difficult to measure due to the close-lying intense Pb $K\alpha_2$ X-ray at 72.8 keV. But in the planar detector the two lines were partially resolved, and it was found that the 72.2 keV γ-ray is coincident with all the strong lines in the main cascade. With the placement firmly established from energy loops involving parallel decay branches the α_{tot} value was obtained as 7.3(30), giving magnetic dipole character for the 72.2 keV transition.

The ^{153}Tm level scheme up to 57/2 at 9.2 MeV excitation energy was established from the γγ-coincidence data. The three lowest stretched E2 transitions establish the spins up to $23/2^-$ at 1.786 MeV. The M1 nature of the two next higher γ-rays solidify the tentative $25/2^-$ and $27/2^-$ assignments for the 1.879 MeV and 2.240 MeV states proposed in the previous work[Rat 84].

All the levels shown to the left of Fig 3.3.1 above the $27/2^-$ state decay through stretched E2 transitions; only the 148 keV line is firm M1 from its α_{tot} value. This unambiguously assigns the spin values and odd parity for all states.

Similar as in the ^{151}Ho isotone, we also in ^{153}Tm find a side branch from the negative parity level sequence through a group of rather closely spaced levels in the 2.5 to 4 MeV region, but in ^{153}Tm the main fraction of the yrast cascade proceeds through this group of states. The γ-cascade departs from the 4.186 MeV $37/2^-$ level through a 191 keV E1 transition and proceeds through an intense 907 keV E2–72 keV M1–766 keV dipole triple-cascade back to the $27/2^-$ state at 2.240 MeV, which assigns $35/2^+$, $31/2^+$, and $29/2^+$ to the three intermediate states. Two additional stretched E2 decay branches from the $35/2^+$ state at 3.995 MeV determine $31/2^+$ for the 3.660 and 3.423 MeV levels, and the ADO-data for their de-excitation γ-rays support these assignments. A 205 keV–932 keV dipole-cascade connects the 3.016 MeV $29/2^+$ level to the $25/2^-$ yrast state. The intensity of the 204.8 keV line is poorly known since it is not resolved from the coincident 204.1 keV doublet partner, and therefore level energy and parity for the intermediate state are tentative. For the 4.149 MeV level the 154 keV M1 de-excitation γ-ray gives $I^\pi=37/2^+$, but for all above lying states shown to the right in Fig. 3.3.1 the parities are not determined although their spins are firm.

3.4 The nucleus $^{154}_{70}$Yb$_{84}$

The even-even N=84 nucleus $^{154}_{70}$Yb consists of eight valence particles moving around the ^{146}Gd core. The 0^+ ground state with a half-life of 0.42s was established [Hag 77] from the dominant $\Delta l=0$ α-decay to the four-proton nucleus ^{150}Er, and independently [Vie 88] from the fast $0^+\longrightarrow1^+$ Gamow-Teller decay (log ft =3.6) to the 133 keV $(\pi h_{11/2}\nu h_{9/2})1^+$ excitation in ^{154}Tm.

The β^+-decay of the $^{154}_{71}$Lu high-spin activity to ^{154}Yb was first investigated by Rathke et al. [Rat 84] using the ^{60}Ni(^{96}Ru,pn)^{154}Lu reaction, where also in-beam $\gamma\gamma$- and γ-singles data on ^{154}Yb excited through 2p evaporation were recorded. From their studies an yrast cascade up to 5.7 MeV was established, based on $\gamma\gamma$-coincidence results taken with one coaxial and one large-volume planar Ge-detector. A half-life of 51(5)ns was attributed to the presumed 8^+ state decaying through an unobserved low energy E2 γ-ray to the 1.949 MeV 6^+ level firmly assigned from ^{154}Lu β-decay and the level energy systematics in doubly-even N=84 nuclei. In a later study of ^{154}Lu β-decay [Vie 88] this presumed low-energy γ-line was observed to have 96.6 keV and the measured α_k-value established its E2 character, confirming the earlier [Rat 84] tentative suggestion.

We have investigated the ^{154}Yb yrast states using the ^{106}Cd(^{54}Fe,α2p) reaction. The experiment was performed with the Osiris γ-spectrometer, where a 1.2mg/cm^2 thick 90.8% enriched ^{106}Cd, backed by 15mg/cm^2 ^{208}Pb, was irradiated with a 300ns-pulsed ^{54}Fe beam of 255MeV. The large-volume neutron detector combined in this experiment with the Osiris γ-ray detectors aided to identify other largely unknown fusion-evaporation products.

Eleven coaxial and one planar Ge-detector were used in the Osiris measurements. With a beam current of 0.8 nA we obtained a $\gamma\gamma$-coincidence counting rate of about 600 events/sec. A total of 47 million good coincidence events were accumulated, of which 0.6 million are γ-γ-n coincidence events. From the detailed reaction cross-section anslysis [Bro 91] of the present data we found that the α2p exit channel leading to ^{154}Yb contributes about one tenth to the total fusion-evaporation cross-section(Fig. 2.4.2). However, in our collisions of ^{54}Fe and ^{106}Cd 30 MeV above the Coulomb barrier, by far the largest fraction of the emitted γ-rays comes from numerous nuclei produced in binary reactions, such that the α2p fusion evaporation exit channel carries only ~1% of the total in-beam γ-ray intensity.

Of the two other experiments giving angular distributions for ^{154}Yb γ-lines (Table 1.1), the quality of the Nordball data with the ^{130}Ba(^{28}Si,4n) reaction was much superior. The beam energy in this experiment was 140 MeV, and the >99% enriched ^{130}Ba target was prepared from 14% pre-enriched material by direct ion beam deposition in the mass-seperator at Orasy on an 8mg/cm^2 ^{208}Pb recoil stopper foil.

The results from the two experiments are summarized in Table 3.4, and in the level scheme of Fig 3.4.1. As before, the energies and relative intensities of the ^{154}Yb

γ-lines were extracted from coincidence data with three lowest yrast transitions; the spectrum measured with ($^{54}Fe,\alpha 2p$) is shown in Fig 3.4.2. Three crucial α_{tot} values for the intense low-energy γ-transitions of 97, 160, and 182 keV are listed in column 5, and compared with calculated values in Fig 3.4.3. The ADO ratios and the γ-intensities obtained in the ^{28}Si-experiment are also given in the table.

From our coincidence data the energy levels in ^{154}Yb were constructed and the spins assigned up to I=24 at the 7.610 MeV level. An important result here is the finding of a new yrast 16^+ isomeric state at 4.479 MeV, decaying via eight stretched E2 transitions to the ground state. Its half-life

$$T_{1/2}(^{154}\text{Yb}, 16_1^+) = 18.6(15)\ \text{ns}$$

was extracted from the $t_{\gamma RF}$ data for the 622, 782, and 869 keV transitions following the 16^+ isomer decay, as shown in Fig 3.4.4. The half-life of the previously known 8^+ isomer shown below was redetermined using the $t_{\gamma\gamma}$ data from full-absorption coincidence events between the three strongest transitions below and above it. The resulting

$$T_{1/2}(^{154}\text{Yb}, 8^+) = 28(2)\text{ns}$$

half-life is about twice shorter than the value [Rat 84] from the earlier measurement. No apparent delay was recognized in the $t_{\gamma RF}$ distribution of the γ-transitions above the 16^+ isomeric state. The three examples of $\gamma\gamma$-coincidence spectra with specifically chosen timing conditions shown in Fig 3.4.5 conclusively demonstrate which of the ^{154}Yb γ-rays occur above the two nanosecond-isomers, between them, and below both isomers.

Up to the 16^+ state at 4.479MeV the level spins and parities are already clear from the E2 nature of the eight transitions in the de-excitation cascade. The six above-lying intense transitions in the main cascade all have dipole character, giving the spin values up to 22 at 7.187 MeV. The level parities are specified up to 18^+ at 5.177

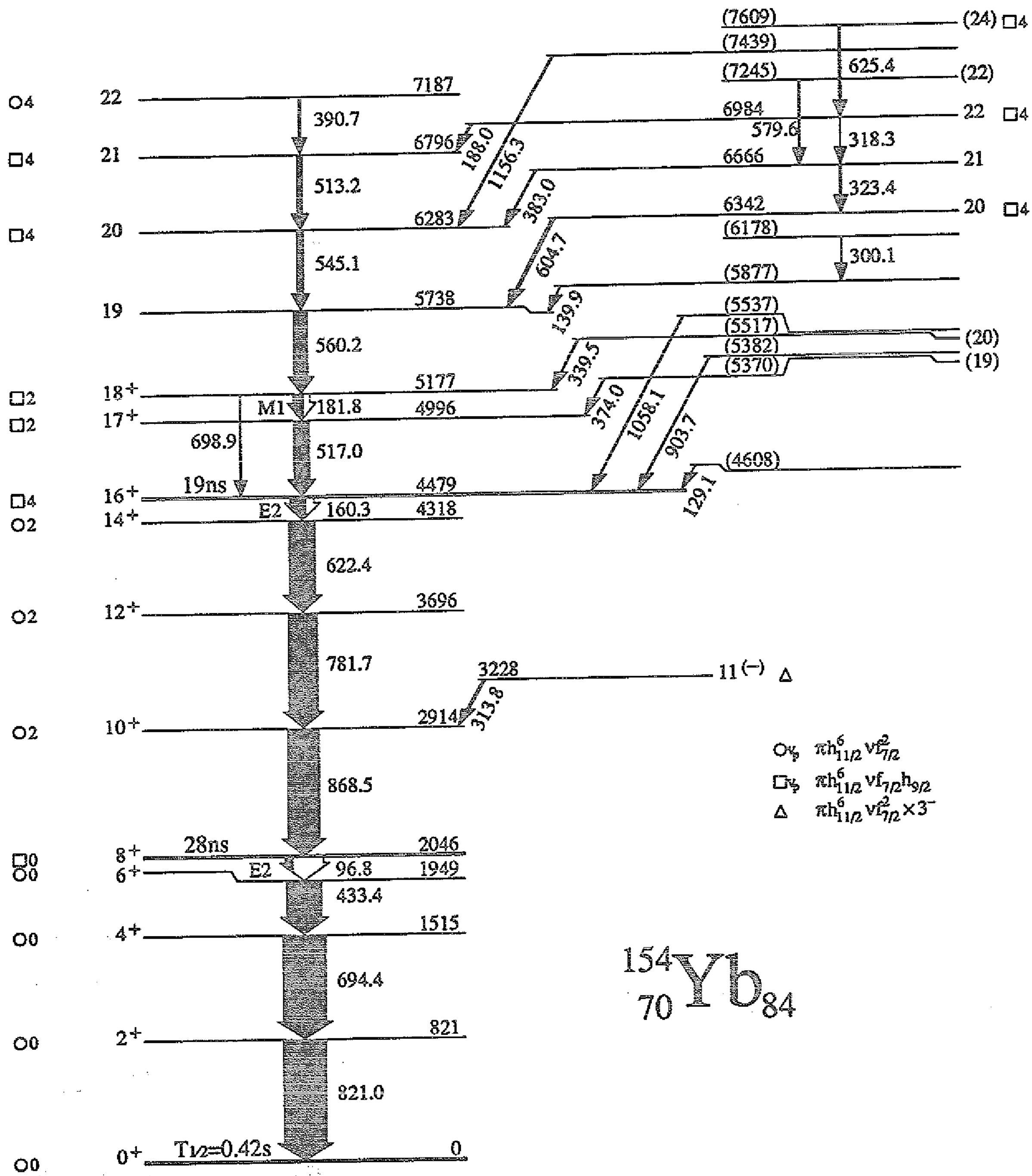

Fig. 3.4.1 The ^{154}Yb high-spin states observed in the ^{106}Cd(^{54}Fe,α2p) reaction (cf. caption to Fig. 3.1.1).

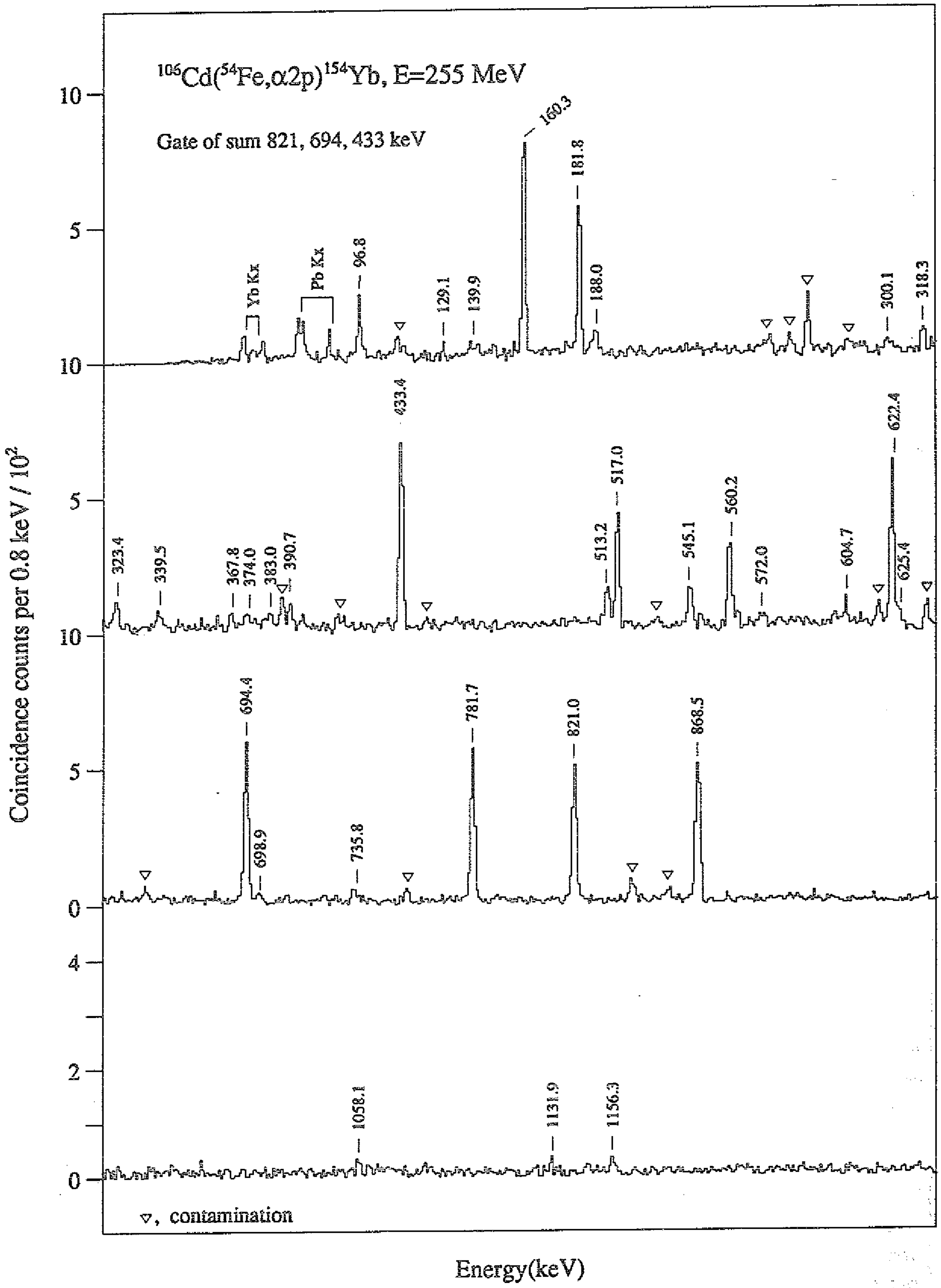

Fig. 3.4.2 *The* ^{154}*Yb* γ*-rays observed in the summed gates of lowest three yrast* γ*-transitions.*

Table 3.4: Gamma-transitions in ^{154}Yb observed in the ^{130}Ba(^{28}Si,4n) reaction at 140 MeV performed on Nordball and in the ^{106}Cd(^{54}Fe,α2p) reaction at 255 MeV on Osiris

E_γ^a (keV)	Rel. γ-ray Intensity[b] (^{28}Si,4n)	(^{54}Fe,α2p)	ADO[c] ratio	α_{tot}^d	Multi-polarity[e]	Placement E_i(keV)	$I_i^\pi \rightarrow I_f^\pi$
96.8(1)	163(6)	178(28)	1.68(8)	3.88(20)	E2	2046	$8^+ \rightarrow 6^+$
129.1(2)	11(2)	14(3)	1.66(64)			4608	
139.9(1)	21(2)	19(3)				5877	
160.3(1)	386(13)	381(10)	1.46(3)	0.47(3)	E2	4479	$16^+ \rightarrow 14^+$
181.8(1)	243(11)	250(6)	0.82(2)	0.82(6)	M1	5177	$18^+ \rightarrow 17^+$
188.0(1)	28(2)	50(4)	0.58(8)			6984	
300.1(1)		26(4)				6178	
313.8(1)	127(4)	63(7)	0.82(5)			3228	$11^{(-)} \rightarrow 10^+$
318.3(2)	35(2)	17(4)	0.93(10)			6984	
323.4(1)	51(2)	63(4)	0.69(7)			6666	
339.5(1)	17(2)	35(6)	1.15(26)			5517	
363.1(1)							
367.8(1)		23(5)					
374.0(1)	32(3)	31(6)				5370	
383.0(1)	38(3)	34(5)	0.84(10)			6666	
390.7(1)	54(3)	75(6)	0.78(8)			7187	
411.8(2)		19(6)					
433.4(1)	987(10)	824(30)	1.35(2)			1949	$6^+ \rightarrow 4^+$
508.5(1)		33(6)					
513.2(1)	69(3)	143(8)	0.87(5)			6796	
517.0(1)	423(12)	382(11)	0.81(2)			4996	$17^+ \rightarrow 16^+$
545.1(1)	84(3)	161(9)	0.55(4)			6283	
560.2(1)	481(12)	342(11)	0.95(2)			5738	
572.0(1)		32(7)					
579.6(1)	28(3)	42(6)	0.87(8)			7245	
604.7(1)	72(4)	74(11)	0.87(22)			6342	
622.4(2)	671(14)	623(15)	1.36(2)			4318	$14^+ \rightarrow 12^+$
625.4(2)	60(4)	61(7)	1.24(6)			7609	
694.4(1)	1000(13)	1000(28)	1.35(2)			1515	$4^+ \rightarrow 2^+$
698.9(2)	58(4)	41(7)	1.31(16)			5177	$18^+ \rightarrow 16^+$
735.8(1)		32(7)					
781.7(1)	807(13)	678(17)	1.38(3)			3698	$12^+ \rightarrow 10^+$
821.0(1)	1000(13)	1000(28)	1.33(3)			821	$2^+ \rightarrow 0^+$
868.5(1)	1000(13)	742(20)	1.31(2)			2914	$10^+ \rightarrow 8^+$
903.7(1)		33(5)				5382	
913.9(2)		25(8)					
1058.1(2)	56(4)	36(9)	0.67(10)			5537	

to be continued

Table 3.4: continued

Eγ (keV)	Rel. γ-ray Intensity (^{28}Si,4n)	Rel. γ-ray Intensity (^{54}Fe,α2p)	ADO ratio	α_{tot}	Multi-polarity	Placement E_i(keV)	$I_i^\pi \rightarrow I_f^\pi$
1131.9(2)		22(8)					
1156.3(2)		40(9)				7439	
1228.8(3)		12(7)					
1240.4(3)		26(7)					
1273.5(3)		20(7)					

[a] For errors cf. Sect. 2.3.1
[b] Extracted from coincidence data.
[c] Coincidence intensity ratio I(37°)/I(79°) determined in sum gates of γ-transitions in coincidence with analysed γ-ray, cf. Sect. 2.4. Data originate from (^{28}Si,4n) reaction
[d] Determined from intensity balance
[e] Multipolarity listed when obtained from α_{tot} data, possible E2 contributions to M1 transitions not listed

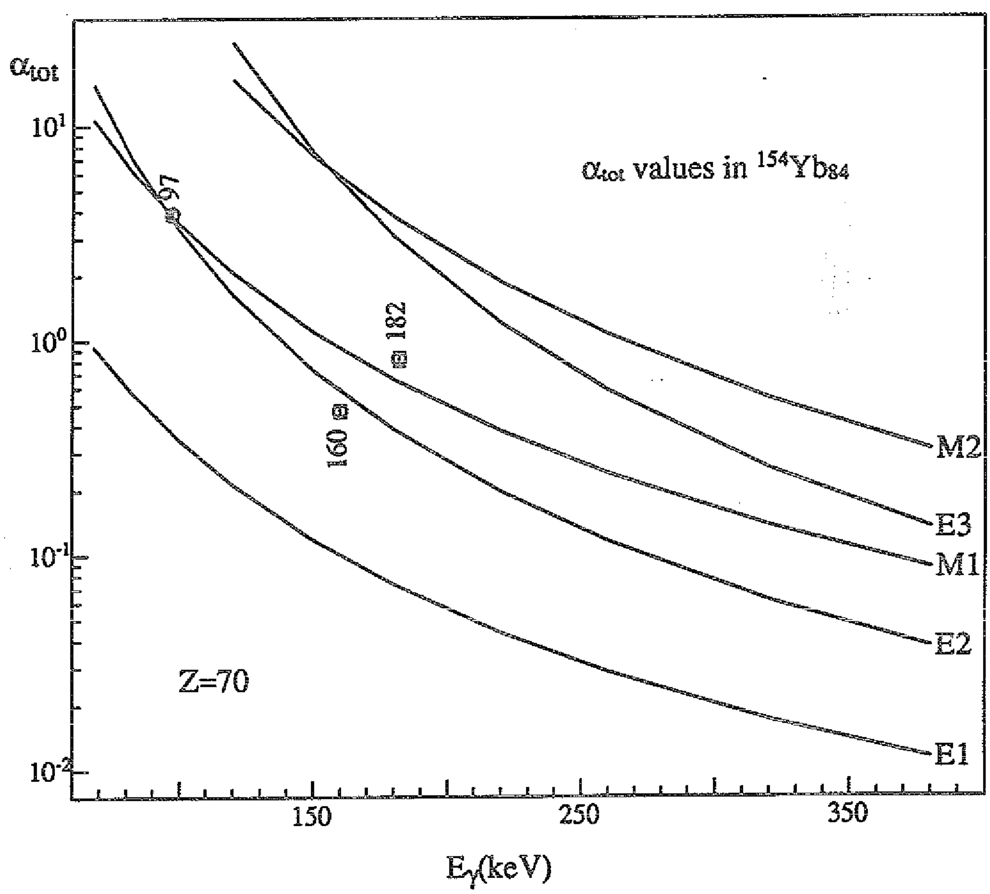

Fig. 3.4.3 Total conversion coefficients from intensity balance of transitions in ^{154}Yb.

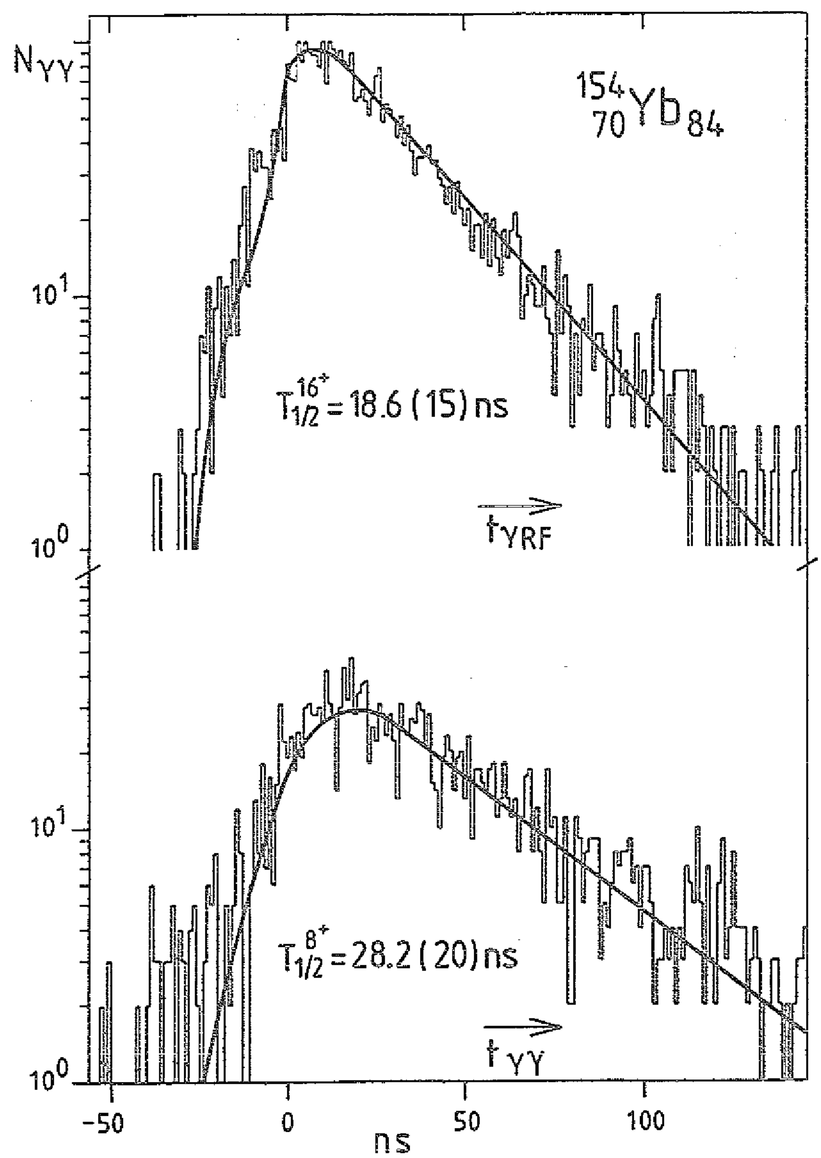

Fig. 3.4.4 Isomer half-lifes in ^{154}Yb. The upper curve displays $t_{\gamma RF}$ – data for the 622, 782, and 869 keV lines which were accepted only when in coincidence with other intense ^{154}Yb yrast transitions. The data points in the lower curve display $t_{\gamma\gamma}$ for the 9 possible pairs of intense γ-transitions with energy above 350 keV that have the 8^+ isomer between them. Both curves were analyzed by deconvolution with the pertinent prompt response function.

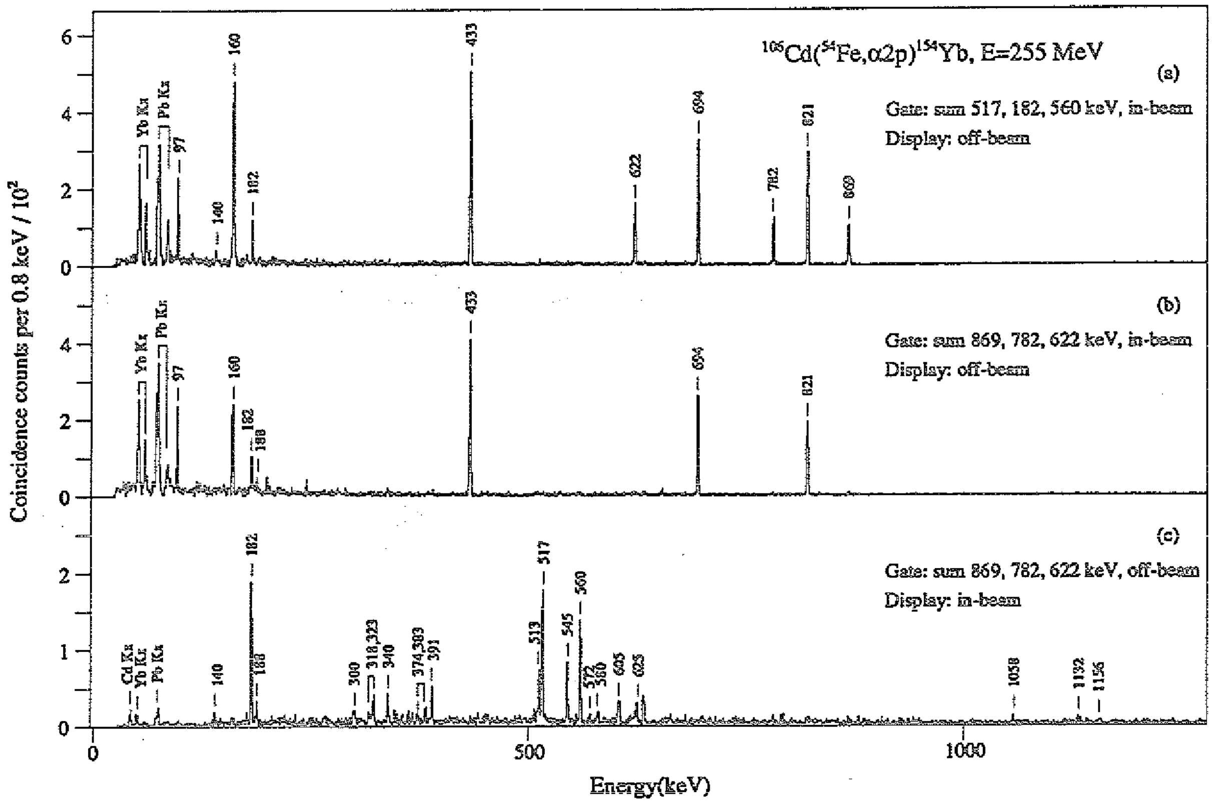

Fig. 3.4.5 Coincidence spectra for ^{154}Yb γ-rays with timing conditions chosen to locate the displayed γ-rays relative to the two isomeric states at $I^{\pi}=8^{+}$ and 16^{+}.

MeV from the M1 nature of the 182 keV $18^{+}\longrightarrow 17^{+}$ transition and the competing 699 keV cross-over γ-ray to the 16^{+} level which has stretched quadrupole character. This result is in significant contrast to the lower-Z doubly-even N=84 isotones where the E2 yrast cascade continues up to 18^{+}, as we will discuss below.

Moreover, a number of additional levels above the 18^{+} state are weakly populated and decay preferably to the main yrast states. Most of them are only established by a single de-excitation γ-ray and therefore remain tentative; only for three levels the excitation energies and spins are reasonably firm.

Finally, we assign the low-lying state at 3.228 MeV as $11^{(-)}$ from the level energy systematics to be discussed below and in accord with the measured dipole nature of the 314 keV sole de-excitation γ-ray.

4 Shell Model Analysis

We will discuss the observed high-spin states in the four N=84 isotones in terms of multiparticle shell model configurations. It will be shown that the $\pi h^n_{11/2}\nu f^2_{7/2}$ and $\pi h^n_{11/2}\nu f_{7/2}h_{9/2}$ configurations up to their respective maximun spins will be prominent in the lower part of the N=84 yrast lines. We base our identifications on the comparison with shell model calculations which reveal irregular seniority for the $h_{11/2}$ protons in the $\pi h^n\nu fh$ yrast line, in agreement with our data. For levels with opposite parity configuration assigments are less straightforward and may involve the 3^- core excitation, but we can suggest such assignments in cases where they are well supported by the comparison with excitations in neighbouring nuclei which involve similar configurations.

4.1 Multiparticle shell model calculations

We calculate the N=84 yrast states in terms of angular momentum coupled multinucleon configurations as implemented by the shell model. As it is often done in shell model calculations for heavy nuclei we use empirical values for the single particle energies and the residual nucleon-nucleon interactions.

The input data needed to calculate our configurations can be found in spectroscopic data for the two one-nucleon nuclei ^{147}Tb and ^{147}Gd, and for the three two-particle neighbours of ^{146}Gd, namely ^{148}Gd, ^{148}Tb, and ^{148}Dy(see Fig. 4.1.1). They are listed in Table 4.1, where also the references are given, and also shown in Fig. 4.1.2. The $\pi h_{11/2}$ single particle state lies at 51 keV in ^{147}Tb, and the $\nu f_{7/2}$ and $\nu h_{9/2}$ single particle energies are represented by the $7/2^-$ ground state and the 1397keV $9/2^-$ state in ^{147}Gd. The two-body interactions are taken from the respective two-body multiplets. The $\pi h_{11/2}\pi h_{11/2}$ interaction is fully specified by the six lowest even-parity yrast states of ^{148}Dy with spins 0 to 10. The $\nu f_{7/2}\nu f_{7/2}$ two-nucleon interactions, similarly, are observed in ^{148}Gd as the four lowest positive-parity yrast excitations with 0 to 6. Of the 1^+ to 8^+ eight-level $\nu f_{7/2}\nu h_{9/2}$ multiplet only the three highest members are identified in experiment; the interactions for the low spin members should be moderate and we use the estimated excitation energies as specified. In the odd-odd ^{148}Tb nucleus the eight members of the $\pi h_{11/2}\nu f_{7/2}$ multiplet were all identified in in-beam experiments by J. Styczen et. al, whereas it was much more difficult to see the $\pi h_{11/2}\nu h_{9/2}$ states. The 1^+ coupling is firmly identified at 620 keV in ^{148}Dy $(\pi h^2_{11/2})0^+ \longrightarrow$ ^{148}Tb $(\pi h_{11/2}\nu h_{9/2})1^+$ GT-decay, but the other members lie at~1.5 MeV excitation, and the in-beam experiments could only establish candidates for the 10^+, 9^+ and 8^+ members, while the six remaning excitation energies for I=2^+ to 7^+ are estimated.

Yb			$\pi h^6\nu fh$ $\pi h^6\nu f^2$
Tm			$\pi h^5\nu fh$ $\pi h^5\nu f^2$
Er			$\pi h^4\nu fh$ $\pi h^4\nu f^2$
Ho			$\pi h^3\nu fh$ $\pi h^3\nu f^2$
Dy	$\pi h\pi h$		
Tb	πh	$\pi h\nu h$ $\pi h\nu f$	
Gd	Core	νh νf	$\nu f\nu h$ $\nu f\nu f$
	82	83	84

Fig. 4.1.1 The four N=84 isotones investigated in this thesis with their yrast line configurations, and the one- and two-valence particle nuclei of ^{146}Gd giving the input data for the shell model calculations.

These input data fully specify all dynamic quantities needed for the shell model analysis. Our theoretical treatment thus reduces exclusively to the calculation of the angular momentum recoupling which is exact. With all dynamic input quantities taken from measured (or in some cases previously adopted) level energies it is obvious that our calculation is strictly parameter-free.

It furthermore is apparent that our calculation ignores configuration mixing (since the numerous off-diagonal (inter-configuration) matrix elements can not be extracted from accessible experimental data), and that we calculate relative excitation energies only. Absolute excitation energies can in principle be calculated with incorporation of the ground state masses, but practically the experimental error of this mass term becomes unusefully large and we therefore normalize our calculated level energies to the nuclear ground state.

The calculations were carried out with the angular momentum recoupling part of the OXBASH shell model code [Oxb 85], and the results for the two configurations in the four N=84 isotones (see Figs. 4.2.1 to 4.2.4) were obtained from separate matrix diagonalizations for both configurations and all spin values from the ground state up to the maximum aligned state. The matrix dimensions are indicated in the figures showing the results.

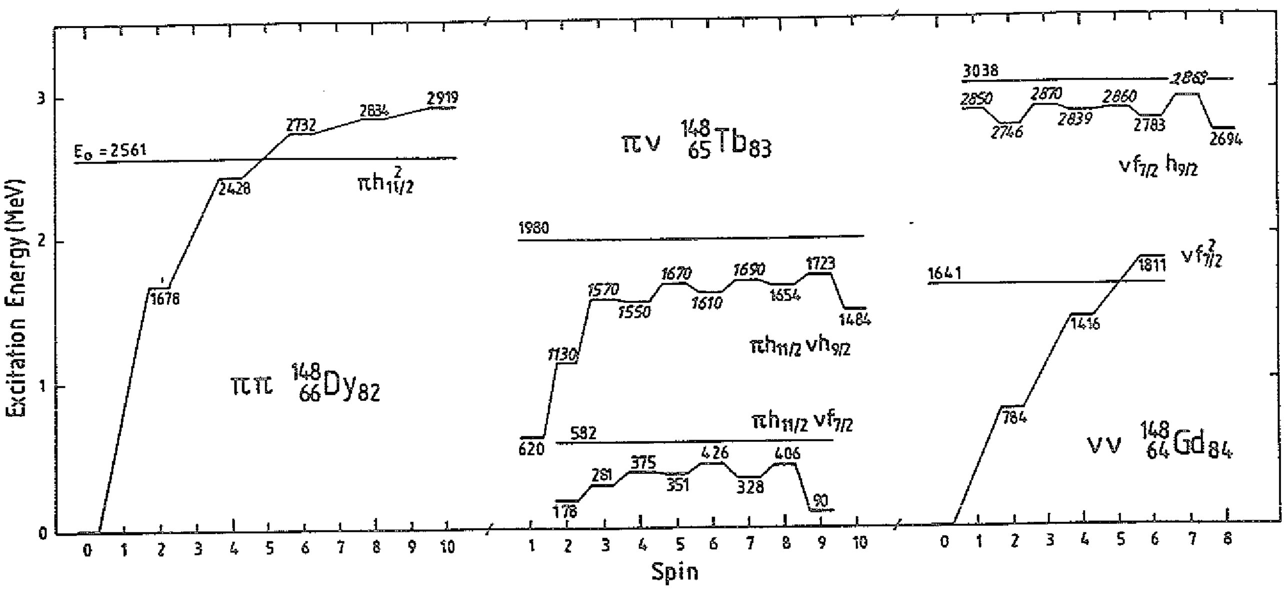

Fig. 4.1.2 Two-nucleon multiplets in ^{148}Dy, ^{148}Tb, and ^{148}Gd specifying the two-body interactions used in the shell model calculations. Observed excitation are given in keV, in skew numbers when estimated.

Table 4.1: Two-body residual-interaction and single particle energies used in the present shell model calculations

Configuration	Spin I^{π}	Excit. energy (keV)	Nucleus	Ref.
$\pi(h_{11/2})^2$	0^+	0	^{148}Dy	Dal 80
	2^+	1678		Dal 80
	4^+	2428		Dal 80
	6^+	2732		Dal 80
	8^+	2834		Dal 80
	10^+	2919		Dal 80
$\nu(f_{7/2})^2$	0^+	0	^{148}Gd	Pii 90
	2^+	784		Pii 90
	4^+	1416		Pii 90
	6^+	1811		Pii 90
$\nu f_{7/2} \nu h_{9/2}$	1^+	2850*	^{148}Gd	Men 91
	2^+	2746*		Men 91
	3^+	2870*		Men 91
	4^+	2839*		Men 91
	5^+	2860*		Men 91
	6^+	2783		Pii 90
	7^+	2869		Col 93
	8^+	2694		Pii 90
$\pi h_{11/2} \nu f_{7/2}$	2^+	178	^{148}Tb	Sty 87
	3^+	281		Sty 87
	4^+	375		Sty 87
	5^+	351		Sty 87
	6^+	426		Sty 87
	7^+	328		Sty 87
	8^+	406		Sty 87
	9^+	90		Sty 87
$\pi h_{11/2} \nu h_{9/2}$	1^+	620	^{148}Tb	Sty 87
	2^+	1130*		Sty 92
	3^+	1570*		Sty 92
	4^+	1550*		Sty 92
	5^+	1670*		Sty 92
	6^+	1610*		Sty 92
	7^+	1690*		Sty 92
	8^+	1654		Sty 92
	9^+	1723		Sty 92
	10^+	1484		Sty 92
$\pi h_{11/2}$	$11/2^-$	51	^{147}Tb	Lia 87
$\nu h_{9/2}$	$9/2^-$	1397	^{147}Gd	Led 78
$\nu f_{7/2}$	$7/2^-$	0	^{147}Gd	Led 78

*, Estimated energy

Table 4.1: Continued

Configuration	Spin I^π	Excit. energy (keV)	Nucleus	Ref.
$\pi h_{11/2} \pi d_{3/2}$	4^-	2995	^{148}Dy	Tai 89
	5^-	3172		Tai 89
	6^-	3323		Tai 89
	7^-	2739		Tai 89
$\pi d_{3/2} \nu f_{7/2}$	2^-	0	^{148}Tb	Sty 87
	3^-	714		Sty 87
	4^-	596		Sty 87
	5^-	496[a]		Sty 87
$\pi d_{3/2}$	$3/2^+$	253	^{147}Tb	Nag 81

a, the $(\pi d_{3/2} \nu f_{7/2})5^-$ excitation, originally given in Ref. [Sty 87] at 345 keV, was changed to the 5^- level at 496 keV [Sty 93]

4.2 Configuration assignments

The in-beam experiments have firmly identified in the N=84 isotones of Ho, Er and Tm (Figs. 4.2.1 to 4.2.3) sequences of high-spin levels with firm spins and parities at energies very close to the calculated yrast states of the $\pi h^n_{11/2} \nu f^2_{7/2}$ and $\pi h^n_{11/2} \nu f_{7/2} h_{9/2}$ configurations ranging from the ground state up to their maximum spins. In ^{154}Yb (Fig. 4.2.4), the highest(I^π=26$^+$) state is not observed, and the proposed candidates for the states with I >18 are tentative as their parities are unclear. We note that throughout all cases the agreement of theory with experiment is excellent, in particular having in mind the elementary nature of our theoretical calculation. For the $\pi h^n \nu f^2$ families the average (and maximum) deviations of theory from experiment are between 30 and 60 keV (below 100 keV); the corresponding numbers for the $\pi h^n \nu fh$ levels are between 70 and 150 keV (below 280 keV).

The slightly increased deviations in the latter case are in part related to the constant value of 1397 keV for the $\nu h_{9/2}$ single particle energy used in all four calcula-

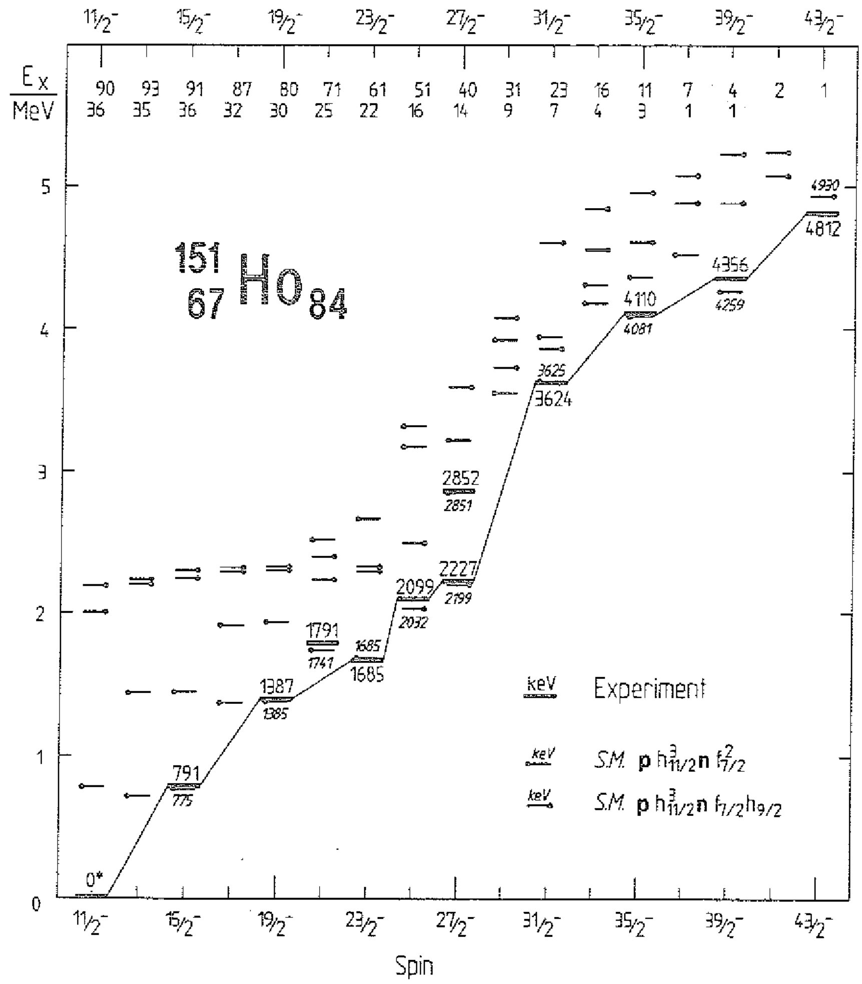

Fig. 4.2.1 The observed ^{151}Ho high-spin states compared to results from shell model calculations. For each spin value the two lowest states of the $\pi h^3_{11/2}\nu f^2_{7/2}$ and $\pi h^3_{11/2}\nu f_{7/2}h_{9/2}$ configurations are shown. Specified on top are the dimensions for the matrix diagonalizations at each spin value.

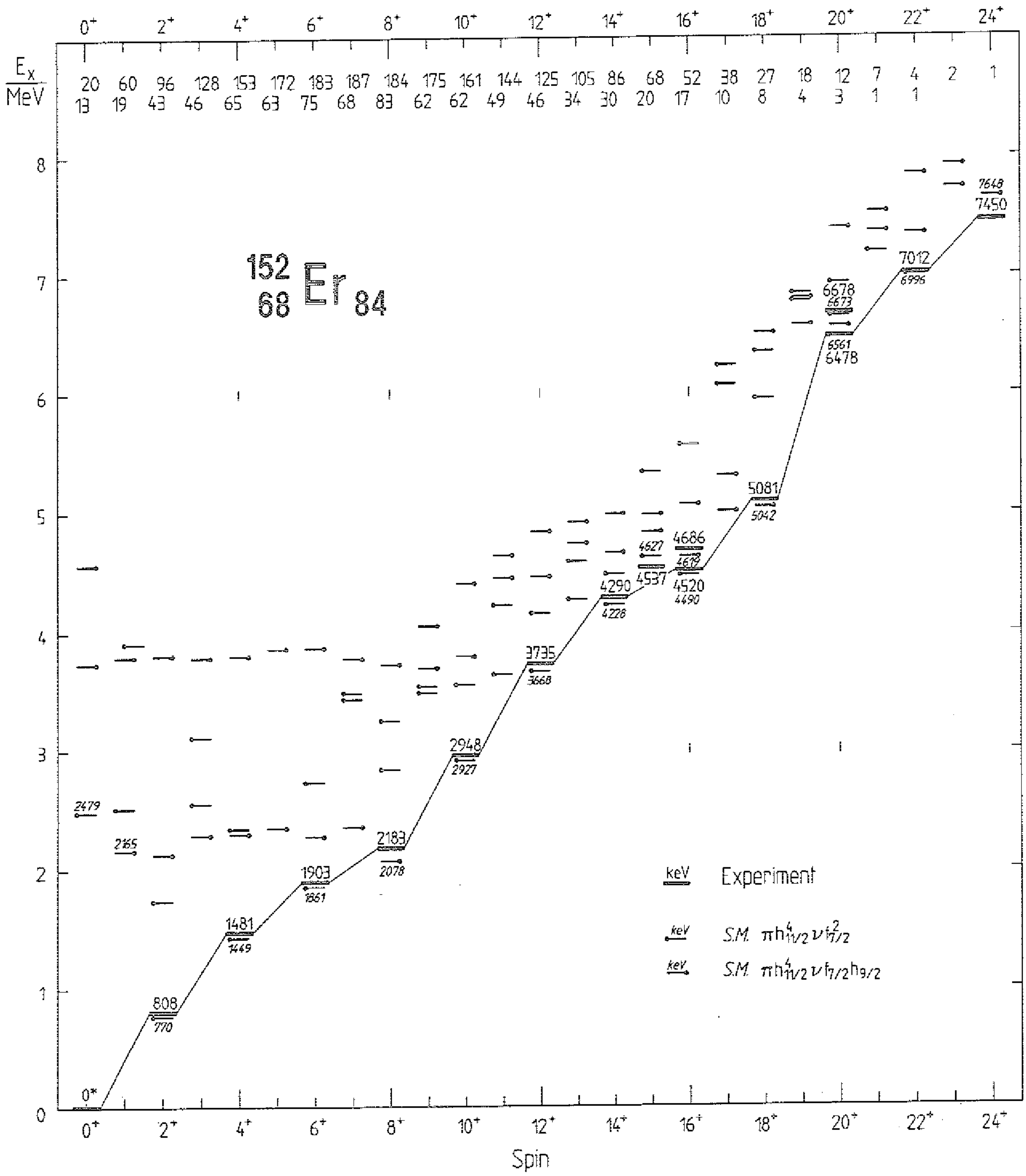

Fig. 4.2.2 The observed ^{152}Er high-spin states compared to results from shell model calculations (cf. caption to Fig. 4.2.1).

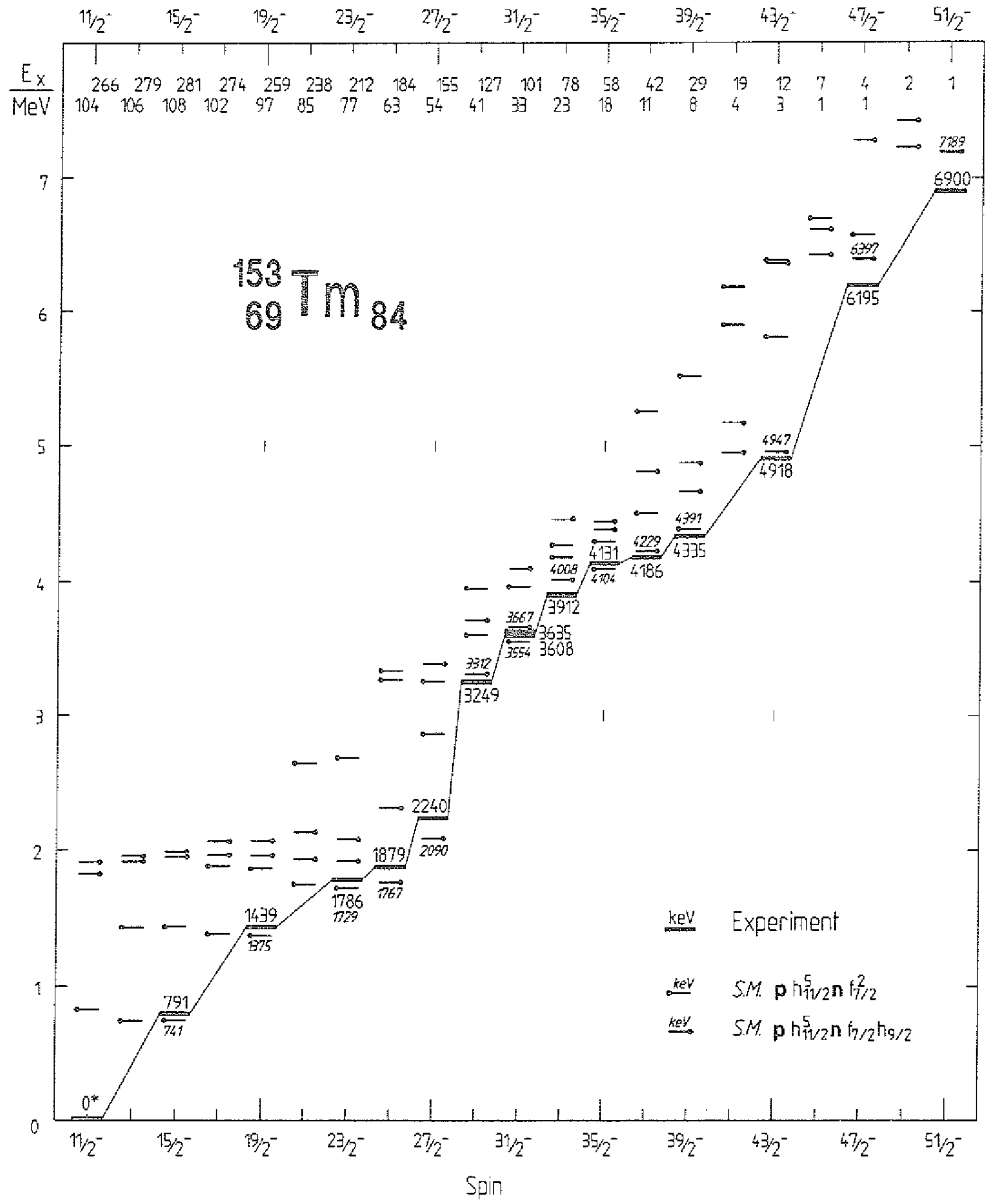

Fig. 4.2.3 The observed ^{153}Tm high-spin states compared to results from shell model calculations (cf. caption to Fig. 4.2.1).

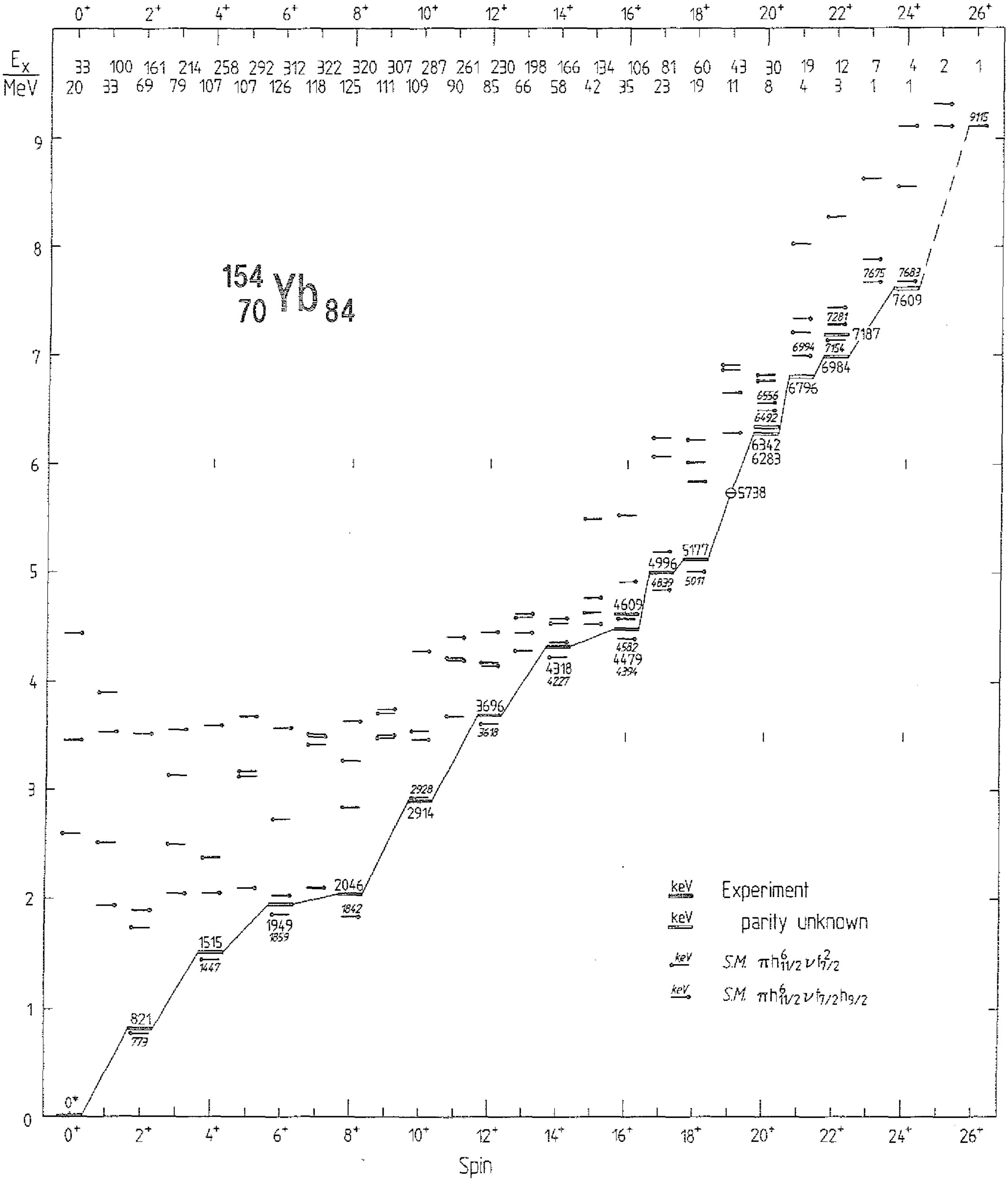

Fig. 4.2.4 The observed ^{154}Yb high-spin states compared to results from shell model calculations (cf. caption to Fig. 4.2.1).

tions. Adjustments between −9 keV and −37 keV would reproduce the 6^+ to 8^+ in the even-Z, and the equivalent $23/2^-$ to $27/2^-$ separations in the odd-Z cases, which would result in better overall agreement with experiment for the $\pi h^n \nu fh$ states. Thus, a −19 keV $\nu h_{9/2}$ energy adjustment would be required for ^{154}Yb to reproduce the observed 98 keV E2 decay of the 8_1^+ state, while from Fig. 4.2.4 it would be an α–decay isomer. Such minute alterations are definitely below the expected accuracy of the bare $h_{9/2}$ single particle energy as measured in ^{147}Gd when up to 6 protons are added to it. Still, we prefer to show theoretical energies obtained with constant $\nu h_{9/2}$ energy for the sake of simplicity, despite the unfortunate calculated 8_1^+ energy for ^{154}Yb.

Another apparent mismatch occurs for the calculated maximum spin state within the $\pi h^n \nu fh$ configuration. It lies 100 to 300 keV above the measured energy, significantly more than the average deviation in the configuration. This effect can be related to a similar difficulty encountered already in the pure valence proton nuclei at N=82, which might relate it to the $\pi h_{11/2}^2$ two-body matrix elements. The effect has also been traced in N=83 nuclei [McN 86], and corresponding data are available for Er and Ho. In Fig. 4.2.5 we have compiled the data for the Tm nuclei with 82 to 84 neutrons and indicate the difference for the calculated and measured energy separation of aligned states formed with maximum and maximum−2 seniority of the protons. In Tm, the associated $I_{max}-2$ states are also lower and shown in the figure to have similar but slightly smaller disagreement. Corresponding data for the Er and Ho isotones are compiled in the Table 4.2 and reveal the systematic occurence of the effect, which supports the configuration assignment despite the unusually large deviation of up to 300 keV from the theoretical energy.

Having moreover in mind that the calculated yrast levels of the two configurations are usually clearly separated from the next higher level of the same spin parity, and similarly that in experiment the assigned states are well isolated from alternate candidates, we conclude that our configuration assignments are firm. In the six cases, where theory predicts the next higher-lying state within less than 200 keV of the yrast level we have indeed identified the two states, although in a few cases (at

$I^{\pi}=20^{+}$ and 22^{+} in ^{154}Yb) the configuration assignments are tentative as the level parities are not measured.

An important result of our studies is the distinct qualitative difference of the yrast lines in the two configurations (Figs.4.3.2, 4.3.3). In all four nuclei the $\pi h^n \nu f^2$ yrast line is quite smooth while the $\pi h^n \nu fh$ yrast line has more pronounced dips related to the breaking of a proton pair. This effect is in quantitative agreement with the shell model results and we will discuss it in the following section.

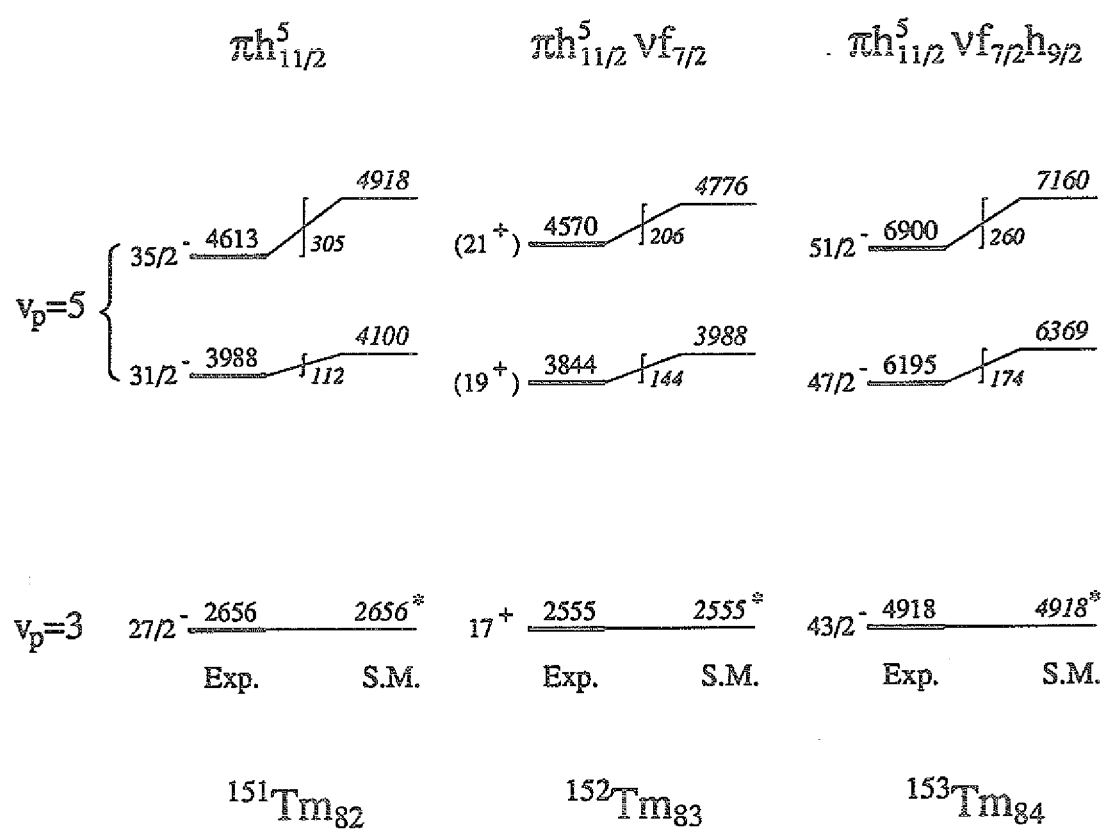

Fig. 4.2.5 The v_p=5 $\pi h^5_{11/2}$ excitations in Tm nuclei with 82,83,or 84 neutrons compared to values calculated from the shell model relative to the corresponding maximum aligned v_p=3 states.

Table 4.2: Observed energy separations of the maximum aligned v_p=n and v_p=n-2 states in $\pi h^n_{11/2}$ nuclei with 0, 1, or 2 valence neutrons compared to results from shell model calculations.

N=		82			83			84		
		$I_{max}^{v_p=n}$	$I_{max}^{v_p=n-2}$	$\Delta E_{Exp.}-\Delta E_{SM}$	$I_{max}^{v_p=n}$	$I_{max}^{v_p=n-2}$	$\Delta E_{Exp.}-\Delta E_{SM}$	$I_{max}^{v_p=n}$	$I_{max}^{v_p=n-2}$	$\Delta E_{Exp.}-\Delta E_{SM}$
Tm	5	35/2	27/2	-305	21	17	-206	51/2	43/2	-260
Er	4	16	10	-241	39/2	27/2	-----	24	18	-237
Ho	3	27/2	11/2	-119	17	9	-79	43/2	27/2	-147

4.3 Characteristic properties of the $\pi h^n_{11/2}\nu f^2_{7/2}$ and $\pi h^n_{11/2}\nu f_{7/2}h_{9/2}$ yrast lines

The two multiparticle configurations which are prominent in the yrast lines of our nuclei from the ground state up to 4 –10 MeV excitation clearly reflect the features of the yrast spectra for the n valence protons and the two valence neutrons. The valence proton spectra for two to six $h_{11/2}$ particles are well known from calculations[Law 81] based on the $^{148}_{66}Dy_{82}$ ($\pi h^2_{11/2}$) 0^+ to 10^+ level energies, which reproduce the experimental energies quite well. They have pure $\Delta I=2$ yrast sequences, with characteristic j^n-type energy spacings, but extend up to respectively higher spins for increasing proton number. These calculated energies are shown in Fig. 4.3.1.

The characteristic energy spectra of the always two valence neutrons present in our nuclei are shown to the right. While the two $f_{7/2}$ particles form a regular even-spin 0^+ to 6^+ yrast sequence up to 1.8 MeV, the $f_{7/2}h_{9/2}$ family has essentially only one single 8^+ yrast state, ~0.9 MeV above the νf^2 6^+ level. The remaining 1^+ to 7^+ f h couplings all lie in the energy range up to 0.2 MeV above it (Fig. 4.1.2), and are not significant for the yrast line.

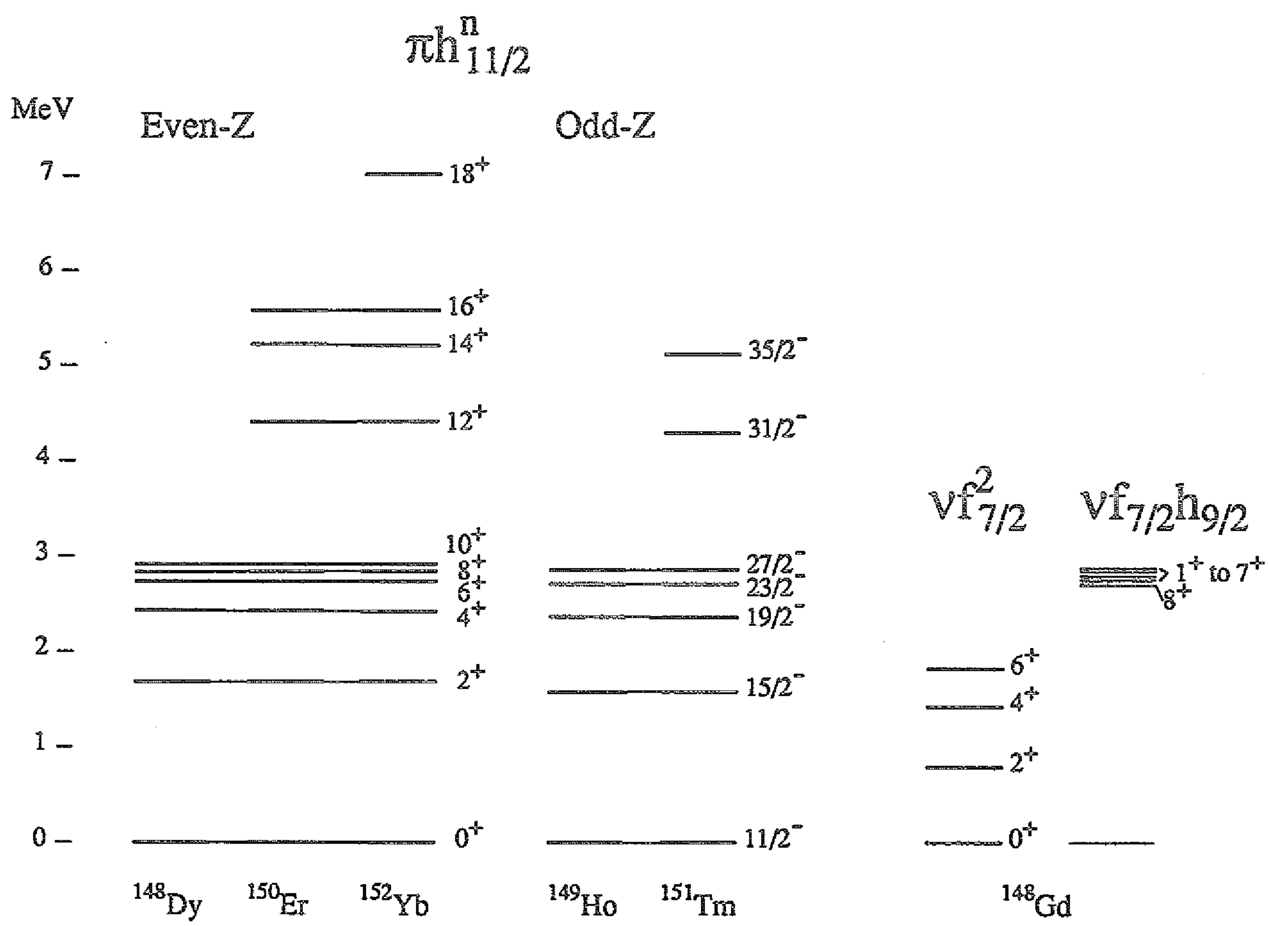

Fig. 4.3.1 Calculated $\pi h^n_{11/2}$ yrast spectra relevant for the $\pi h^n \nu^2$ yrast lines at N=84, and the $\nu f^2_{7/2}$ and $\nu f_{7/2} h_{9/2}$ two-particle spectra.

We therefore expect that the multinucleon $h^n f^2$ yrast lines will always reveal the three νf^2 $\Delta I=2$ spacings that are much smaller than those of the protons, while the $\pi h^n \nu fh$ yrast line will more closely follow the πh^n $\Delta I=2$ separations. These ideas are also summarized in the Fig. 1.2 shown in the introduction to this thesis. Important modifications of this first order picture will be caused by the proton-neutron two-body interaction. These effects will give rise to interesting new structure features which we will discuss below.

4.3.1 The $\pi h^n_{11/2}\nu f^2_{7/2}$ yrast line

The yrast lines of the $\pi h^n_{11/2}\nu f^2_{7/2}$ configuration in the N=84 isotones represent an example for an unusually regular yrast sequence in spherical nuclei. In the Fig. 4.3.2 we show the calculated configuration yrast lines for the six nuclei, where they are experimentally well investigated, separated for even-Z and odd-Z.

From the Figs. 4.3.1 and 4.3.2 it is apparent that in the even-Z isotones the two $f_{7/2}$ valence neutrons will form the lowest 2^+ excitation and the following states up to 6^+. For the pure $\pi h^n \nu f^2$ configuration the two next states are the dominant $(\pi h^2 \nu f^2_0)8^+$ and 10^+ levels, where the former, however, is bypassed in the yrast decay, which proceeds through the below-lying $(\nu fh)8^+$ state(Figs. 4.2.2, 4.2.4). From 10^+ to 16^+ the states have more dominant $\pi h^2_{10}\nu f^2_{0\,to\,6}$ character, and above 16^+ the next proton pair must be activated to form the spins 18 to 24 involving the 12^+ to 16^+ yrast states of ${}^{152}_{68}Er_{82}$, with the neutrons largely in 6^+ coupling. Again the $(\pi h^4_{12}\nu f^2_6)18^+$ level lies much above the $(\pi h^2_{10}\nu fh_8)18^+$ state which receives the entire yrast decay intensity. The 24^+ yrast state becomes available in Yb, with $18\hbar$ angular momentum from the six protons (Fig. 4.2.4). The pure proton character of the yrast line steps above 16^+ becomes apparent from the accurate energy agreement with the ^{152}Yb yrast states that are included in the figure normalized at the $(\pi h^6_{10}\nu f^2_6)16^+$ level.

The yrast lines built on the $\pi h_{11/2}$ ground state of the odd-Z nuclei are principally very similar, with the natural difference that here the maximun aligned seniority v_p=3 $27/2^-$ proton state can directly connect through a single E2 to the v_p=1 $(h_{11/2}\,\nu f^2_6)23/2^-$ state. Above the $(\pi h^3_{27/2}\nu f^2_6)39/2^-$ state further angular momentum can only be gained by breaking the last proton pair in Tm. Analogous as in the even nuclei, the yrast decay bypasses the $(\pi h^3_{27/2}\nu f^2_0)27/2^-$ and $(\pi h^5_{31/2}\nu f^2_6)43/2^-$ states (Figs. 4.2.1, 4.2.3), and proceeds through the lower states with the same spin formed with the $(\nu fh)8^+$ coupling.

A remarkable finding in our full shell model calculations is that the respective por-

Table 4.3.1: The energy differences (in keV) between corresponding νf^2 states in different N=84 nuclei as observed in experiment and as calculated from the shell model

Spin		2	4	6	10	12	14	16	18	20	22
Scatter	Exp.	18	58	98	112	139	47	89			16
	S.M.	3	11	13	31	133	9	194	68	85	215
Spin		15/2	19/2	23/2	27/2	31/2	35/2	39/2			
Scatter	Exp.	5	93	149		16	21	21			
	S.M.	99	16	94	15	98	23	132			

tions of the configuration yrast lines result to have essentially equal energies despite the variation in proton number from 2 to 6. This feature is borne out by experiment, where the $\pi h^n \nu f^2$ yrast lines up to 16^+ and $39/2^-$ have been completely identified except the one state above the νfh_8 coupling. The Table 4.3.1 gives the maximum energy differences ΔE_I between the calculated yrast states for the same spin I but in different odd-Z or even-Z nuclei, and compares them with the same differences obtained from exclusively the experimental data. These ΔE_I values found in experiment and calculation in general are quite similar, occasionally somewhat bigger in experiment than in our calculation that was limited to a single configuration.

4.3.2 The significant impact of the strong $(\pi h_{11/2} \nu h_{9/2})1^+$ attraction on the $\pi h^n_{11/2} \nu f_{7/2} h_{9/2}$ yrast line

The $\pi h^n_{11/2} \nu f_{7/2} h_{9/2}$ yrast lines at N=84 (Fig. 4.3.3) apparently differ much from those of the $\pi h^n_{11/2} \nu f^2_{7/2}$ configuration just discussed. The closer similarity with the pure N=82 πh^n excitations apparent here is a straightforward consequence of the sole 8^+

yrast state in the $\nu f_{7/2}h_{9/2}$ two-nucleon configuration. Naturally, the lowest state of these yrast lines is the $\pi h^n \nu fh_8$, and the yrast states at lower spins reflect the νfh 1^+ to 7^+ two-body interactions. $I^\pi=0^+$ can only be formed if a proton pair is broken.

Below spin 18 or 43/2 the entire yrast lines constantly drop in energy by a few 100 keV with the addition of each proton pair, and moreover, the calculations reveal local irregularities for the spins $25/2^-$, 16^+, and $37/2^-$. These features both are related to the strong $h_{11/2}h_{9/2}$ proton-neutron residual interaction, which on the average is much more attractive than in the $\pi h \nu f$ case, particularly for the $(\pi h \nu h)1^+$ coupling which has the large attraction of −1.4 MeV (cf. Fig. 4.1.2).

The energy shift for the entire yrast line directly reflects the increased binding of the $h_{9/2}$ neutron (relative to $f_{7/2}$) when proton pairs are added in the nuclei above Gd. This effect has quantitatively been studied in the even-Z N=83 nuclei, where the $\nu h_{9/2}$ single particle state has been observed from Gd up to Yb. The Fig. 4.3.4.a compares these data with a shell model calculation [Men 91] using the $\pi h \pi h$ and $\pi h \nu h$ two-body energies of Table 4.1. That the same effect is responsible for the shift at N=84 can be tested e.g. from the observed N=84 6^+ to 8^+ level energy spacings that should reflect the $\nu h_{9/2}$ energy at N=83, however modified by the νf^2_6 and νfh_8 residual interactions, which are expected to be constant. Therefore,

$$E_8 - E_6 = E_{9/2} + V_{f^2,6} + V_{fh,8}$$

or

$$E_8 - E_6 - E_{9/2} = V_{f^2,6} + V_{fh,8} \approx \text{const.}$$

For Gd, Dy, Er, and Yb we find the quite similar values of 514, 540, 522 and 470 keV for the sum of the two residual interactions. For the same differences calculated with the shell model the agreement is similarly good(Fig. 4.3.4.b), thus supporting the above interpretation.

In the intermediate range from spin 9 to 17, where one proton pair is broken, the

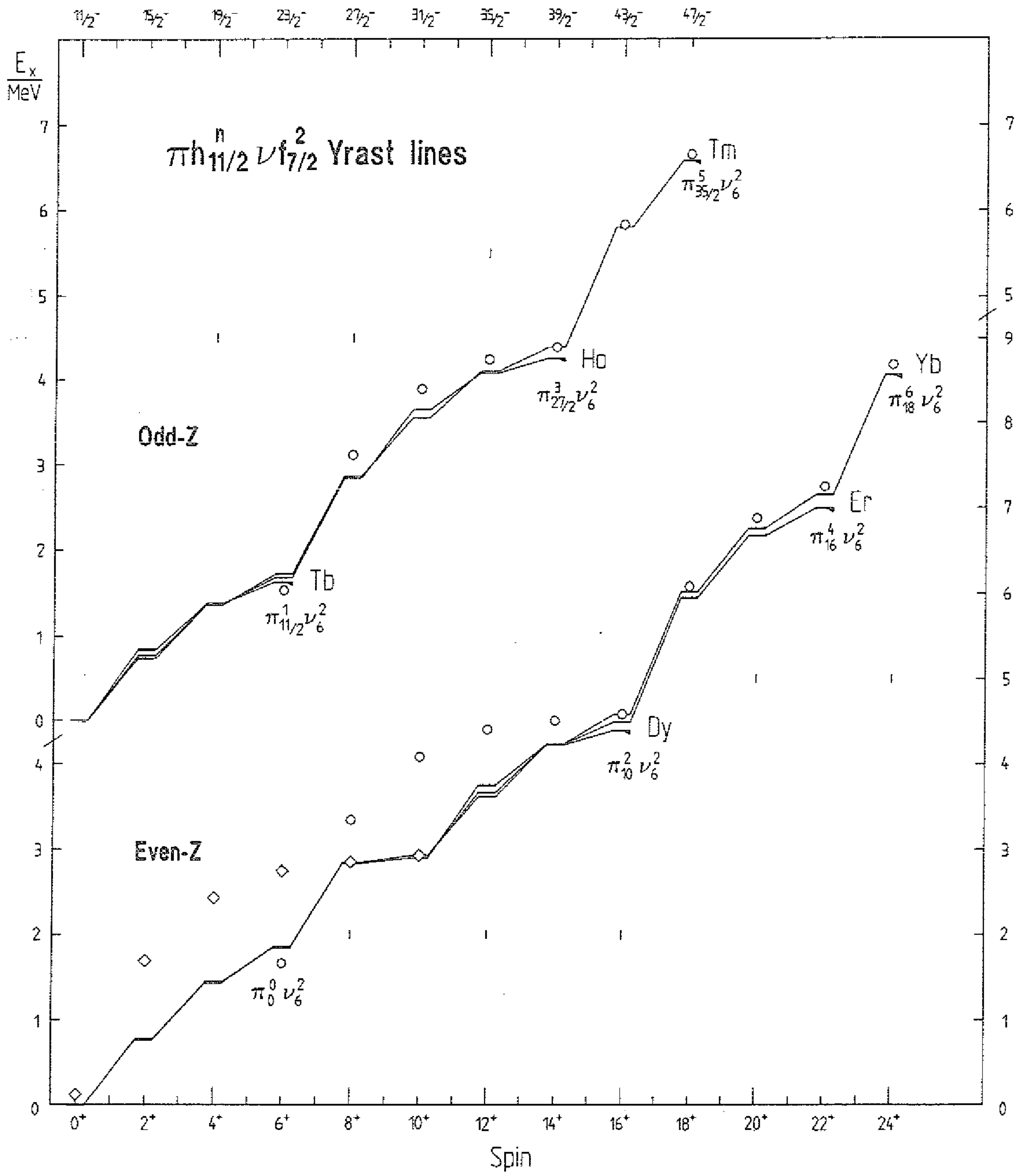

Fig. 4.3.2 Comparison of the $\pi h^n_{11/2}\nu f^2_{7/2}$ configuration yrast lines calculated for the six N=84 isotones from ^{149}Tb to ^{154}Yb. The calculated bare $\pi h^n_{11/2}$ yrast energies of ^{152}Yb and ^{151}Tm are shown as bubbles, normalized at the 16^+ and $39/2^-$ states at N=84. For even-Z, the 0^+ to 10^+ level energy sequence of ^{152}Yb is also given normalized at the N=84 10^+ energy (diamonds). Aligned valence particle configurations, and the elements for the respective yrast line terminations are indicated.

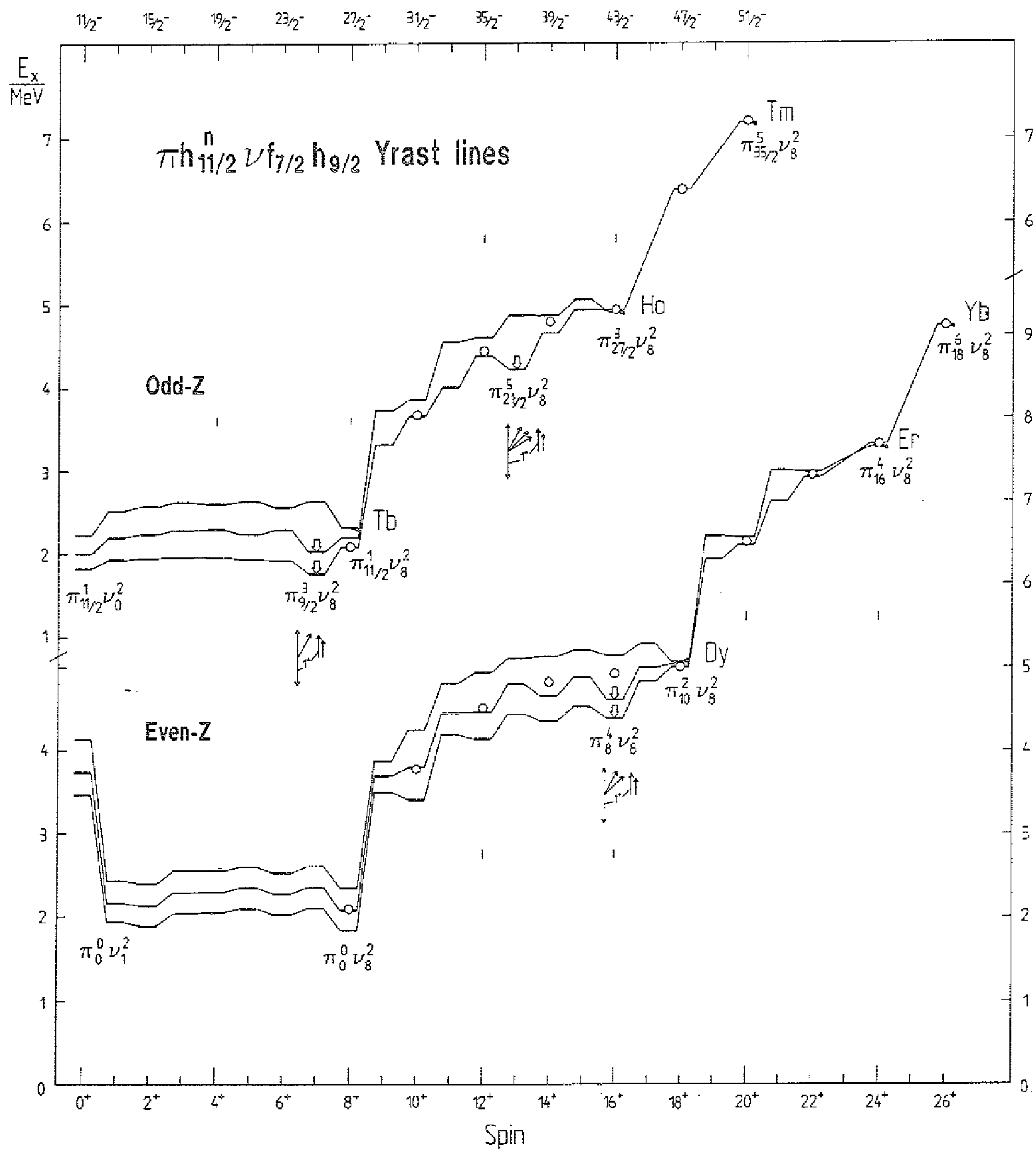

Fig. 4.3.3 Comparison of the $\pi h^n_{11/2}\, \nu f_{7/2} h_{9/2}$ configuration yrast lines calculated for the six N=84 isotones from ^{149}Tb to ^{154}Yb. The calculated bare $\pi h^n_{11/2}$ yrast energies for the N=82 nuclei ^{152}Yb and ^{151}Tm are shown as bubbles,normalized at the 18^+ and $43/2^-$ states at N=84. Elements for the respective yrast line terminations and aligned valenceparticle configurations are indicated, where the exponent to the proton gives the seniority v_p(rather than n). The seniority inverted states are marked by open arrows, and in each case the respective angular momentum vector diagram for the contributing valence particle is given,with the two neutrons in 8^+ coupling shown to the right.

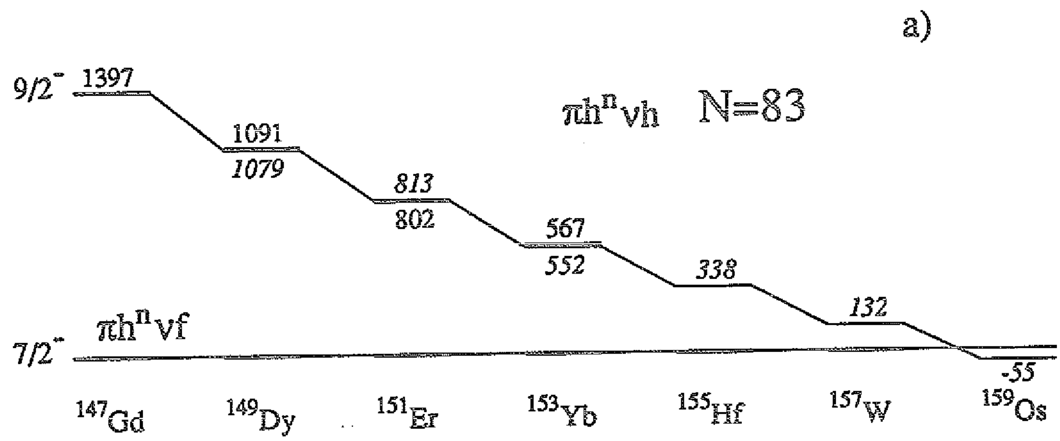

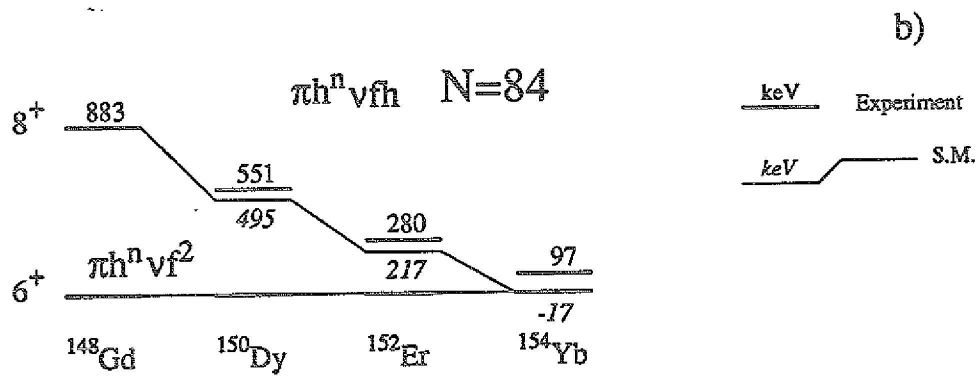

Fig. 4.3.4 a) The observed $\nu h_{9/2}$ states at N=83 compared to the results of multi-particle shell model calculations of the $\pi h^n \nu f$ and $\pi h^n \nu h$ configurations normalised at the $\nu f_{7/2}$ level (from Ref. [Men 91]).

b) The same comparison for the νfh_8 excitations above the νf_6^2 states in N=84 nuclei.

yrast energy displacement between the isotones scatters slightly more for two reasons: First, now two $h_{11/2}$ protons always occupy various combinations of two $h_{11/2}$ substates, and second, in this region the next-higher state of the same configuration lies much closer in energy than below spin 9 (Figs. 4.2.2, 4.2.4). Specifically, if the 11/2 substate is blocked, as e.g. in the 18^+ state with πh^2_{10}, the particularly strong $(\pi h \nu h)1^+$ interaction of –1.4 MeV cannot contribute to the $\nu h_{9/2}$ energy lowering, which greatly reduces the 18^+ energy shift between the isotones. Similar aguments hold for the four even spins above 18^+, for $43/2^-$ and principally also for the $27/2^-$ state.

In the effects considered so far, related to the lowering of the $\nu h_{9/2}$ energy, the interacting $h_{11/2}$ proton always is one member of a 0^+ pair, and therefore all the (unblocked) $\pi h \nu h$ residual attractions will contribute with their respective statistical weights to the energy shifts. There exist also cases where the $(\pi h \nu h)1^+$ attraction is selectively activated in the particular configuration of the state. Such cases are the strongly suppressed $25/2^-$, 16^+, and $37/2^-$ states of Fig. 4.3.3. They are of particular interest because these states drop down to the yrast line from the level family with next higher proton seniority.

The principle mechanism of this seniority inversion can be visualized in Fig. 4.3.5. It shows the maximum aligned states for the possible values of proton seniority v_p of the πh^n, $\pi h^n \nu h$, and $\pi h^n \nu h f_8$ configurations at N=82 to 84. For Tb, the respective configuration ground states are $\pi h_{11/2}$, $(\pi h \nu h)_{10}$, and $(\pi h_{11/2} \nu^2_8)_{27/2}$. In Dy v_p=2 allows spins up to 10^+, $29/2^-$, and 18^+, and no yrast state of v_p=2 occurs below the respective aligned v_p=0 level. The same rule holds for $^{149}Ho_{82}$, but it is violated in the N=83 and 84 neighbours when an $h_{9/2}$ neutron is present. This valence neutron can couple with the lowest lying v_p=3 j–1=$9/2^-$ state which is presented by the symbolic angular momentum vector diagrams shown on top of the figure. It is clear that an $h_{9/2}$ neutron can couple with the three proton structure to maximum spin 9, thus fully exploiting the $(\pi h \nu h)1^+$ attraction. Hereby, this v_p=3 state is lowered below the 10^+ v_p=1 yrast state. Of quite analogous nature is the $25/2^-$ v_p=3 state in ^{151}Ho which is observed 129 keV below the $27/2^-$ v_p=1 level.

The 9^+ v_p=3 and the presumably above lying v_p=1 10^+ states in $^{150}Ho_{83}$ have not yet been discovered, but in the ^{152}Tm and ^{154}Lu isotones [McN 86, McN 90], both the 10^+ and 9^+ states were observed. Their assignment as $\pi h^n \nu h$ states was based on the comparison with calculated energies using renormalized Schiffer-True[Sch 76] interactions, and their relative energies were interpreted in terms of the $\nu h_{9/2}$ energy lowering caused by the addition of proton pairs, which is partially blocked in the

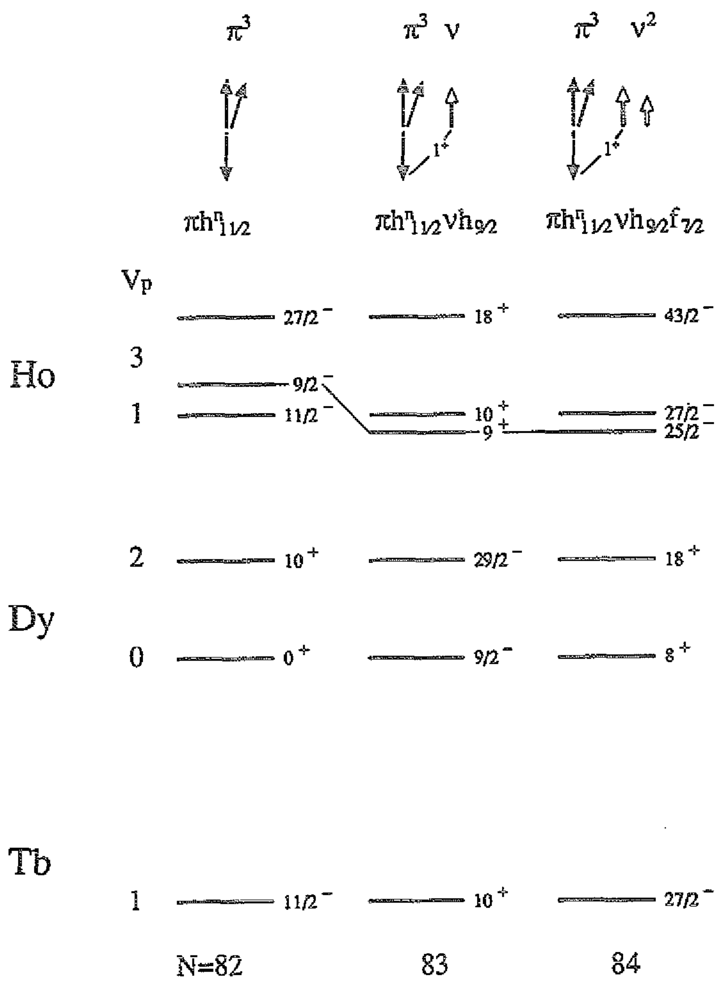

Fig 4.3.5 Proton seniority inversion in Ho and the principle $\pi h^n_{11/2} \nu h_{9/2}$ aligned yrast states for N=82, 83 and 84 nuclei. The figure displays that the v_p=3 $(h^3_{11/2})_{9/2}^-$ coupling in Ho drops down in energy below the v_p=1 $h_{11/2}$ state at N=83 and 84, where one $h_{9/2}$ neutron is present. This $h_{9/2}$ neutron couples with the anti-aligned $h_{11/2}$ proton, thus exploiting the $(\pi h_{11/2} \nu h_{9/2})1^+$ attraction.

10^+ coupling. Also the ^{151}Ho $25/2^-$ state is known since long [Giz 81] but no interpretation of its nature was so far forwarded.

From the above it is evident that seniority inverted yrast states should also occur in even-Z nuclei with at least 4 protons. Here, the v_p=4 proton structure with two anti-aligned $h_{11/2}$ protons, analogous to the 9/2 structure of ^{150}Ho, has spin 8, which together with the νfh_8 gives $I^\pi=16^+$, two units below the v_p=2 maximum aligned 18^+ level in the $\pi h^4 \nu fh$ configuration. In the present study we have identified in ^{154}Yb this v_p=4 ($\pi h^6_8 \nu fh_8$)16^+ state, which drops down in energy even below the v_p=2 ($\pi h^6_{10} \nu f^2_6$)16^+ level [Zha2 93]. In the ^{152}Er isotone two 16^+ states were observed [Kuh 92], and are supported by our data (Fig. 3.2.1), where the higher one is the v_p=4 ($\pi h^4_8 \nu fh_8$)16^+ seniority inverted state, 395 keV below the v_p=2 ($\pi h^4_{10} \nu fh_8$)18^+ level, but here still above the 16^+ level of νf^2 character.

Principally, a seniority inverted yrast state can be formed whenever an extra proton pair is still available to be activated, i.e when v_p can be increased by 2. Consequently, the ^{153}Tm$_{84}$ nucleus, with five $h_{11/2}$ valence protons, is the first case where a second inverted yrast state can occur. That state should be a v_p=5 $37/2^-$ level of the configuration $\pi h^5_{21/2} \nu fh_8$ and lie below the v_p=3 ($\pi h^5_{27/2} \nu fh_8$)$43/2^-$ aligned state assigned at 4.918 MeV. In experiment we have clearly identified this inverted state, at 4.186 MeV, 43 keV below its predicted energy (Fig. 4.2.3). This assignment is firm since the lowest ($\pi h^5 \nu f^2$)$37/2^-$ level is calculated at 4.506 MeV, significantly above the $39/2^-$ and $35/2^-$ neighbours of the same configuration, which both are populated in the yrast decay.

The only other case, where a second inverted state could occur is ^{154}Yb. Its nature is v_p=6 ($\pi h^6_{12} \nu fh_8$)20^+, and the state is expected at about 7 MeV excitation. Since however the configuration yrast line in this region is dominated by the steep 10^+ to 14^+ πh^6 yrast sequence (cf. Fig. 4.3.3), the expected 20^+ state will not form a configuration yrast pocket. Since in addition our data are marginal in that region we were not able to identify this higer seniority 20^+ state in our present experiment.

In the above discussions we have throughout based upon the shell model level ener-

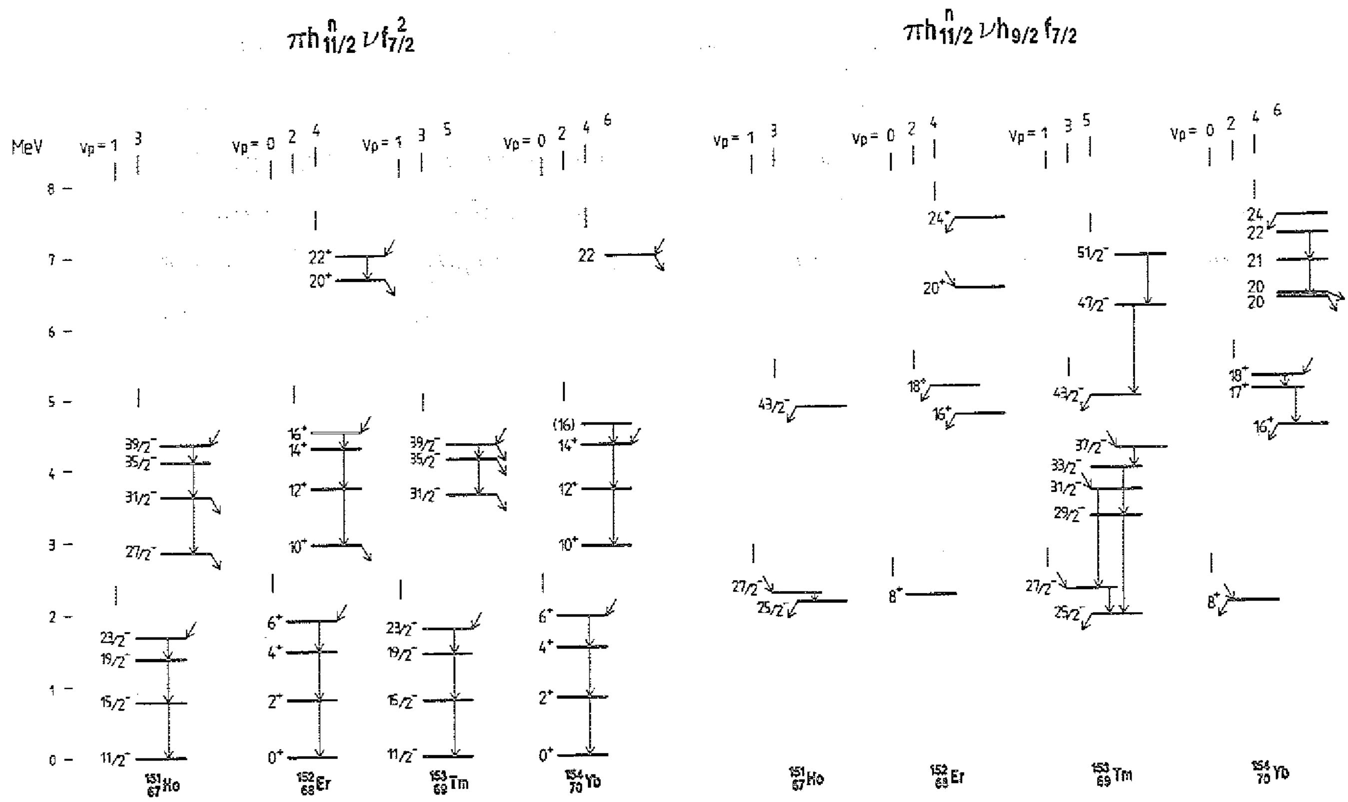

Fig. 4.3.6 Summary of the experimental results. The observed yrast states are shown with the yrast line sections for different proton seniority v_p horizontally displaced, and the main γ-decay of the levels indicated. The results for the $\pi h^{n}_{11/2}\nu f^{2}_{7/2}$ configuration (left) demonstrate the regular proton seniority increasing with higher spins, and the significant similarlity of the yrast states for the four isotones. The results for the $\pi h^{n}_{11/2}\nu f_{7/2} h_{9/2}$ configuration shown the five cases where seniority inversion occures.

gies of the two principle yrast configurations shown in Figs. 4.3.2 and 4.3.3 . Because of these complete level sequences it is more easy to recognize delicate systematic features and to discuss their structural significance. In the Fig. 4.3.6 our experimental data on these two multiparticle configurations are summarized. Naturally, the results for the $\pi h^{n}\,\nu f^{2}$ configuration, with smooth yrast line, and largely lying below the $\pi h^{n}\,\nu fh$ states, are more complete up to 4.5 MeV and confirm the predicted unusual similarity of these yrast lines in the isotones. For the fh configuration we obtained the best results in ^{153}Tm, the only nucleus where the fh configuration yrast line is calculated to lie below the f^2 yrast states over a wide range of spins(Fig. 4.2.3). In our experiments on the N=84 isotones we have found all 8 states predicted in the four nuclei where the νfh_8 attraction causes a dip in the yrast line, with the spins 8^+, $27/2^-$, 18^+ , $43/2^-$,and 24^+. A new discovery in this study is the systematic idenfication of the seniority inverted yrast states at their calculated energies and spins, of $25/2^-$ in ^{151}Ho and ^{153}Tm, 16^+ in ^{152}Er and ^{154}Yb, and also $37/2^-$ in ^{153}Tm which is the first nucleus where a second inverted yrast state becomes possible.

5 Low-Lying High-Spin States of Opposite Parity

The yrast states discussed in the previous section, formed by the valence protons in $h_{11/2}$, and the two valence neutrons in $f_{7/2}$ or $h_{9/2}$, have positive parity in the even-A, and negative parity in the odd-A nuclei, and our results have shown that these configurations dominate the N=84 yrast decay. There are three possibilities to form high-spin configurations of opposite parity at low excitation, which however are limited to lower maximum spin and are in general not strongly fed in the yrast cascade.

First, one valence proton particle can be displaced from the $h_{11/2}$ into $s_{1/2}$ or $d_{3/2}$ orbital. These $\pi h^{n-1}_{11/2}\pi d_{3/2}$ and $\pi h^{n-1}_{11/2}\pi s_{1/2}$ configurations form respectively 7^- and 5^-, or in odd-A nuclei $23/2^+$ and $19/2^+$ states that are well known yrast levels in the N=82 isotones [Dal 80, Wil 80, Chu 84, McN 86, Nol 82].

Another possibility is the promotion of one valence neutron into the $i_{13/2}$ orbital, the only remaining high-spin single particle state of the 82 to 126 major shell. This orbital however couples with a large matrix element (−0.8MeV) to the $\nu f_{7/2}\times 3^-$ core excitation. The effect has been extensively discussed [Pii 90], and essentially precludes to recoginize such levels as simple multiparticle configurations.

The only remaining possibility to form low-lying opposite parity states is to invoke core excitations across the Z=64 proton gap, where the 3^- octupole state has the lowest energy. But at N>82 these excitations are complicated through the mixing with the $i_{13/2}$ neutron state as just pointed out.

In the even-Z N=84 nuclei firmly assigned negative parity states do not occur below 5 MeV, but in the odd-Z ^{153}Tm, and probably also in ^{151}Ho, groups of opposite parity states are observed in the region above 2.5 MeV. Of the odd-parity two-proton particle excitations the stretched $\pi h_{11/2}\pi d_{3/2}$ 7^- state should be quite pure since no other 7^- state lies close-by. The two-body matrix elements to calculate the expected $(\pi h^{n-1}_{11/2}\, d_{3/2}\, \nu f^{2}_{7/2})35/2^-$ states in odd-Z N=84 nuclei are all known from the $\pi d_{3/2}\nu f_{7/2}$ and $\pi d_{3/2}\pi h_{11/2}$ quartets observed in ^{148}Tb and ^{148}Dy, which are also listed in Table 4.1. In the Fig. 5.1 we show the calculated energies for the N=82 to 84 Ho and Tm isotopes with none, one, or two $f_{7/2}$ valence neutrons, where one of the valence protons is in $d_{3/2}$. The calculated $(\pi h^{n-1} d\, \nu f^2)35/2^+$ energies for the two N=84 isotones are in good agreement with observed $35/2^+$ states in Ho and Tm, where however only in Tm the parity is established from experiment. The calculation also predicts the $33/2^-$ state above, and thus inter-configuration M1 decay of this $35/2^+$ yrast level is excluded. The lowest $31/2^+$ and $29/2^+$ states in the two nuclei should lie less than 220 and 390 keV below it, but our data give no obvious candidates for those levels. Above the $35/2^+$ state, one would expect a $(\pi h^{n-1}_{11/2} d_{3/2}\, \nu f h_8)39/2^+$ level, but since the $\pi d \nu h$ two-body interactions are not known we cannot calculate the level energy. Also configurations involving an $s_{1/2}$ proton cannot be predicted satisfactorily by the shell model since the $\pi h \pi s$ two-body states in ^{148}Dy are known [Tai 89] to mix strongly with close-lying neighbouring levels.

The simplest octupole state that we have observed in our experiments is the 3.228 MeV 11^- level in ^{154}Yb although the level parity is not yet measured. The state has the configuration $\pi h^6_0 \nu f h_8 \times 3^-$. Analogous states have also been identified in the even-Z isotones lying below and were discussed in Ref. [Pii 90]. In this $\nu f h_8 \times 3^-$ coupling the νf will cause a lowering of the 11^- octupole state compared to the phonon energy at N=82 through the coupling to the $i_{13/2}$ neutron. In contrast, the $h_{9/2}$ neutron has no suitable single particle partner to form 3^-, and therefore should remain a spectator, such that the stretched 11^- octupole energy should be the same as the stretched $(\nu f_{7/2} \times 3^-)13/2^+$ energy in the N=83 neighbours. The Fig. 5.2 gives the energy systematics for the N=83 and 84 nuclei from Gd to Yb, which is in excellent agreement with this simple expectation and strongly supports the assignment in ^{154}Yb.

Also from the energy systematics of octupole excitations it is tempting to assign the low-lying $27/2^+$ and $29/2^+$ states in Tm and their probable counterparts in Ho as octupole excitations built on the maximum aligned $(\pi h_{11/2} \nu f^2_6)23/2^-$ level. The two

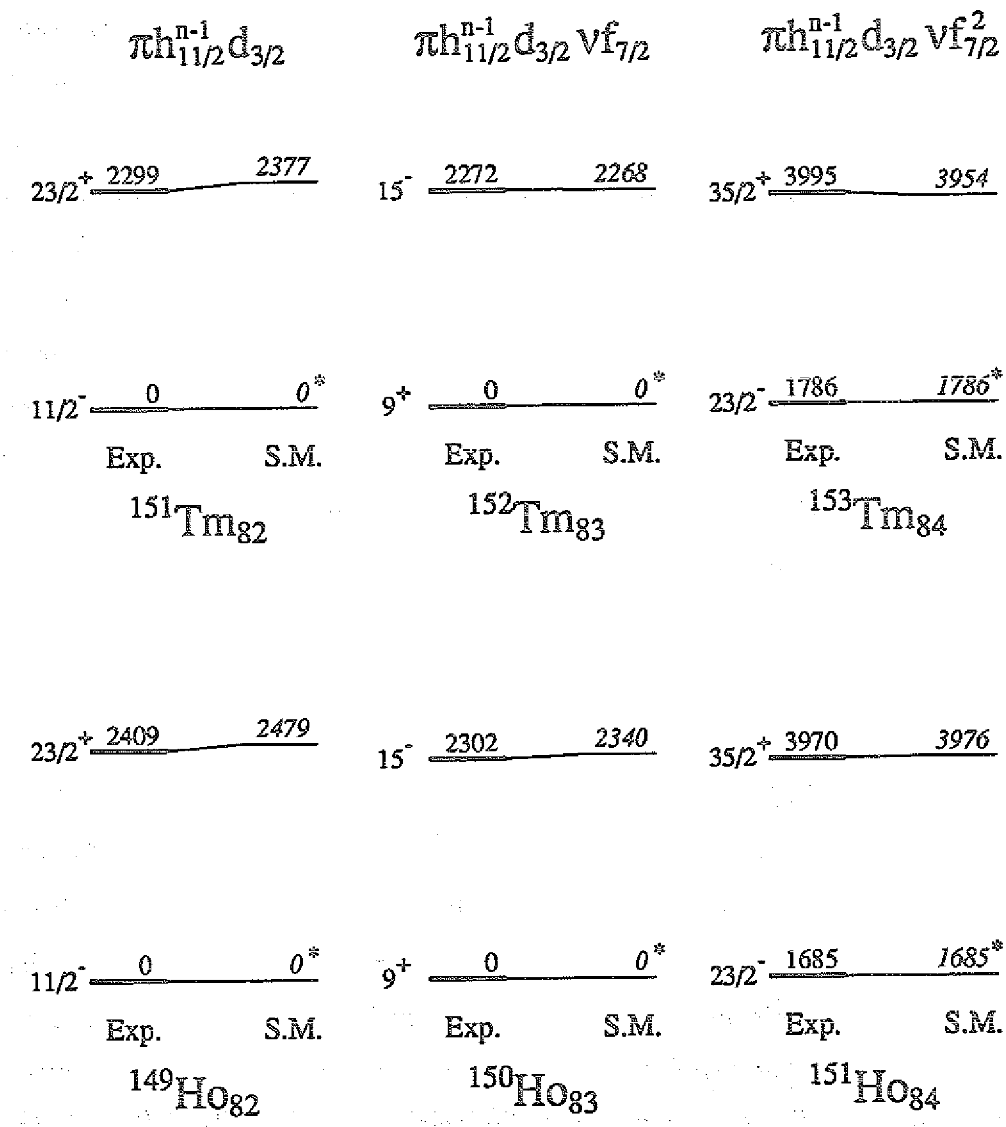

Fig. 5.1 The energy of the $(\pi h^{2}_{11/2})0^+$ to $(\pi h_{11/2}d_{3/2})7^-$ excitation in multiparticle states of Ho and Tm involving 1 to 3 aligned spectetor nucleons, compared with the results from shell model calculations.

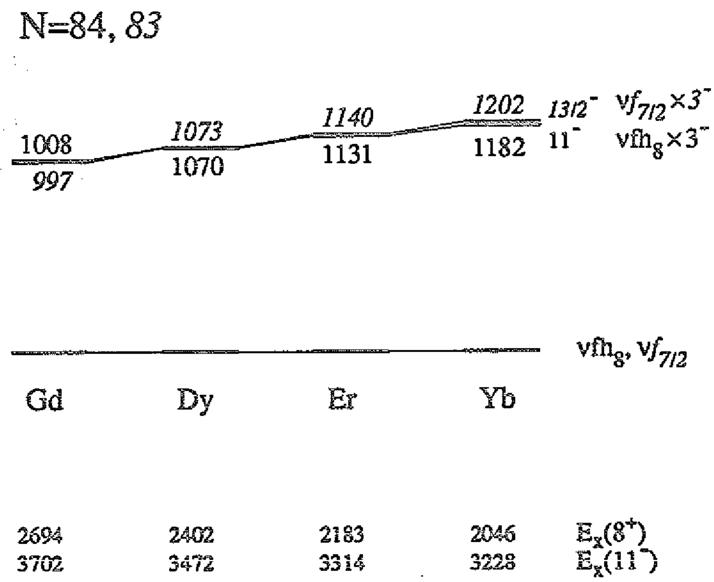

Fig. 5.2 Comparison of the yrast 8^+ to 11^- energy separations in N=84 nuclei with the lowest $13/2^+$ excitation energy of their N=83 neighbours. Below are given the excitation energies in the N=84 nuclei.

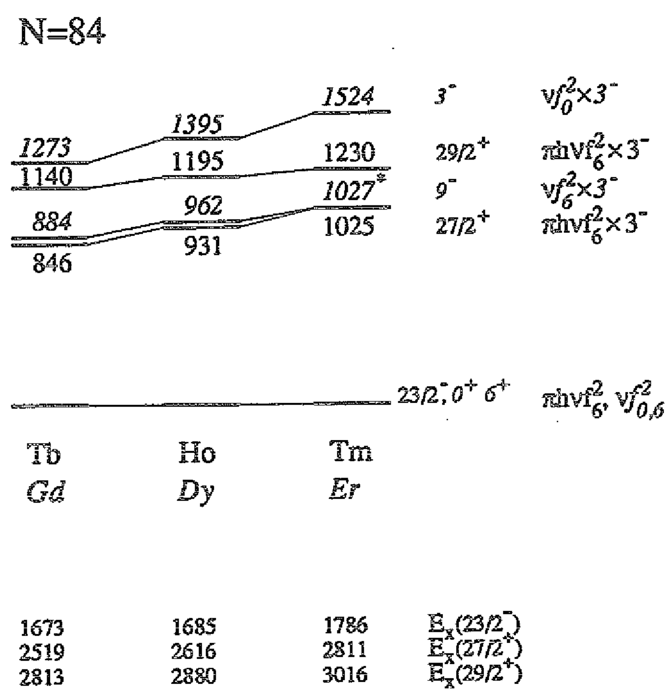

Fig. 5.3 Energy comparison of octupole excitations built on the aligned $(\nu f^2_{7/2}\pi h_{11/2})23/2^-$ states in odd-A N=84 nuclei with those built on the νf^2_6 and νf^2_0 states in the even-Z isotones.

analogous states are also identified in ^{149}Tb, and it is well known [Lac 91] that in the presence of one $h_{11/2}$ proton the lowest lying octupole septet yrast excitation has $\Delta I=2$, while the maximum coupling $\Delta I=3$ state lies higher in energy. Most clearly, this feature is observed in $^{147}Tb_{82}$ and is attributed to the exchange interaction of the $h_{11/2}$ valence proton with the large $\pi h_{11/2} d^{-1}_{5/2}$ particle-hole component in the octupole phonon [Bro 79]. The effect naturally prevails when valence neutrons are added. The data from $^{149}Tb_{84}$ are compared with our results for $^{151}Ho_{84}$ and $^{153}Tm_{84}$ in the Fig. 5.3, where we also include the νf^2_6 to $\nu f^2_6 \times 3^-$ 6^+ to 9^- spacings and the lowest 3^- excitations in the below-lying even–Z neighbours. Although the comparision supports the above interpretation, the assignments here are tentative since 27/2 and 29/2 even-parity states may also be formed in this energy region by other configurations.

Opposite parity core excited states should also become yrast at higher angular momentum when the $\pi h^n \nu^2$ valence particle spin is exhausted. But since so far only in ^{152}Er odd-parity levels have firmly been established above 5 MeV a systematic study of these excitations is still precluded.

6 Synopsis

In in-beam experiments using the γ-spectrometers Nordball at the Niels Bohr Institute and Osiris at the Hahn-Meitner Institute we populated the four N=84 isotones ^{151}Ho, ^{152}Er, ^{153}Tm and ^{154}Yb through compound evaporation reactions induced with medium HI beams of masses ranging from 28 to 56. All observed γ-transitions with intensities above 1% (5% in ^{154}Yb) of the respective exit channel were placed in the level schemes, with spins established up to 10 MeV (8 MeV for ^{154}Yb) and parities up to between 5 and 7 MeV.

We have found that in these N=84 nuclei the multi-valenceparticle configurations $\pi h^n_{11/2}\nu f^2_{7/2}$ and $\pi h^n_{11/2}\nu f_{7/2}h_{9/2}$ are strongly populated in the yrast cascades, and we have observed them up to their maximum spins of $43/2^-$ in Ho (at 4.8 MeV), 24^+ in Er (7.5 MeV), $51/2^-$ in Tm (6.9 MeV), and only up to 24^+ in Yb, 0.5 MeV below the fully aligned 26^+ state expected at 9.1 MeV. The $\pi h^n \nu f^2$ configuration forms smooth sections of the yrast line, while the more irregular yrast line of the $\pi h^n \nu fh$ character reflects the strong $(\nu fh)8^+$ two-body attraction which gives rise to pronounced yrast line dips.

We have also carried out full shell model calculations of these yrast lines, which are in excellent agreement with the experimental data. Since we take all dynamic input values, i.e. the two-body matrix elements and the single particle energies, from experiment, the calculations are free of any adjusted parameter.

An interesting new result is the systematic identification in the $\pi h^n_{11/2}\nu fh$ configuration of yrast states formed by specific proton couplings, where the strongly attractive $(\pi h_{11/2}\nu h_{9/2})1^+$ interaction is activated. As a consequence these states drop down to the yrast lines and in energy below the maximum aligned state of the next lower proton seniority. These seniority inverted yrast states were systematically identified in the four N=84 nuclei, including two such states in ^{153}Tm, the first N=84 nucleus where a second seniority inverted yrast state can be formed.

References

[Bar 88] R. Barden, A. Plochocki, D. Schardt, B. Rubio, M. Ogawa, P. Kleinheinz, R. Kirchner, O. Klepper, J. Blomqvist, Z. Phys. A329(1988)11

[Bro 79] R. Broda, M. Behar, P. Kleinheinz, P.J. Daly, J. Blomqvist, Z. Phys. A293(1979)135

[Bro 91] R. Broda, C.T. Zhang, P. Kleinheinz, R. Menegazzo, K.–H. Maier, H. Grawe, M. Schramm, R. Schubart, M. Lach, S. Hofmann, Jül-Spez-2590, (1991)85

[Col 93] R. Collatz, privite communication 1993

[Chu 84] Y.H. Chung, P.J. Daly, H. Helppi, R. Broda, Z.W. Grabowski, M. Kortelahti, J. McNeil, A. Pakkanen, P. Chowdhury, R.V.F. Janssens, T.L. Khoo, J. Blomqvist, Phys. Rew. C29, (1984)2153

[Dal 80] P.J. Daly, P. Kleinheinz, R. Broda, S. Lunardi, H. Backe, J. Blomqvist, Z. Phys. A298(1980)173

[Dri 90] M.W. Drigert, M. Piiparinen, R.V.F. Janssens, R. Holzmann, I. Ahmad, J. Borggreen, R.R. Chasman, P.J. Daly, B.K. Dichter, H. Emling, U. Garg, Z.W. Grabowski, T.L. Khoo, W.C. Ma, M. Quader, D.C. Radford, W. Trzaska, Nucl. Phys. A515(1990)466

[Fer 65] A.J. Ferguson,'Angular Correlation Methods in Gamma-ray Spectroscopy', North-Holland Publishing Co., Amsterdam (1965)

[Fir 88] R.B. Firestone, J.M. Nitschke, P.A. Wilmarth, K. Vierinen, J. Gilat, K.S. Toth, Y.A. Akovali, Phys. Rev. C39, (1988)219

[Giz 81] J. Gizon, A. Gizon, S. Andre, J. Genevey, J. Jastrzebski, R. Kossakowski, M. Moszynski, Z. Preibisz, Z. Phys. A301(1981)67

[Hag 77] E. Hagberg, P.G. Hansen, J.C. Hardy, P. Hornshoj, B. Jonson, S. Mattsson, P. Tidemand-Petersson, and the Isolde Collaboration, Nucl. Phys. A293 (1977)1

[Her 86] Bent Herskind, Nucl. Phys. A447(1985)395c

[Kor 89] M.O. Kortelahti, K.S. Toth, K.S. Vierinen, J.M. Nitschke, P.A. Wilmarth, R. B. Firestone, R. M. Chasteler, A. A. Shihab-Eldin, Phys. Rev. C39, (1989)636

[Kuh 88] A. Kuhnert, Dissertation, HMI Berlin, 1988

[Kuh 92] A. Kuhnert, D. Alber, H. Grawe, H. kluge, K.H. Maier, W. Reviol, X. Sun, E. M. Beck, A.P. Byrne, H. Hübel, J.C. Bacelar, M.A. Deleplanque, R.M. Diamond, F.S. Stephens, Phys. Rev. C46, (1992)484

[Kra 73] K.S. Krane, R.M. Steffen and R. M. Wheeler, Nucl. Data Tables 11(1973)351

[Lac 91] M. Lach, P. Kleinheinz, M. Piiparinen, M. Ogawa, S. Lunardi, M.C. Bosca, J. Styczen, J. Blomqvist, Z. Phys. A341(1991)25

[Law 81] R.D Lawson, Z. Phys. A303(1981)51

[Led 78] Table of Isotopes, 7th Edn., C.M. Lederer, V.S. Sherley(Eds.), (Wiley, New York, 1978)

[Lia 87] C.F. Liang, P.Paris, P. Kleinheinz, B. Rubio, M. Piiparinen, D.Schardt, A.

[Lie 84] R.M. Lieder, H. Jäger, A. Neskakis, T. Venkova, C. Michel, Nucl. Instr. and Meth. 220(1984)363

Plochocki, R. Barden, Phys. Lett. 191B, (1987)245

[McN 86] J. McNeill, R. Broda, Y.H. Chung, P.J. Daly, Z.W. Grabowski, H. Helppi, M. Kortelahti, R.V.F. Janssens, T.L. Khoo, R.D. Lawson, D.C. Radford, J. Blomqvist, Z. Phys. A 325(1986)27

[McN 90] J.H. McNeill, J. Blomqvist, A.A. Chishti, P.J. Daly, W. Gelletly, M.A.C. Hotchkis, M. Piiparinen, B.J. Varley, P.J. Woods, Z. Phys. A335(1990)241

[Mec 89] W. Meczynski, K. Zuber, R. Broda, R. Menegazzo, P. Kleinheinz, M.C. Bosca, P. Paris, C.F. Liang, J. Blomqvist, Jül-Spez-562, (1990)50, and Proc. Conf. NFFS6+ AMC09, Bernkastel-Cues, Germany (1992)695

[Men 91] R. Menegazzo, Dissertation, KFA Jülich, Jül-2529, Sep. 1991

[Nag 81] Y. Nagai, J. Styczen, M. Piiparinen, P. Kleinheinz, D. Bazzacco, P. v. Brentano, K.O. Zell, J. Blomqvist, Phys. Rev. Lett 47(1981)1259

[Nol 82] E. Nolte, G. Korschinek, Ch. Setzensack, Z. Phys. A309(1982)33

[Oxb 85] 'The Oxford-Buenos-Aires-MSU Shell-Model Code', B.A. Brown, A. Etchegoyen, W.D.M. Rae, MSUCL report 524.

[Pii 90] M. Piiparinen, P. Kleinheinz, S. Lunardi, M. Ogawa, G. de Angelis, F. Soramel, W. Meczynski, J. Blomqvist, Z. Phys. A337(1990)387

[Rat 84] G.E. Rathke, Diplomarbeit, TU München, 1984

[Saa 93] A. Saad, C.T. Zhang, P. Kleinheinz, R. Collatz, R. Broad et. al, to be published

[Sch 76] J. Schiffer, W.W. True, Rev. Mod. Phys. 48(1976)191

[Sch 87] D. Schardt, R. Barden, R. Kirchner, O. Klepper, A. Plochocki, E. Roeckl, P. Kleinheinz, M. Piiparinen, B. Rubio, K. Zuber, C. F. Liang, P. Paris, A. Huck, G. Walter, G. Marguier, H. Gabelmann, J. Blomqvist, Proc. Conf. Nuclei far from Stability, Ontario, Canada (1987)477

[Sle 89] G. Sletten, J. Gascon, J. Nyberg, Proc. of the Int. Conf. on the Spectroscopy of Heavy Nuclei, June 1989, Crete. Institute of Physicis Conference Series Number 105 (IOP Publishing, Bristol) p. 125

[Ste 75] R.M. Steffen and K. Alder, in: The Electromagnetic Interaction in Nulear Spectroscopy, ed., W.D. Hamilton (North-Holland, Amsterdam, 1975) p. 505

[Sty 87] J. Styczen, P. Kleinheinz, W. Starzecki, B, Rubio, G. de Angelis, H.J. Hähn, C.F. Liang, P. Paris, R. Reinhardt, P. von Brentano, J. Blomqvist, Proc. 5th Int. Conf. on Nuclei far from Stability, Rosseau Lake 1987, I. S. Towner(ed.), (New York: AIP Conf. Proc. 164), p. 489

[Sty 92] J. Styczen, unpublished data, quoted in P. Kleinheinz, J. Styczen, R. Menegazzo, H. Grüven, D. Schardt, G. Walter, A. Huck, G. Marguier, J.L. Tain, J. Blomqvist, and the ISOLDE collaboration, Proc. NFFS & AMC09, Inst. of Phys. Conf. Ser. 132, Bristol and Philadelphia 1992, p691, cf. also M. Lach, P. Kleinheinz, M. Piiparinen, M. Ogawa, S. Lunardi, M.C. Bosca, J. Styczen, J. Blomqvist, Z. Phys. A341(1991)25

[Sty 93] J. Styczen, privite communication 1992

[Tai 89] J.L. Tain, B. Rubio, P. Kleinheinz, D. Schardt, R. Barden, J. Blomqvist, Z. Phys. A333(1989)29

[Tot 79] K.S. Toth, C.R. Bingham, H.K. Carter, B.G. Ritchie, D.C. Sousa, D.R. Zolnowski, Phys. Rev. C20, (1979)298

[Vie 88] K.S. Vierinen, A.A. Shihab-Eldin, J.M. Nitschke, P.A. Wilmarth, R.M. Chasteler, R.B. Firestone, K.S. Toth, Phys. Rev. C38, (1988)1509

[Wil 80] J. Wilson, S.R. Faber. P.J. Daly, I. Ahmad, J. Borggreen, P. Chowdhury, T.L. Khoo, R.D. Lawson, R.K. Smither, J. Blomqvist, Z. Phys. A296(1980)185

[Zha1 93] C.T. Zhang, P. Kleinheinz, R. Broda, M. Piiparinen, R. Collatz, G. Sletten, et. al, to be published

[Zha2 93] C.T. Zhang, R. Broda, R. Menegazzo, P. Kleinheinz, R. Collatz, H. Grawe, S. Hofmann, M. Lach, K.H. Maier, M. Schramm, R. Schubart, J. Blomqvist, Z. Phys. A345(1993)327

Acknowledgement

I acknowledge with sincere gratitude Prof. Yukun Ho for his recommendation and Prof. Dr. Otto Schult for the possibility to carry out this work at the Institut für Kernphysik, KFA Jülich. The thanks are extended to the KFA Jülich for the full financial support under the duration of my research project.

I am in particular grateful to Dr. Peter Kleinheinz for his continuous guidence, invaluable help and his constant encouragement throughout the course of this work.

I wish also to experess my warmest thanks to Prof. Dr. Rafal Broda for his friendship, his assistance and for many helpful discussions.

Furthermore, I am indebted to our collabrators at the Hahn-Meitner Institute and the Niels Bohr Institute, especially, to Dr. Matti Piiparinen, Dr. Hugo Meier, Dr. Hubert Grawe and Dr. Geirr Sletten, who contributed a great deal to the success of the experiments carried out for this thesis. I would also like to extend my gratitude to Prof. Jan Blomqvist for his friendly cooperation in the work of the theoretical interpretations of the experimental results, and to Rüdiger Collatz, Roberto Menegazzo and Peter Wieder for their friendly support in the work.

My sincere thanks go to Mrs. Hiltrud Schult and Mrs. Ankel Kleinheinz for their hospitality, and for their kind help in solving the problems of daily life.

Most of all, I want to thank my wife, Zhihong, for her understanding and constant support.

FORSCHUNGSZENTRUM JÜLICH GmbH

KFA

Jül-2857
Dezember 1993
ISSN 0944-2952